UMS
UNIVERSITI MALAYSIA SABAH

BORNEO SCIENCE

The Journal of Science and Technology

ONLINE ISSN : 2231-9085 | ISSN : 1394- 4339

BORNEO SCIENCE

A JOURNAL OF SCIENCE AND TECHNOLOGY

BORNEO SCIENCE is a journal of science and technology published twice a year. It publishes original articles on all aspects of research in science and technology of general or regional interest particularly related to Borneo. Manuscripts submitted must not have been published, accepted for publication, or be under consideration elsewhere. Borneo Science welcomes all categories of papers: full research papers, short communications, papers describing novel methods, review papers and book reviews. Views expressed in the articles do not represent those of the Editorial Board and the University.

BORNEO *SCIENCE* *merupakan jurnal sains dan teknologi yang diterbitkan dwitahunan. Jurnal ini menerbitkan artikel asli dalam kesemua bidang sains dan teknologi secara umum mahupun dalam kepentingan serantau, terutamanya yang berkaitan dengan Borneo. Manuskrip yang dihantar bukan yang telah diterbitkan, telah diterima untuk diterbitkan, atau sedang dipertimbangkan untuk diterbitkan. Borneo Science mengalu-alukan semua jenis kertas kerja sama ada hasil penyelidikan, komunikasi pendek, penjelasan suatu kaedah, ulasan kertas kerja atau ulasan buku. Pandangan yang ditulis dalam artikel Borneo Science tidak menggambarkan pendapat Sidang Editor dan Universiti.*

DOI: https://doi.org/10.51200/bsj.v43i2

BORNEO SCIENCE
A JOURNAL OF SCIENCE AND TECHNOLOGY

BORNEO SCIENCE

A JOURNAL OF SCIENCE AND TECHNOLOGY

ONLINE ISSN 2231-9085 | ISSN 1394-4339

BORNEO SCIENCE

A JOURNAL OF SCIENCE AND TECHNOLOGY
JURNAL SAINS DAN TELNOLOGI

Volume 43 Issue 2

October 2022

CONTENT
KANDUNGAN

Page
Muka
Surat

ORIGINAL ARTICLES

BorneoScience
The Journal of Science & Technology
Volume 43 Issue 2 : Oct 2022
Online ISSN : 2231-9085 | ISSN : 1394-4339

PROFILING ENVIRONMENTAL LEADERS AMONG SOCIAL INFLUENCERS: PERSPECTIVES OF SOCIAL FOLLOWERS

Nor Azira Mohd Radzi[1], Latisha Asmaak Shafie[2], Nor Alifah Rosaidi[3], Razlina Razali[4], Lew Ya Ling[5] and Ku Azlina Ku Akil[6]

[1, 2,3,4,5] Academy of Language Studies,
[6] Faculty of Computer & Mathematical Sciences,
Universiti Teknologi MARA Cawangan Perlis,
Kampus Arau, Perlis, Malaysia

Received 13th Nov 2021; accepted 29th Mei 2022
Available online 1st Nov 2022
DOI: https://doi.org/10.51200/bsj.v43i2.4506

ABSTRACT. *Opinion leaders or social influencers possess the conviction of their followers in making personal and professional decisions. Their posts or sharing on social media may strongly influence their followers' decision to practise some environmental actions in their daily lives. They are often labelled as the current thought leaders among the Millennials. Considering the critical environmental issues faced, many social influencers play important roles to show their willingness to change human destructive behaviours and conserve the environment for the future. Realising their influence on their followers, these environmental influencers relentlessly encourage their followers to support their missions. Thus, the study attempted to profile successful environmental leaders among social influencers from the views of their followers. The study was a qualitative multiple case study on five informants. The informants volunteered to participate and were from 100 university students. They were interviewed in a written semi-structured interview and researchers could reach them if clarification was needed. Data were analysed using thematic analysis. Peer debriefing was used to increase trustworthiness. The findings revealed that effective environmental leaders possessed these criteria: a) credibility; b) generosity; c) responsible creators; d) influential figures; e) trust builders. The informants believed that these social influencers are as real as offline leaders even though they only knew these social influencers in online contexts. The ability of environmental social influencers to reach and convince multiple audiences to participate and support various environmental initiatives via social media platforms made them powerful thought leaders.*

KEYWORDS. social influencers, followers, environmental awareness, pro-environmental behaviours

INTRODUCTION

Natural resource depletion and the rise of consumerism lead to environmental disasters. In recent years, environmental leaders in the form of social influencers use social media to increase environmental awareness by opinion leaders, and pro-environmental behaviours among millennials. Millennials in this study refer to the digital natives who were born between 1981 to 2000 (Fry, 2016). This generation spends a substantial amount of time communicating, connecting, unwinding, making content and being updated with recent events using social media platforms (Dwivedi & Lewis, 2020). Not only that,they are able to connect with society and tend to be the agent of change. Concurrently,they have to keep abreast with the latest social issues and always be prepared to interact with their followers. However, the role of social influencers in communicating pro-environmental behaviours among millennials is not well understood. It is important to identify how social influencers can be used as an enabler for promoting pro- environmental behaviours in the context of Malaysian millennials because there are limited studies on the influence of these influencers on their followers regarding environmental issues (Saghati, Sanaz & Khalid, 2021). Social influencers like Melissa Tan, Deborah Henry, Seri Mizani, Taylor Bright and Shellbizlee can convince their followers in making personal and professional decisions.

They are often labelled as the current thought leaders among the Millennials. Considering the critical environmental issues the world is facing, many social influencers play important roles to show their willingness to change human's destructive behaviours and to conserve the environment for the future (Awang et al., 2021; Okuah et al., 2019). For instance, Melissa Tan advocates eco-awareness lifestyles by embracing vegan food, participating in environmental campaigns and starting an eco-awareness platform (The Green Guerilla). Tasnim Shah, Shariffudin Azhar Omar and Muhammad Nazirul Ahmad Fauzi collaborated with Nuffnang to raise funds for environmental causes (Raihan, 2021).

Furthermore, millennials are more acquiescent to ethical issues and are conscious of the environment as compared to the other generations (Bedard & Tolmie, 2018). Millennials are considered the most well-informed and conscious age group when it comes to environmental issues (Bureau, 2015). However, there is an incongruence between millennials' claimed intentions and actual behaviours toward pro-environmental. Naderi & Van Steenburg's study (2018) indicates that millennials have not truly begun to fully integrate their beliefs and actions. In other words, they are green in attitude, but they may not take actual environmental actions in their daily lives. Therefore, the pro-environmental behaviour of the environmental influencers nowadays needs more attention. We want to know further the behavioural characteristics of these environmental influencers which allow them to encourage their followers to support their missions and promote environmental awareness among the millennials, and play their part to tackle certain issues. Thus, this study attempted to profile successful environmental leaders among social influencers from the views of their followers. The study aims to see the potential of social influencers in making a difference to the environment.Successful environmental leaders are social influencers who can exhibit pro-environmental behaviours and persuade their followers to emulate their pro-environmental lifestyles. Future research could look into the dynamics of environmental issues championed by these opinion leaders or social influencers in order to encourage future generations to adopt pro-environmental behaviours.

LITERATURE REVIEW

Current and future societies require their citizens to rectify their self-destructive behaviours on the environment (Razak & Sabri, 2019). Recently, environmental awareness has increased in developed countries as consumers opt for green-conscious products and services (Naderi & Steenburg, 2018). The growing segment of consumers consists of the Millenials. Millennials were born between 1981 to 2000 (Fry, 2016), and they are known for their informative experiences with being adaptable, risk-taking and pleasure-seeking (Aker, 2018; Weber, 2017) as well as today's technology-savvy (Twenge et al., 2010). These definitions are adopted in Malaysian contexts (Abd Majid et al., 2016). Thus, it creates a growing body of research on emerging millennial leaders to cater for the millennials' needs and demands for leaders. Long (2017) reveals that millennials are inspired by servant leadership, ethical leadership and transformational leadership. On the other hand, Indonesian millennials prefer democratic leadership (Mustomi & Reptiningsih, 2020). Similarly, Basit and Sebastian (2017) advocate that democratic leadership is effective to lead the millennials. In developing pro-environmental behaviours among the Millennials, they need to feel attached to nature (Gräntzdörffer, James & Elster, 2019).

Educating individuals to become environmentally friendly society members is achieved through lifelong environmental education (Clugston, 2004). Therefore, society members need to be educated on environmental problems to enhance their environmental knowledge which will facilitate pro-environmental behaviours. Pro-environmental behaviours protect the environment (Razak & Sabri, 2019). As the Millennials constantly use social media, they can be educated through the use of social media sites to encourage environmental awareness among young people. For instance, modern zoos engage their customers using their social media sites to enhance awareness of conservation and ecology (Rose, Hunt & Riley, 2018). Millennials in higher education are green consumers because they are influenced by future- oriented mindsets despite not being financially stable as they will reap the benefits of their pro-environmental behaviours (Naderi & Steenburg, 2018).

The popularity of Youtube, Instagram, Twitter and Facebook has propelled the influence of social influencers to engage the audience and create awareness to their followers (Lokithasan, Simon, Jasmin & Othman, 2019). Social influencers influence their followers through strong persuasive content (Audrezet, de Kerviler, & Moulard, 2017). They become role-models to their followers by being authentic and promoting their causes and lifestyles through their contents (Casaló, Flavián & Ibáñez-Sánchez, 2018; Puteri, 2018). Social influencers connect brands/companies/organisations to their followers (Lim, Radzol, Cheah & Wong, 2017) and cultivate ecocentrism (Liobikien˙e & Poškus, 2019). These social influencers have established their credibility by highlighting their authenticity while curating their social media accounts. Social influencers engage their followers with exciting content on environmental awareness like biodiversity, climate change and sustainability and influence the audience to persuade them to form pro-environmental behaviours. In China, social influencers used Weibo to promote environmental consumerism by educating their followers on environmental issues and asking their followers to purchase products based on environmental considerations (Skoric & Zhang, 2019).

However, there are not many studies conducted on the characteristics of social media influencers who attracted and influenced followers (Ki, 2018). There are limited studies on the effects of social influencers and social media on environmental issues as previous studies tended to focus on the impact of social influencers on marketing in retaining and engaging customers (Hassan et al., 2021; Javed, Rashidin & Xiao, 2021; Nafees et al., 2021). A common theme in these studies is that social media influencers are seen as credible, trustworthy and relatable sources of information that have a big impact on the purchasing behaviours and decisions of their followers (Djafarova & Rushworth, 2017; Lou & Yuan, 2019).

Expertise and trustworthiness are seen as two contributing factors that indicate the credibility of influencers for followers to encourage their pro-environmental intentions (Awang, Syed Annuar& Gisip, 2019). This finding contradicts Lim, Cheah and Wong (2017), who advocated that the credibility of social influencers failed to encourage desired attitude and attention. Expertise and credibility are seen as two enablers that indicate the credibility of influencers to followers to encourage their environmental intentions (Awang, Syed Annuar & Gisip, 2019). This finding contradicts Lim, Cheah, and Wong (2017), who argue that the credibility of social influencers fails to encourage the attitudes and attention that people expect. In addition, research on pro-environmental behaviours also uses various theories, such as the Theory of Planned Behavior (TPB), Normative Activation Model (NAM), Normative Theory of Value Beliefs (VBNT), and Theory of Protective Motivation (PMT), etc. to explain what drives the followers to pro-environmental attitude. From this, it is worth further exploring what influences the local followers to follow their influencers.

Therefore, this paper intended to profile environmental leaders among social influencers in the eyes of followers who were university students. Higher education plays an important role to promote pro-environmental behaviours in a sustainable environment (Akhtar et al., 2022; Cuadrado et al., 2022; Huang & Yu, 2022; Jusoh et al., 2020; Lee et al., 2020). Therefore, it is necessary to profile environmental leaders among social influencers in the eyes of followers who were university students.

METHODOLOGY

The study was a qualitative multiple case study on five informants. Qualitative research method enables researchers to explain the informants' perspectives on the phenomenon (Denzin & Lincoln, 2011). A multiple case study enables researchers to grasp a comprehensive understanding and connect the most insightful experiences of the informants (Stake, 2006). Qualitative multiple case study allows the researcher to investigate individuals or organisations, simple to complex interventions, relationships, communities, or programmes, and it facilitates the deconstruction and subsequent reconstruction of various phenomena (Baxter & Jack, 2008). Purposive sampling was used to gather rich information in limited resources (Patton, 2002).

Five informants were chosen from the survey which involved 100 social influencers that was conducted prior to this study. These Malay informants were chosen because they volunteered to participate in a written semi-structured interview. During semi-structured interviews, participants were asked to respond to questions on demographic information, the effects of the leadership qualities of micro-influencers, motivation to exhibit pro-environmental behaviours and levels of advertising literacy.

Pseudonym	Gender	Age
Informant 1	F	23
Informant 2	M	23
Informant 3	F	23
Informant 4	M	24
Informant 5	F	23

The researchers could reach them if clarification was needed. Data were analysed using thematic analysis. This involved a thorough reading of interview transcripts as well as comparing each transcript to generate common themes about the case. Similar data analysis approach has been conducted by researchers such as Zamari et al. (2022) and Mijar and Manaf (2021) in qualitative case studies involving Malaysian social media influencers. Peer debriefing was used to increase trustworthiness.

FINDINGS AND DISCUSSION

The analysis produces five themes. The findings revealed that effective environmental leaders possessed these criteria: a) credibility; b) generosity; c) responsible creators; d) influential figures; e) trust builders. Participants were asked these questions during semi-structured interviews to evaluate characteristics of these environmental leaders : i) Why do you trust social-influencers? ii) How do you judge the reliability of the message? iii) How do micro-influencers influence you to increase your pro-environmental behaviours? iv) What are the strategies they use to persuade you to support their environmental campaigns? v) Why do you trust micro-influencers in promoting environmentally friendly lifestyles?

Theme 1: Credibility

WOM (Word of Mouth) adoption is predicted by credibility (Erkan and Evans, 2016). It is commonly acknowledged that word-of-mouth is a potent tool. Social influencers, as potent sources of cultural meaning, play an important role in the diffusion of meanings. According to WOM, this is a must-have. Credibility, which is derived from a social influencer's reputation, is an important part of the endorsement process. Credibility is achieved when followers assume that social influencers had experiences and knowledge about environmental issues/challenges/products. A study by Mijar and Manaf (2021) demonstrated that Malaysian influencers had to frequently update their social media content on relevant environmental issues in order to build credibility among their followers. This shows that social presence and relatable content are important factors that social influencers need to consider if they are to influence followers to undertake significant pro-environmental actions.

Three informants reported that their social influencers had environmental leadership when these social influencers had credibility as illustrated in Extract 1, 2 and 3.

Extract 1	They have knowledge in their respective fields (Informant 4) Shows the example on what needs to be done themselves (not just saying what need to be done)
Extract 2	There's this one influencer Melissa Tan, she is on a journey to a zero-waste lifestyle where she uses stainless steel straw instead of the plastic one and also uses reusable container or bottle. (Informant 5)
Extract 3	- mempunyai pengalaman dan pengetahuan tentang sesuatu product (Informant 3) -They have experience and knowledge of a product (Informant 3)

This suggests that environmental leaders for the Malaysian Millenials need to have a believability factor before they emulate pro-environmental behaviours. This is so as followers are more likely to be more influenced by their behaviours if the influencers possess expertise in the content that they promote (Lou & Yuan, 2019). Moore, Yang, and Kim (2018) also discovered that influencers must demonstrate authenticity, likability, and authority to gain followers' trust. They have consistently provided important and honest information to their followers, thus their perspectives are more credible. A similar pattern of results was obtained in previous studies (Kumar & Polonsky, 2019; Tarhini, Alalwan, Shammout, & Al- Badi,2019).

Theme 2: Generosity

Environmental leaders are perceived as someone who generously shared his/her experiences and knowledge on their social media. The informants believed that social media influencers needed to be generous in sharing and showing them to be involved in environmental challenges.

Extract 4	Gather follower to do it together and do it the way that people tend to love doing it. For example, selfie with clean environment after cleaning it and post it on media social to attract more people to do it like what Maya Karin did last time. It is a good campaign where a lot of her followers take part of it even from different location. (Informant 4)
Extract 5	She conducts workshops, talks and also creates customised programs and campaigns to suit different needs. (Informant 5)
Extract 6	Dengan sentiasa memuat naik aktiviti memelihara alam sekitar di media sosial. (Informant 1) By constantly uploading environmental conservation activities on social media. (Informant 1)
Extract 7	Dari segi cara perkongsian yang dilakukan… dengan perkongsian tentang alam sekitar (Informant 3) In terms of the way the partnership is done… with the partnership about the environment (Informant 3)

Research shows that in utilising social media influencers for environmental awareness, three basic communication processes are used to influence and engage target audiences towards the desired response: awareness, instruction, and persuasion (Thompson et al., 2011). Social influencers publish information about pro-environmental activities and activities continue to input a kind of awareness information to the public. Awareness messages keep people known of what they should do, who

should do it, where and when to do it. Instruction messages instruct people on how to do it, and persuasive messages provide reasons why the audience should have pro-environmental behaviour (Thompson et al., 2011). When answering how social influencers influence her pro-environmental behaviour, Informant 4 stated that it is important for social influencers to share actively and generously because their sharing influences others to follow them, "…gather followers to do it together and do it the way that people tend to love doing it. For example, take a selfie with clean environment after cleaning it and post it on media social to attract more people to do it like what Maya Karin did last time. It is a good campaign where a lot of her followers take part of it even from different locations." This informant's answer pointed out that social influencers used their personal practices to guide others on how to conduct pro-environmental activities, subconsciously input the awareness of "pro-environmental is important", and further persuaded other followers from different regions to do the pro-environment activities with her. Pro-environmental social influencers must also be activists. Research found that the influence of peer recommendations and actions is higher than the information shared by official organisations or higher authorities (Moser, 2010). They either bring their followers for activities or show activism to them at home, of course, often through the media, "…dengan sentiasa memuat naik aktiviti memelihara alam sekitar di media sosial (…by constantly uploading environmental conservation activities on social media)" (Informant 1).

In addition, it should be noted that the methods or strategies shared by social influencers are also extremely important. Research shows that originality and uniqueness are crucial factors for social media influencers as opinion leaders (Casaló et al., 2020). While micro- influencers share their private news generously, social timing is also very important so that they know how to publish posts on the right day and time to increase likes, shares and clicks (Patel, 2017). Through the feedback of the informant, we found that besides originality, uniqueness and social timing, some social influencers will share different activities which they had done according to different needs, "She conducts workshops, talks and also creates customised programs and campaigns to suit different needs." (Informant 5). Although followers are aware of environmental issues, if credible information such as pro-environmental knowledge is inadequate, it will also prevent followers from adopting green behaviour (Nguyen & Zhang, 2020). Therefore, it is very important for social influencers as a leader to generously share their knowledge and experience appropriately.

Theme 3: Responsible Creators

Theme 3 which is responsible creators indicates that social influencers were environmental leaders when they include facts to support and verify their claims.

Extract 8	Research back for what they had said from trusted sources (Informant 4)
Extract 9	I will do a background check first, then evaluate them based on how they approach their audience and on the quality on their social media content.
Extract 10	Mungkin dengan cara melihat komen, cerita atau maklum balas orang lain (Informant 1) Maybe by looking at other people's comments, stories or feedback (Informant 1)
Extract 11	menilai mengikut sumber mesej tersebut (Informant 2) Evaluate according to the source of the message (Informant 2)

Responsible creators cannot talk in vain. Followers will use different methods to detect their authenticity. The online world is now a virtual "real world", speech is relatively free, open, and more influential. For example, Instagram users around the world participate in and maintain dialogue by sharing, liking and leaving their personal views in the comments area. Followers' messages are conversations with social media influencers and other followers, so this will not be the monologue of social media influencers, but the interaction between followers and stories and their narrators (Junior, 2020), or even the communication of a group of people. In this situation, everyone's comments are clear at a glance, which also increases its credibility. As the research found, social media influencers' messages are perceived as "one of the few forms of real, authentic communication" (Scott, 2015). Informant 4 said that she will evaluate how the social influencers approach their audience and their social media content. Informant 1 also said that he would pay attention to micro- influencers' responsibility "by looking at other people's comments, stories or feedback". Social influencers generally allow followers to express their thoughts and opinions online, and they also interact with users in the comment section. Social media influencers pay attention to the voices in the comment section and react to them, which will make followers feel listened to and give them a deeper understanding of the direction of the conversation (Okuah et al., 2019). This is one of the ways for followers to detect whether micro-influencers are the responsible leaders.

Since social media influencers establish more harmonious and friendly connections and relationships with the audience, compared with traditional celebrities, social media influencers are seen as more credible and trustworthy (Djafarova & Rushworth, 2017). Followers feel that they know the creator of the content; they have a relationship with the creator of the content, albeit a one-sided relationship (Lockie, 2019). Followers sure will also think about the authenticity of these social media influencers' messages based on their wisdom. Informant 2 said that he did not trust some social influences because they "kurang pengaruh fakta kukuh (less influence of solid facts)" and said he would "menilai mengikut sumber mesej tersebut (evaluate according to the source of the message)". Li Ziqi, one of the most successful social media influencers in China in the research context, has more than 8.7 million international subscribers on YouTube. She has a powerful communication impact in terms of ecological lifestyle to the audiences, especially the young generation. (Nguyen & Zhang, 2020) She showed her self-sufficient and leisurely rural life in the video. Even though her sharing is so amazing, because her green life involves a lot of work that requires self-reliance, some followers also doubt its authenticity (Wu & Jiang, 2021). After confirming that all these were fragments of her former life, she has received a large number of positive responses from followers. To lead millennials most effectively, leaders must operate with integrity. Informant 4 said he would "research back for what they had said from trusted sources" instead of accepting all information without thinking. Informant 3 would detect whether social influencers would "memaparkan bukti yang telah berjaya mereka peroleh (display the evidence they have successfully obtained)".

From the feedback of the interviewees, it can be found that the followers are always checking whether the social media influencer is a responsible creator. In general, a social media influencer is monitored by the public, and irresponsible social media influencers will be eliminated by the society at any time.

Theme 4: Influential figures

Theme 4 which is influential figures indicate that environmental leaders must have the power to **Profiling**

influence their followers to their causes. The number of followers became an indicator of social influencers' persuasive power. A large number of followers would be another indicator of the social power a social influencer has.

Extract 12	Lots of follower and have knowledge. They also can act as the voice of the people. (Informant 4)
Extract 13	Yes, they are someone that can give a big impact on a person decision as they can encourage their fans through social media. (Informant 5)
Extract 14	Kerana pempengaruh mikro pada masa kini semakin popular dan dilihat memainkan peranan khususnya kepada golongan anak- anak muda yang mana mereka suka mengikuti selebriti atau orang yang digemari di media sosial. (Informant 1) Because social influencers are now increasingly popular and are seen to play a role especially to young people who like to follow celebrities or favorite people on social media. (Informant 1)
Extract 15	kerana mereka boleh menarik lebih ramai orang untuk menyertai program yang diadakan (Informant 3) because they can attract more people to join the program held (Informant 3)

The current study reflects that Malaysian Millennials perceive influencers as powerful figures who are capable of influencing others through their opinions. Similarly, Yeo, Carter and Khor (2019) demonstrated that Malaysian Millennials regarded influencers as opinion leaders who played a huge role in the decision-making of followers. In line with previous studies, the finding shows that influential figures possessed an inviting factor to influence the attitude and decisions of their followers for particular products (Byrne, Kearney & MacEvilly, 2017). Marketing by social influencers creates more appeal as compared to the traditional celebrity-based and media advertising (Müller, Mattke & Maier, 2018). Desirable attitudes of the product which lead to higher purchase and recommendation intentions can be achieved if there is a strong congruence between consumer and product (Belanche et al., 2021). However, a study by Marjerison, Yipei and Chen (2021) revealed that influential figures among bloggers in China did not significantly motivate customers in purchasing products and purchase intention. Likewise, Cooley and Parks-Yancy (2019) pointed out that Millennials were more likely to emulate the behaviours of influencers whom they knew personally regardless of their status as celebrities or not.

Theme 5: Trust Builders

Theme 5 which is Trust Builders emphasises that social influencers spent time to make their followers trust them as environmental leaders. The informants deemed social influencers as trustworthy environmental leaders when they were engaged with their followers by exchanging opinions, environmental activities and sharing their lifestyles.

Extract 16	Social influencer is not like any typical celebrities they have more engagement with their audience thus I can say that trust is built between them and the audience. (Informant 4)
Extract 17	Social influencer has a lot more engagement with the audience thus trust is build. You can trust the influencer as is you are their friend and family, beside they also provide prove about their lifestyle. (Informant 5)
Extract 18	Dengan cara mereka menunjukkan keprihatinan mereka terhadap alam sekitar ….Dengan sentiasa memuat naik aktiviti memelihara alam sekitar di media sosial. (Informant 1) In a way they show their concern for the environment… .By constantly uploading environmental preservation activities on social media. (Informant 1)
Extract 19	memaparkan bukti yang telah berjaya mereka peroleh (Informant 3) Display the evidence they have successfully obtained (Informant 3)

The current study demonstrates that Malaysian Millennials regard the influencers as trustworthy enviromental leaders because they are able to engage with the contents delivered by the influencers at a personal level. This is not surprising given that Malaysians are more likely to be influenced by people who are in their immediate surroundings such as peers, family, and friends (Yeo et al., 2019). Furthermore, this finding is consistent with what has been found in previous studies that trust is a source of credibility in engaging awareness (Awang, Syed Annuar & Gisip, 2019) and product purchasing (Hassan, Teo, Ramayah & Al-Kumaim, 2021). Furthermore, it must be pointed out that trust is a favourable element in enhancing advertising effectiveness (Chekima, Chekima & Adis, 2020). Similarly, Cooley and Parks-Yancy (2019) found that Millennials were more likely to purchase a product based on recommendations made by people they knew personally compared to celebrities due to the level of trust they had in the former.

CONCLUSION

In the current study, the findings revealed that effective social influencers possessed these five criteria: credibility, generosity, responsible creators, influential figures and trust builders. The informants believed that these social influencers are as real as offline leaders even though they only got to know the influencers through the online world. The results showed that these environmental social influencers have the ability to reach and convince multiple audiences in social media platforms to participate and support various environmental initiatives, making them powerful thought leaders. This is something to reckon when it comes to the effects that they could make in helping with environmental issues that we are facing nowadays.

To date there is very limited studies on the role of social media influencers in influencing pro-environmental behaviours to their followers even when social media has become more significant in our life these days (Hamid et al., 2017). Despite the small scale of our study, we hope that it will

provide some valuable insights on how opinion leaders or social influencers possess the power to convince their followers in making personal and professional decisions. The social influencers are powerful enablers for promoting pro-environmental behaviours in the context of Malaysian millennials. The findings also help shed some light on other influencers to learn more about their role in spreading environmental awareness among their followers. They could use the findings as a metric or reference point to look at what or why their followers are actually reaching out for them.

The study was aimed at profiling environmental leaders among social influencers from university students' perspectives. As the informants were Malay, the study did not study social influencers of other races. The findings of this study add to the knowledge of characters of digital environmental leaders among social influencers who influence the Millennials. In making digital environmental campaigns and activities, management at higher education can include social influencers to participate in the events. These social influencers can be selected among their students. The contents of digital campaigns should reflect credibility, generosity, responsibility, influence and trustworthiness. In addition, content writing can be taught as one of the courses in higher education that can enhance the graduates' employability skills and as a skill that allows them to spread environmental awareness successfully. Future studies could be carried out to study more about the dynamic of environmental issues championed by these opinion leaders or social influencers to carry out pro-environmental behaviours for the future generation.

ACKNOWLEDGEMENT

The researchers are grateful for the financial fund received from Universiti Teknologi MARA (UiTM) through its internal grant (600-UiTMPs (PJIM & NPI-DPPD 04). The researchers are thankful to the participants of the research for their participation.

REFERENCES

Abd Majid, F, Syed Mustafa, S.M., Jais, I, Shahril, W., Subramaniam, K., & Halim, M. (2016). A preliminary study on selected Malaysian Millennials: Their characteristics and its implications on teaching innovation. 10.1007/978-981-287-664-5_54.

Akers, K. L. (2018). Leading after the boom: Developing future leaders from a future leader's perspective. Journal of Management Development, 37(1), 2-5. https://doi.org/10.1108/JMD-03-2016- 0042

Akhtar, S., Khan, K. U., Atlas, F., & Irfan, M. (2022). Stimulating student's pro-environmental behaviour in higher education institutions: An ability–motivation–opportunity perspective. Environment, Development and Sustainability, 24(3), 4128–4149.

Awang, S. F. L. Q., Annur, S. N. S., & Gisip, I. A. (2021). The effect of social media in-fluencer attributes towards pro-environmental intentions. Romanian Journal of Information Technology and Automatic Control, 31(1), 111–124.

Awang, S.F.L.Q., Syed Annuar, S.N., & Gisip, I.A . (2019). The effect of social media influencer towards pro-environmental intention. The Business and Management Review, 10(3), 63-68. 9 th International Conference on Restructuring of the Global Economy, University of Oxford, UK,8-9 th July 2019.

Audrezet, A., de Kerviler, G., & Moulard, J. G. (2017). Authenticity under threat: when social media influencers need to go beyond passion. Paper presented at the 2017 Global Fashion Management Conference at Vienna.

Basit, A., & Sebastian, V. (2017). Impact of Leadership Style on Employee Performance (a Case Study on a Private Organisation in Malaysia). 5(2), 112–130.

Baxter, P., & Jack, S. (2008). Qualitative Case Study Methodology: Study Design and Implementation for Novice Researchers. The Qualitative Report, 13(4), 544-559. https://doi.org/10.46743/2160- 3715/2008.1573

Belanche, D., Casal´o, L.V., Flavi´an, M., & Ib´a˜nez-S´anchez, S. (2021). Understanding influencer marketing: The role of congruence between influencers, products and consumers. https://www.sciencedirect.com/science/article/pii/S0148296321002307?via%3Dihub

Bureau, U. S. C. (2015). Millennials outnumber baby boomers and are far more diverse, Census Bureau reports. Author Washington, DC. https://www.census.gov/newsroom/press-releases/2015/cb15-113.html

Byrne, E, Kearney, J, & MacEvilly, C. (2017) The role of influencer marketing and social influencers in public health. Proceedings of the Nutrition Society. 76, E103-E103.

Casaló, L. V., Flavián, C. and Ibáñez-Sánchez, S. (2018). Influencers on Instagram: Antecedents and consequences of opinion leadership. Journal of Business Research. 10.1016/j.jbusres.2018.07.005

Chekima, B., Chekima, F. Z., & Adis, A. A. A. (2020), Social Media Influencer in Advertising: The Role of Attractiveness, Expertise and Trustworthiness. In: Journal of Economics and Business. 3(4), 1507-1515.

Clugston, R.M.(2004). Foreword. In P.B. Corcoran, & A.E. Wals, A.E.(Eds.), Higher Education and the Challenge of Sustainability: Problematics, Promise and Practice (pp. 3–6). Kluwer Academic Publishers: Dordrecht, The Netherlands.

Cuadrado, E., Macias-Zambrano, L. H., Carpio, A. J., & Tabernero, C. (2022). The moderating effect of collective efficacy on the relationship between environmental values and ecological behaviours. Environment, Development and Sustainability, 24(3), 4175–4202.

Cooley, D., & Parks-Yancy, R. (2019). The effect of social media on perceived information credibility and decision making. Journal of Internet Commerce, 18(3), 249-269.

Denzin, N. K., & Lincoln, Y. S. (2011). The SAGE Handbook of Qualitative Research. Thousand Oaks, CA: Sage.

Djafarova, E., & Rushworth, C. (2017). Exploring the credibility of online celebrities' Instagram profiles in influencing the purchase decisions of young female users. *Computers in human behavior*, *68*, 1-7.

Fry, R. (2016, April 25). Millennials overtake baby boomers as America's largest generation. Retrieved from Pew Research Center: http://www.pewresearch.org/fact-tank/2016/04/25/Millennials- overtake-babyboomers/

Gräntzdörffer , A.J., James, A., & Elster, D. (2019). Exploring Human-Nature Relationships amongst Young People: Findings of a Quantitative Survey between Germany and South Africa. International Journal of Environmental & Science Education, 14(7), 417-424.

Hamid, S., Ijab, M.H., Sulaiman, H., Md. Anwar, R., & Norman, A.A. (2017). Social media for environmental sustainability awareness in higher education. International Journal of Sustainability in Higher Education, 18(4), 474-491. doi: 10.1108/IJSHE-01-2015-0010

Hassan, S. H., Teo, S. Z, Ramayah, T., & Al-Kumaim, N. H. (2021). The credibility of social media beauty gurus in young millennials' cosmetic product choice. PLoS ONE 16(3): e0249286. https://doi.org/10.1371/journal.pone.0249286

Huang, R.-T., & Yu, C.-L. (2022). Exploring online green behavior among college students in Taiwan: A moderated mediation model of perceived compatibility. Multimedia Tools and Applications, 81(1), 421–436.

Javed, S., Rashidin, M. S., & Xiao, Y. (2021). Investigating the impact of digital influencers on consumer decision-making and content outreach: using dual AISAS model, Economic Research-Ekonomska Istraživanja, 1-28.

Junior, R. C. G. (2020). Instanarratives: Stories of foreign language learning on instagram. System, 94, 102330.

Jusoh, Syazni & Kamarudin, Mohd khairul amri & Abd Wahab, Noorjima & Saad, Muhammad & Rohizat, Nurul & Mat, Nik. (2018). Environmental Awareness Level among University Students in Malaysia: A Review. International Journal of Engineering & Technology. 7.28.10.14419/ijet.v7i4.34.23575

Ki, Chung-Wha. (2018). The drivers and impacts of social media influencers: The role of mimicry. PhD diss., University of Tennessee. .https://trace.tennessee.edu/utk_graddiss/5070

Kumar, P. & Polonsky, M.J. (2019). In-store experience quality and perceived credibility: a green retailer context. Journal of Retailing and Consumer Services, 49, 23-34.

Lee, A. R., Hon, L., Won, J., You, L., Oloke, T., & Kong, S. (2020). The Role of Psychological Proximity and Social Ties Influence in Promoting a Social Media Recycling Campaign. Environmental Communication, 14(4), 431–449.

Lim, X. J., Radzol, A. F., Cheah, J., & Wong, M. W. (2017). The impact of social media influencers on purchase intention and the mediation effect of customer attitude. Asian Journal of Business Research, 7(2), 19–36. doi:10.14707/ajbr.170035

Lim, X.J., Cheah, J.H. and Wong, M.W. (2017). The Impact of Social Media Influencers on Purchase Intention and the Mediation Effect of Customer Attitude. Asian Journal of Business Research, 7(2), 19-26.

Liobikien˙e , G., & Poškus , M.S. (2019). The Importance of Environmental Knowledge for Private and Public Sphere Pro-Environmental Behavior: Modifying the Value-Belief-Norm Theory. Sustainability, 11(3324), 1-19.

Lockie, M.A. (2018). In Vlogs We Trust: Consumer Trust in Blog and Vlog Content. Unpublished PhD thesis, Auckland.

Lokithasan, K., Simon, S., Jasmin, N. Z., & Othman, N. A. (2019). Male and Female Social Media Influencers: The Impact of Gender on Emerging Adults. International Journal of Modern Trends in Social Sciences, 2(9), 21-30. DOI: 10.35631/IJMTSS.29003

Long, S. 2017. Exploring Which Leadership Styles are Effective with Millennial Employees. (Thesis - Doctoral). Minneapolis, MN: Walden University.

Lou, C., & Yuan, S. (2019). Influencer marketing: how message value and credibility affect consumer trust of branded content on social media. Journal of Interactive Advertising, 19(1), 58-73.

Majid, F. A., Mustafa, S. M. S., Jais, I. R. M., Shahril, W. N. E. H., Subramaniam, K., & Halim, M. A. A. (2016). A preliminary study on selected Malaysian millennials: Their characteristics and its implications on teaching innovation. In 7th International Conference on University Learning and Teaching (InCULT 2014) Proceedings (pp. 685-697). Springer, Singapore.

Marjerison, R. K, Yipei, H, & Chen, R. (2021). The Impact of Social Media Influencers on Purchase Intention Towards Cosmetic Products in China. Journal of Behavioral Studies in Business. 12, 1-12

Mijar, M. A., & Mazinina, A. (2021). Eco-Activist Social Media Influencers (SMI) on Twitter: Does Credibility Matter?. IIUM JOURNAL OF HUMAN SCIENCES, 3(2), 15-26.

Moser, S. C. (2010). Communicating climate change: history, challenges, process and future directions. Wiley Interdisciplinary Reviews: Climate Change, 1(1), 31–53.

Moyer-Gusé, E., and Dale, K. (2017). Narrative persuasion theories. In P. Rössler,P., C. A. Hoffner, and L. van Zoonen (Eds.), The International Encyclopaedia of Media Effects (pp. 1345–1354).

Hoboken, NJ: John Wiley & Sons. Mustomi, D., & Reptiningsih, E. (2020). Gaya Kepemimpinan dalam Perspektif Generasi Millenial. Jurnal Ilmiah MEA (Manajemen, Ekonomi, &Akuntansi), 4(1), 189-199. https://doi.org/10.31955/mea.vol4.iss1.pp189-199

Müller, L., Mattke, J., & Maier, C. (2018). Exploring the effect of influencer marketing on purchase intention. In Proceedings of the 24th Americas Conference on Information Systems (pp. 1–10). New Orleans: Association for Information Systems (AIS).

Naderi, I., & Steenburg, E.V. (2018). Me First, Then the Environment: Young Millennials as Green Consumers. Young Consumers, 19 (3), 280-295.

Nafees, L., Cook, C. M., Nikolov, A. N., & Stoddard, J. E. (2021). Can social media influencer (SMI) power influence consumer brand attitudes? The mediating role of perceived SMI credibility, Digital Business, 1(2), 100008.

Okuah, O., Scholtz, B. M., & Snow, B. (2019). A grounded theory analysis of the techniques used by social media influencers and their potential for influencing the public regarding environmental awareness. In Proceedings of the South African Institute of Computer Scientists and Information Technologists, 1–10.

Patton MQ. (2002). Qualitative research and evaluation methods. 3rd Sage Publications; Thousand Oaks, CA.

Patel, N. (2017). The science of social timing. Kissmetrics

Puteri, R. (2018). The influencer and hedonist lifestyle of digital society. The Journal of Islamic Studies and International Relations, 3(1), 1-14. Available at: http://jisiera.insiera.org/index.php/jisiera/article/view/35 (Accessed: 27 January 2020).

Raihan Hadi. (2021, Oct 15). Nuffnang teams up with APE Malaysia to create social impact. Marketing Magazine. https://marketingmagazine.com.my/nuffnang-teams-up-with-ape-malaysia-to-create-social-impact/

Razak, N.F., & Sabri, M.F. (2019). Pro-Environmental Workplace Intention Behaviour in the Malaysian Public Organization. Asian Social Science, 15(4), 60-68.

Rose, P., Hunt, K.A., & Riley, L.M. (2018). Animals in an online world: an evaluation of how zoological collections use social media. Journal of Zoo & Aquarium Research, 6(2), 57-62.

Saghati Jalali, Sanaz & Khalid, Haliyana. (2021). The Influence of Instagram Influencers' Activity on Green Consumption Behavior. Business Management and Strategy. 12. 78. 0.5296/bms.v12i1.18265.

Scott, D. M. (2015). The new rules of marketing and PR: How to use social media, online video, mobile applications, blogs, news releases, and viral marketing to reach buyers directly. John Wiley & Sons.

Shafiei, A., & Maleksaeidi, H. (2020). Pro-environmental behavior of university students: Application of protection motivation theory. Global Ecology and Conservation, 22(2020), 1-10.

Skoric, M. M., & Zhang, N. (2019). Opinion Leadership, Media Use, and Environmental Engagement in China. International Journal of Communication, 13(2019), 4602–4623.

Stake, R. E. (2006). Multiple case study analysis. New York: The Guilford Press.

Tarhini, A., Alalwan, A.A., Shammout, A.B. and Al-Badi, A. (2019), "An analysis of the factors affecting mobile commerce adoption in developing countries", Review of International Business and Strategy, Vol. 29 No. 3, pp. 157-179

Thompson, T. L., Parrott, R., & Nussbaum, J. F. (2011). The Routledge handbook of health communication. Routledge.

Twenge, J. M., Campbell, S. M., Hoffman, B. J., & Lance, C. E. (2010). Generational differences in work values: Leisure and extrinsic values increasing, social and intrinsic values decreasing, Journal of management, 36(5), 1117-1142.

Weber, J. (2017). Discovering the Millennials' Personal Values Orientation: A Comparison to Two Managerial Populations. Journal of Business Ethics, 143, 517–529. https://doi.org/10.1007/s10551- 015-2803-1

Wu, Y. Y., Jiang, Y. F. (2021). Shenmei shijiao xia Li Ziqi wei jilupian de tupo (The breakthrough of Li Ziqi's micro documentary from the aesthetic perspective). Movie Literature, 3, 55–57. https://www.cnki.com.cn/Article/CJFDTotal-DYLX202103012.htm

Yeo, C.M. A, Carter, S., & Khor, Z. S. (2019). Leadership, Contribution, Language and Shared Content as Metrics in Malaysian Millennials' Decision Making. Journal of Business and Finance in Emerging Markets, 2(2), 153-162.

Zamari, Z. M., Alang, N., Idris, S. L., & Lionel, K. V. (2022). Influencers Er Som Influensa: A Case Study of Malaysian Social Media Influencer Content Development. Journal of Contemporary Social Science and Education Studies (JOCSSES), 2(1), 124-136.

BorneoScience
The Journal of Science & Technology
Volume 43 Issue 2 : Oct 2022
Online ISSN : 2231-9085 | ISSN : 1394-4339

THE 2011 ZEN GARDEN LANDSLIDES: TRIGGER AND CAUSAL FACTORS

Ismail Abd Rahim[1], Hardianshah Saleh[2], Baba Musta[2], Immas Janggok[2] & Amy Natasha Arjali[2]

[1]Natural Disasters Research Unit, School of Sciences & Technology, Universiti Malaysia Sabah, Jalan UMS 88400 Kota Kinabalu, Sabah, Malaysia
[2]Geology Program, Faculty of Sciences & Natural Resources, Universiti Malaysia Sabah, Jalan UMS 88400 Kota Kinabalu, Sabah, Malaysia

Corresponding Author: Ismail Abd Rahim[1]. E-mail: arismail@ums.edu.my

Received 17th Jan 2022; accepted 23th Sept 2022
Available online 31st Oct 2022
Doi: https://doi.org/10.51200/bsj.v43i2.4509

ABSTRACT: *The Zen Garden Resort and its surrounding area are part of the "Kundasang Landslide Complex" and were experiencing reactivation of old landslides on 10 April 2011. Consequently, more than 80 room units of the resort, ten buildings, homes, and local roads were destroyed, uplifted, and damaged as well as disrupted day traffic. About 500m in length and 200m in width of the slope area were slides for 25m. The vertical fall movement in the head section of the landslide is 25m. There is no direct relationship between the 2015 Ranau earthquake and with earlier rotational clay slide of the 2011 Zen Garden Resort landslide. The causing and triggering factor for landslides are generally varied and are always characterized as region-specific and site-specific. Thus, this study was conducted to unravel the triggering and causal factors for the rotational clay slide of the 2011 Zen Garden Resort landslide. The methodology consists of desk study, remote sensing study, geological mapping, geodynamic mapping, laboratory, and data analysis. This study found that the landslides were triggered by prolonged moderate to occasional heavy rainfall. The causal factors are divided into natural factors (tectonic uplift, weak materials, weathered materials, sheared or jointed materials, adversely oriented mass discontinuity or structural discontinuity, and contrast in permeability) while the artificial factor consists of excavation of the slope or its toe, cut and fill, subterranean erosion/ piping, irrigation or water leakage from utilities and deforestation or vegetation removal.*

KEYWORDS: Zen Garden Resort, landslides, Kundasang landslide complex, colluvium, geodynamic, trigger and causal factors

INTRODUCTION

A landslide is a downslope movement of the rock, soil, or debris under the influence of gravity. It becomes a major problem in the mountainous region, as well as plain areas. It causes damage to properties and loss of lives. The causing and triggering factors for a landslide are varied by the location, climate, and local geological setting and a landslide is a region-specific and site-specific character.

Many publications have published the landslide-causing factors such as Highland and Bobrowsky's (2008), Cruden & Lan (2015), Taiwan Geoscience portal (2021), Danish et al. (1994), and Jesus et al. (2017), but Novotný (2012) for triggering factor. The causing factors are divided into natural, physical-artificial, and geomorphological factors.

The natural factor includes the earthquake, tectonic or volcanic uplift, geological rebound, geological meltwater outburst, fluvial erosion of slope toe, wave erosion of slope toe, glacial erosion of slope toe, erosion of lateral margin geology, and climate. The physical-artificial factor consists of flawed design, improper construction, and non-maintenance of slopes, subterranean erosion, deposition loading slope or its crest, subterranean erosion, deposition loading slope or its crest, and groundwater, or water table, thawing, freeze and thaw weathering, shrink and swell weathering, and flooding and oscillation vegetation removal). The geomorphological factor is divided into geology, geological rebound, fluvial erosion of slope toe, wave erosion of slope toe, glacial erosion of slope toe, and erosion of lateral margin.

The triggering factor has been divided into internal (earthquake), external weathering (rainfall, rapid snowmelt, prolonged intense rainfall, rapid downthrown), and human (over-steep slope cutting) factors. Based on the above statement the definition of causing and triggering factors are inconsistent and vital to improvement. On 8-10 April 2011, the huge rotational clay slide (Hungr, et al., 2014) hit the Zen Garden Resort, Kg. Dumpiring and Kg. Kundasang Lama areas in southern Kundasang. These areas are located outside the eight (8) system of 'Kundasang Landslides Complex' (Figure 1) and informally label as system number nine (9) by some local researchers.

After more than two (2) decades of the rotational clay slide of the Zen Garden landslide, the causal and triggering factors have never been documented properly. Thus, this study was conducted to unravel the causal and trigger factors for this landslide.

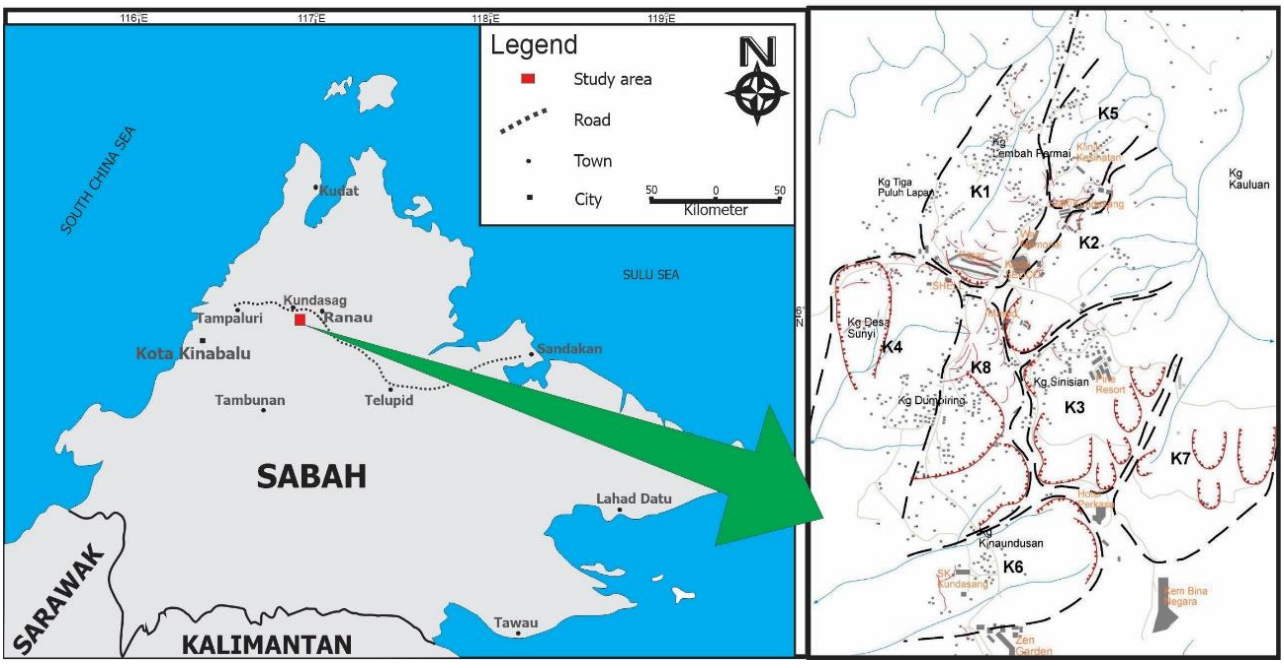

Figure 1 Kundasang landslide complex (Ibrahim Komoo & Lim Sian Choun, 2003).

GEOLOGICAL SETTING

Sabah is currently under a WNW-ESE (west northwest-east southeast) compressive stress which was generated from westward-moving of Philippine-Pacific plate against the southeast moving Eurasian plate. The WNW-ESE compression is being accommodated by northeast-southwest (NE-SW) active thrust faults, active strike-slip faults, and active normal faults of the extensional stress regime all over Sabah. Co-existence has both stress regimes along subduction-accretionary fold-thrust belts may has been attributed to gravitational forces generated by high topography (Sapin *et al*., 2013). The ongoing compressive tectonics, along the northwest (NW) Borneo Trough maybe linked to gravitational forces, collision and gravity sliding (Tongkul, 2017).

The shortening, associated with thrust faults, may have resulted in the thickening of the upper crust as the Dangerous Grounds continental crust is being overthrust by the Sabah ophiolitic oceanic crust. Sabah has been massively uplifted since the Early Miocene, with the Kinabalu pluton emplaced during the early Late Miocene and being exhumed at a rate of 7 mm per year during Late Miocene–Early Pliocene (~ 8–3 Ma ago) as the region continues to rise at a long-term rate of about 0.5 mm each year.

The Kundasang area is underlain by the Paleogene, Neogene, and Quaternary rock units such as Trusmadi formation, Crocker formation, Gravel Pinosuk, and alluvium deposit (including colluvium deposit) (Figure 2). The Trusmadi formation is a deep-sea deposit that metamorphosed to meta-sedimentary rocks. It consists of interbedded sandstone, phyllite, and slate. Some sandstone was metamorphosed into meta-sandstone. The ages of this formation are Paleocene to Late Eocene and overlain the Crocker formation with angular unconformity (Figure 2). This angular unconformity represents a fault line (Jacobson, 1970; Collenette, 1958).

The Kundasang area is underlain by the Paleogene, Neogene, and Quaternary rock units such as Trusmadi formation, Crocker formation, Gravel Pinosuk, and alluvium deposit (including colluvium deposit) (Figure 2). The Trusmadi formation is a deep-sea deposit that metamorphosed to meta-sedimentary rocks. It consists of interbedded sandstone, phyllite and slate. Some sandstone was metamorphosed into meta-sandstone. The ages of this formation are Paleocene to Late Eocene and overlain the Crocker formation with angular unconformity (Figure 2). This angular unconformity represents a fault line (Jacobson, 1970; Collenette, 1958).

The Crocker formation is Late Eocene to late Early Miocene ages and represents flysch deposit. This formation consists of sandstone, siltstone and shale inter-bed and can be divided into three (3) units, i.e., thick sandstone unit, interbedded sandstone-shale unit and shale unit. Nondeposition activities from Middle Miocene to Pliocene was showed hiatus zone in the study area (Kundasang) unless the igneous intrusion during Late Miocene to Early Pliocene (Figure 2).

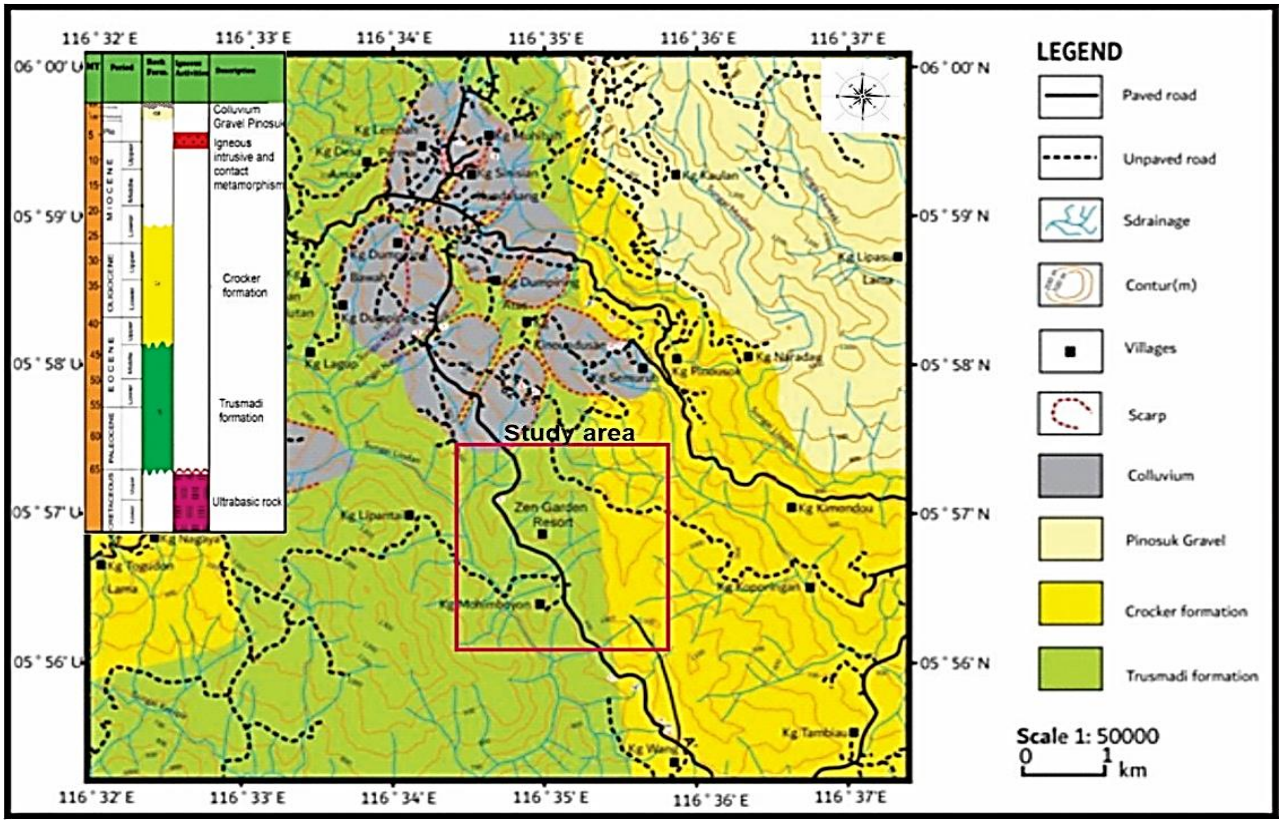

Figure 2 Geological map of the Kundasang area (left) and stratigraphic column (right) (modified from Jacobson, 1970; Immas Jangok, 2021; Amy Natasha Arjali, 2021).

The Pinosuk Gravel of till deposit was deposited during the Pleistocene surrounding Kundasang and Ranau areas. The gravel consists of Mount Kinabalu adamellite, diorite, granodiorite and granite, peridotite, Crocker and Trusmadi sandstone and lesser of basement rock unit which deposited together with/ in a clay matrix.

The alluvium deposit is Quaternary ages and underlain the low land area, along the valley and rivers. It consists of sand, silt, clay, and organic matter. The younger or recent colluvium deposit with Holocene ages locally overlain the alluvium deposit and rock formation of fail slope. This colluvium deposit is considered as in-situ alluvium deposit of the Quaternary ages.

LANDSLIDE MECHANISM

Typical landslide morphology is shown in Figure 3 which is divided into head, body, foot, and toe sections. This landslide is the reactivation of an old dorman landslide (Figure 3) and classified as a rotational clay slide (Hunger et al., 2014). The movement was involving a rotational slide. The materials are colluvium deposits which come from the old landslide and are dominated by matrix material. Then, the slope materials are classified as clay.

Figure 4 shows the chronology of the formation of a rotational clay slide of the 2011 Zen Garden Resort landslide:

A. Natural slope and water table in the Zen Garden Resort area. The slope has been undergoing natural slope equilibrium proses.

B. The morphology of the old Zen Garden landslide but the upper boundary is not found in field investigation and remote sensing study. Interview with surrounding local was made to collect the data. The transverse crack, major and minor scarp, tension crack, 1m down-thrown surface level, undulating resort road, and colluvium deposit of the old landslide are shown in the Photos in Figure 4.

C. Weathering and erosional processes on the slope surface produce smoother slopes but raise the water table. Surface levelling and fertility of secondary plant shows the natural erosional activity, infiltration, and existence of colluvium deposits from an old landslide.

D. After 20 years, the slope becomes smoother due to the natural phenomenon of slope equilibrium. The slide comes once again but moves its position towards the southern part of the study area. The rotational clay slide of the 2011 Zen Garden Resort landslide took place on the transverse crack of the body section of the old dorman landslide. This landslide is caused by about 200 m width, 450 m length, more than 20 m vertical fall, and tens of meter area thrown down the slope as well as the destruction of more than 80 room units, damages of few buildings, roads, homes and a day traffic disruption. The main scarp, tension crack, transverse crack and foot section are clearly shown in the attached Photos in Figure 4.

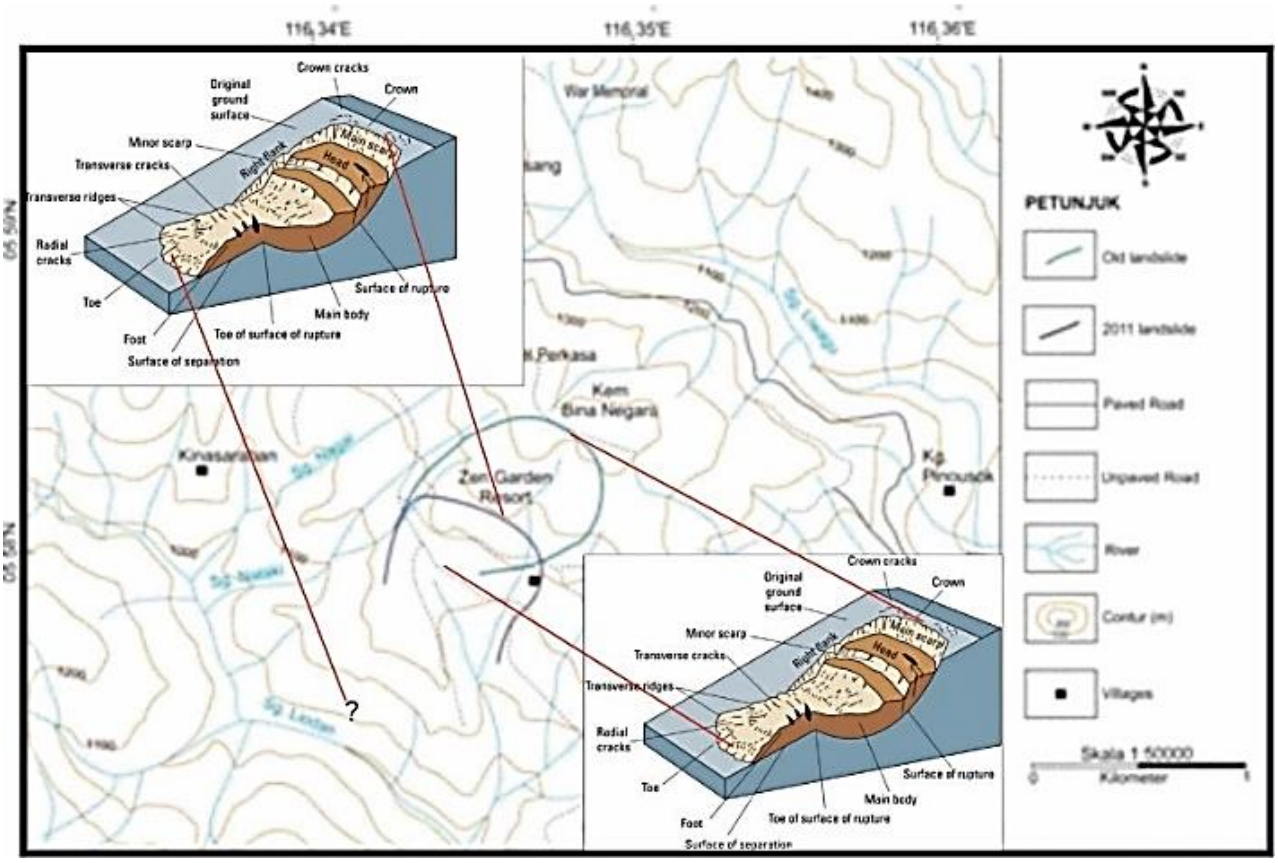

Figure 3 Location and the reactivation on the body (transverse crack) of old landslides. Upper left- old landslide morphology; Lower right- rotational clay slide of the Zen Garden 2011.

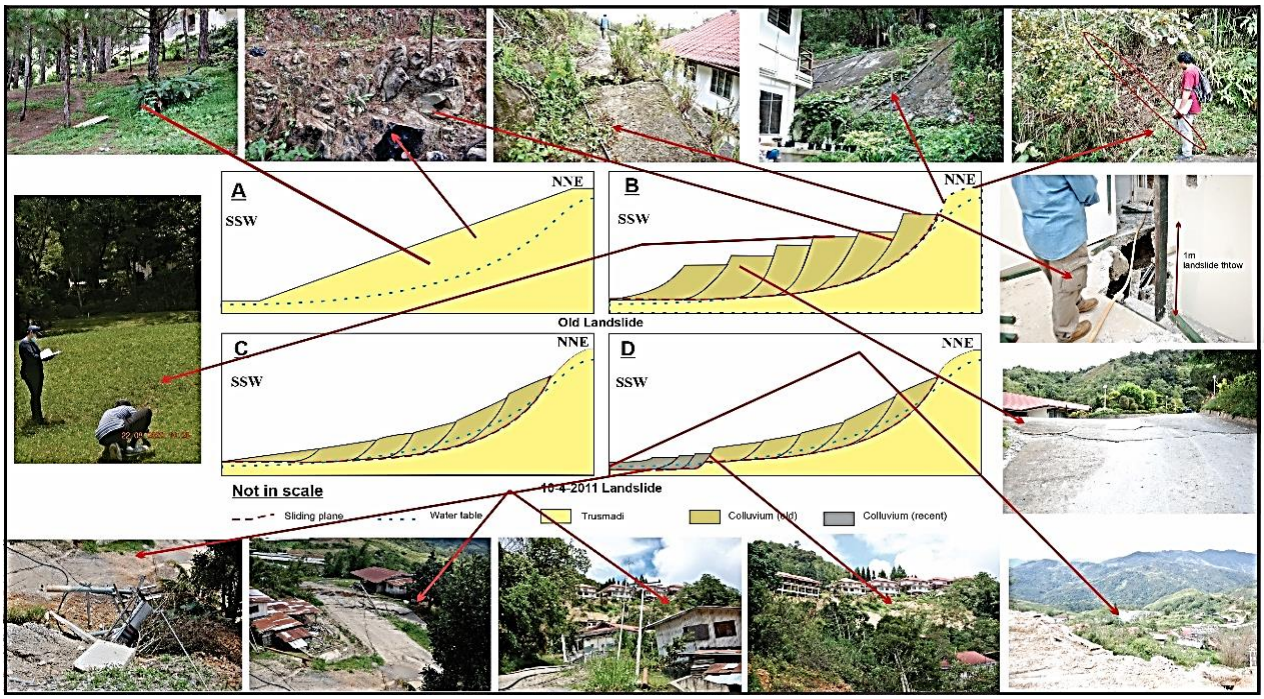

Figure 4 The rotational clay slide of the 2011 Zen Garden Resort Landslide model and the reactivation on the body (transverse crack) of old landslides with attached photos for the selected landslide section. A- Natural slope surface; B- Old landslide mechanism; C- towards natural slope equilibrium; D- rotational clay slide of the 2011 Zen Garden landslide.

TRIGGERING AND CAUSAL FACTORS

The landslides triggering and causing factors for the rotational clay slide of the 2011 Zen Garden landslide were summarized in Table 1. This factor was design base on geological observation and mapping as well as sampling, laboratory, and data analysis studies.

Triggering factors

Triggering factors refer to an event or episode that potentially increases slope instability and is only represented by the prolonged moderate to occasionally heavy rainfall.

Table 1 Summary of the triggering and causal factors for rotational clay slide 2011 of Zen Garden landslide.

Trigger	Causes	
	Natural	**Artificial**
prolonged moderate to occasionally heavy rain	tectonic uplift	excavation of the slope or its toe
	weak material	cut and fill activity
	weathered material	subterranean erosion
	sheared and jointed material	irrigation or water leakage from utilities
	adversely orientated mass discontinuity or structural discontinuity	vegetation removal or deforestation
	contrast in permeability.	
	Water table	

Prolonged moderate to occasionally heavy rainfall

The annual rainfall for the Kundasang area is 2440 mm on average and experienced prolonged light rain type (5-20 mm/days) or moderate with occasional heavy rainfall from January to June 2011. The landslides on 10 April 2011 occured in only 37mm of rainfall but occasional intense rainfall (until 110 mm/day) happened before (Figure 5). That prolonged moderate to occasional heavy rainfall will raise groundwater level rapidly condition to the ground surface and this would result in a sudden increase in pore pressure which would reduce the shearing resistance of geomaterial and finally lead to a failure or landslide.

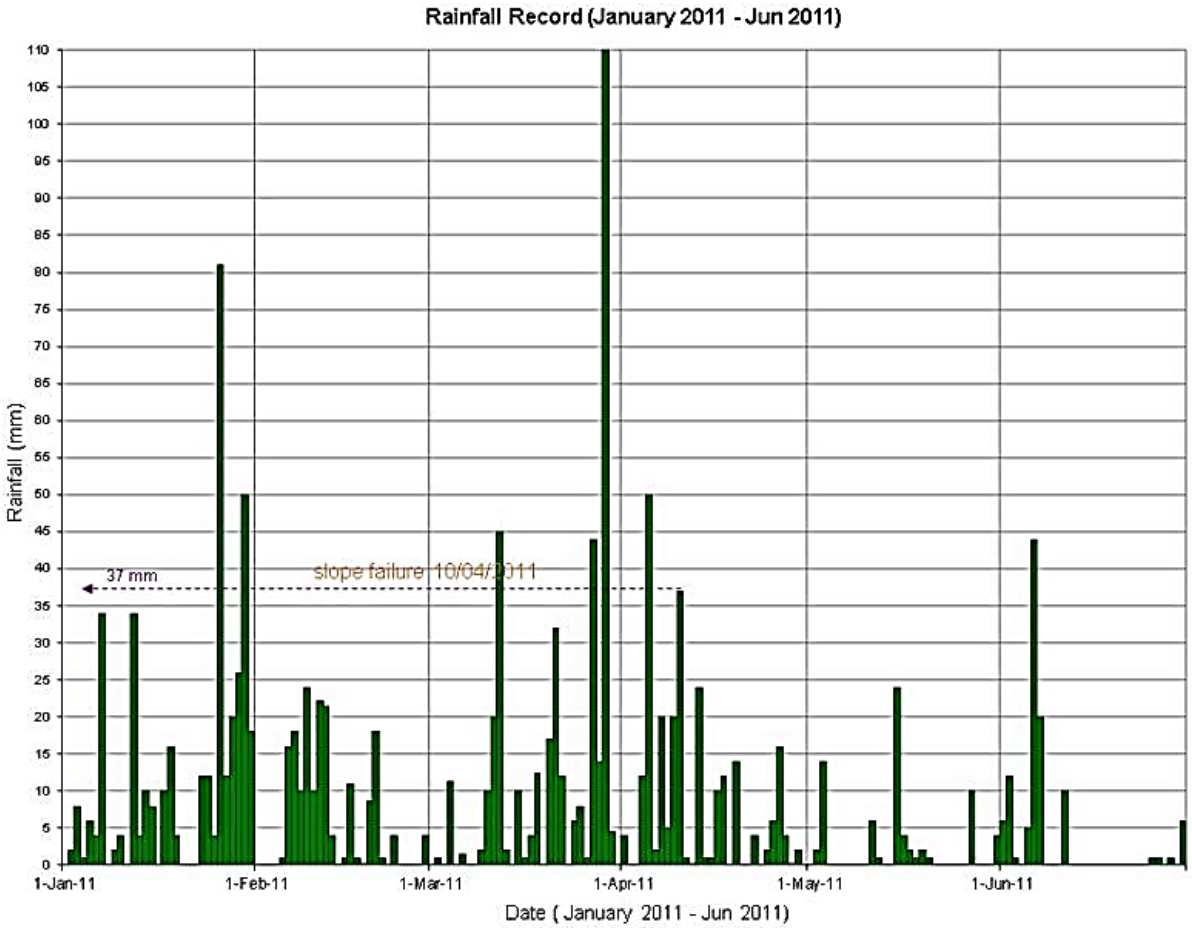

Figure 5 Daily rainfall record from January to June 2011 in the Kundasang area (source from IKRAM, 2011).

Causal factors

The causal factor is "a condition or actions that influence individual assessment of the situation" or refers to an issue, feature, or property that tends to reduce slope stability. The causal factors can be divided into natural and artificial. The natural causal factor consists of tectonic uplift, weak material, weathered material, sheared and jointed material, adversely orientated mass discontinuity or structural discontinuity, contrast in permeability and water level. The artificial causes are related to excavation of the slope or its toe, cut and fill activity, subterranean erosion, irrigation or water leakage from utilities, and vegetation removal or deforestation (Table 1).

Tectonic uplift

The Lobou-lobou fault zone is part of a regional extensional zone trending NW-SE along the west coast of Sabah. The NW-SE trending normal fault appears to be not directly related to the NW-SE compression but is due to gravitational sliding on an uplifted mountain belt. The uplift belt is a tectonic plate collision zone in Sabah, informally referred to as the Sabah Suture Zone (Figure 6). Continued compression in Sabah created differences of roughly around 4000 m in elevation of the upper crust - the Crocker Range is around 2000 m above sea level and the NW Borneo trough around 2000 m below sea level. As mentioned earlier, GPS readings in West Sabah indicate gravity sliding or collapsing the NW in response to significant thickening of the upper crust due to collision (Tongkul, 2015).

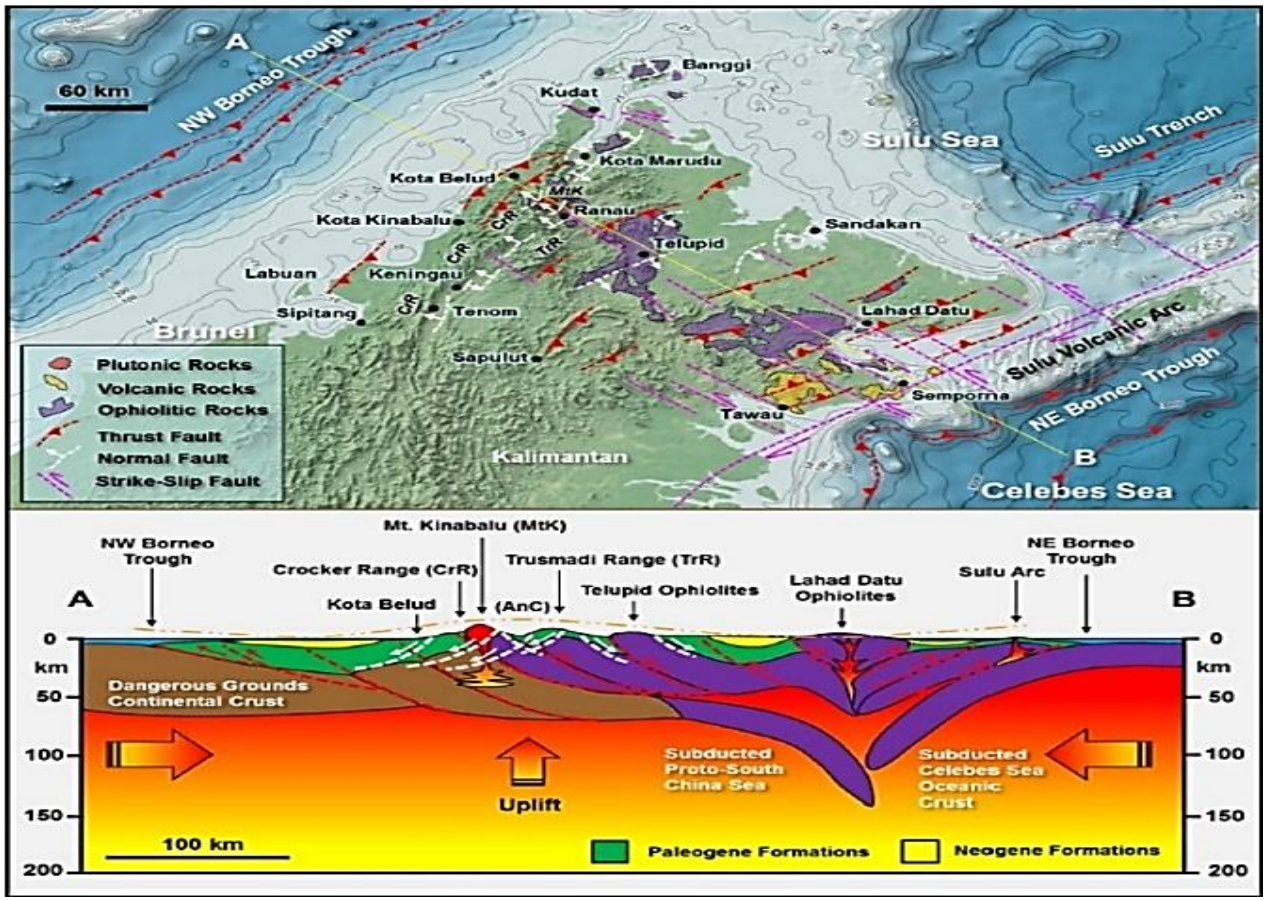

Figure 6 Tectonic cross-section of Sabah showing post-collision collapse due to gravity sliding producing deep-seated normal fault (white line) in response to significant thickening and uplift of the Crocker Range upper crust. A- northwest; B-southeast (adapted from Tongkul, 2015).

The uplift belt or tectonic plate collision zone is continuing to compress and produce high-land areas around Crocker Range including the study area in Kundasang. This high elevation has been reducing the stability of the slopes. The higher the area, the steeper the slope and the less stable the slope. The natural tectonic uplift by collision has caused the slope to decrease in resisting force and become landslide prone.

Weak material

There are four (4) rocks unit underlying the study area namely Trusmadi formation, Crocker formation, Pinosuk Gravel, and Colluvium deposit (alluvium) (Photo 1). Laboratory analysis found

that the Colluvium deposit is weak (19.52 MPa) by Lithological Unit Thickness, LUT method (Ismail Abd Rahim et al., 2009). The characteristics of Pinosuk Gravel which is almost like Colluvium (i.e., unconsolidated deposit and consists of rock block and matrix materials) assumed as a 'weak' rock unit also. The Uniaxial Compressive Test (UCT) was conducted on Trusmadi and Crocker formations rocks and found the strength to be medium (Table 2). Then, it concludes that the strength of rock units varies from 'medium to weak' and is prone to landslides or less resisting force.

Weathered material

Generally, the Kundasang area is experiencing a humid tropical zone of climate with high about 2500 mm of annual rainfall, often seasonal with high temperatures for a longer period. The weathering process is much more progressive due to the abundance of rainfall and moisture, thus accelerating the transformation of homogeneous subsurface material into heterogeneous subsurface materials. The present subsurface materials have suffered from an additional weathering process thus producing another poor rock mass quality. The weathered (class IV) Crocker formation and Trusmadi formation are shown in Figures 7A & 7B, respectively. These weathered rock units are normally characterized as 'weak' rocks which have less resisting force and lead to landslides.

Photo 1 Moderately strong to weak rock units' appearance. A& B- Sheared meta-arenite and meta-argillite (dark) of Trusmadi formation; C- Crocker formation sandstone; D- Pinosuk Gravel; E&F- colluvium deposits.

Table 2 Strength of rocks unit.

Rock unit	***Strength (MPa)***	***Classification***	
			Overall
Crocker formation	*30-40**	*Medium*	*Medium to weak*
Trusmadi formation	*53.6#*	*Medium*	
Pinosuk Gravel	-	*Weak (?)*	
Colluvium (Trusmadi formation)	*19.51#*	*Weak*	

Note: # - Immas Jangok (2021); Amy Natasha Arjali (2021)
* - Ismail Abd Rahim (2011)

In the weathering process especially for class IV, the old discontinuity plane normally disappears. So, the discontinuity observation during the survey depends on relic structures on the limited outcrop. The effect of the weathering activity on discontinuities is the formation of planar failure in the Markland test (Figure 7C). Highly weathered Trusmadi formations (underlain Zen Garden Resort) are locally potential to produce a high concentration of kaolinite and illite. This clay easily absorbs water and expands. Then, facilitate mass movement by reducing the resisting force in slope-forming rock materials, especially during heavy or prolonged rainfall (Baba Musta, 2021).

Figure 7 The weathered (class IV) rock unit. A- Crocker formation; B- Trusmadi formation; C- planar failure.

Sheared and jointed material

Field observation shows that the rock unit was highly jointed and sheared (Photo 2). The discontinuities are varied from four (4) to six (6) sets. Some as individually and some are intersected with other sets to 'daylight' on slope face to form planar, toppling, and/ or wedge types of mode of rock slope failures. These show that the occurrence of joint and shear planes has naturally caused landslides by decreasing resisting force for slope-forming rock materials.

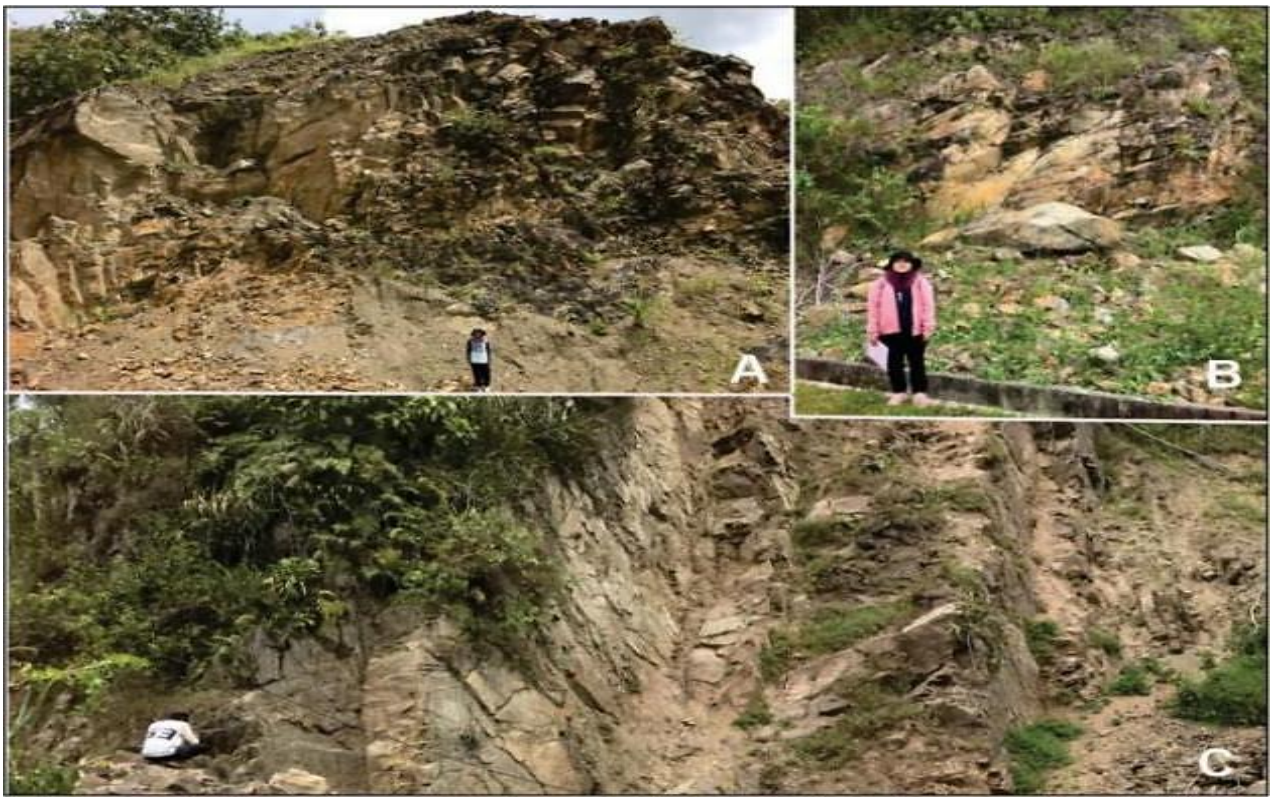

Photo 2 Fractured and sheared meta-sandstone of Trusmadi formation forming the wedge failures, toppling failure, and rock fall (A-C).

Adversely orientated mass discontinuity or structural discontinuity

Adversely oriented discontinuities (bedding) or structural (fault) discontinuity with slope face have been observed in the study area. The first example is shown in Figure 8. This Trusmadi formation was cut by six (6) discontinuity sets including joint, bedding, and fault planes. The intersection of joint 1 (J1) and bedding (B) planes was 'daylight' on slope face or contributed to 'unfavourable' discontinuity orientation. This was causing the formation of potential wedge failure. This indicates that adversely oriented discontinuities are a naturally causal factor for landslides.

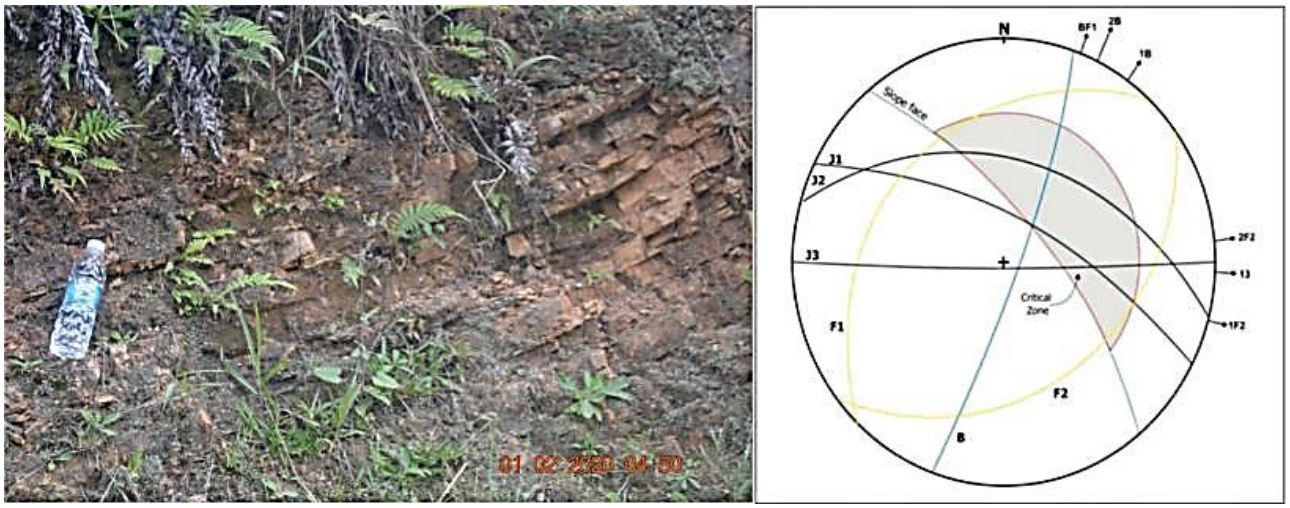

Figure 8 Trusmadi formation's outcrop and wedge failure from Markland test representing adverse discontinuity orientation with slope face.

In general, the Kundasang area is situated at the intersection of major fault zones of the Quaternary ages as highlighted in Tjia (2007) (Figure 9). The study area is situated inside the northern part of Crocker Faults Zone, CFZ which is known as an oblique normal fault of Lobou-Lobou Fault Zone (LFZ). The slope face is facing the lower altitude of sg. Kayongang valley in LFZ and the movement of this fault has broken and fractured the bedrock along the fault line and slope toe (JMGM, 2012). This condition has been reducing toe support and shear strength (resisting force) but raising the driving force (plus the weight or gravity) of the slope forming rock material, especially during rainy days. Then, the adverse orientation of structural discontinuity has been causing a landslide-prone condition in the study area.

Contrast in permeability

Field capacity condition, temporary preached water table, and artesian condition are caused by permeability contrast of colluvium and bedrock unit which accommodate landslide to occur. Field capacities achieve when water drains from the soil (Colluvium) at the same rate as it is added (recharge) by at least 267 mm of rainfall (Campbell, 1975).

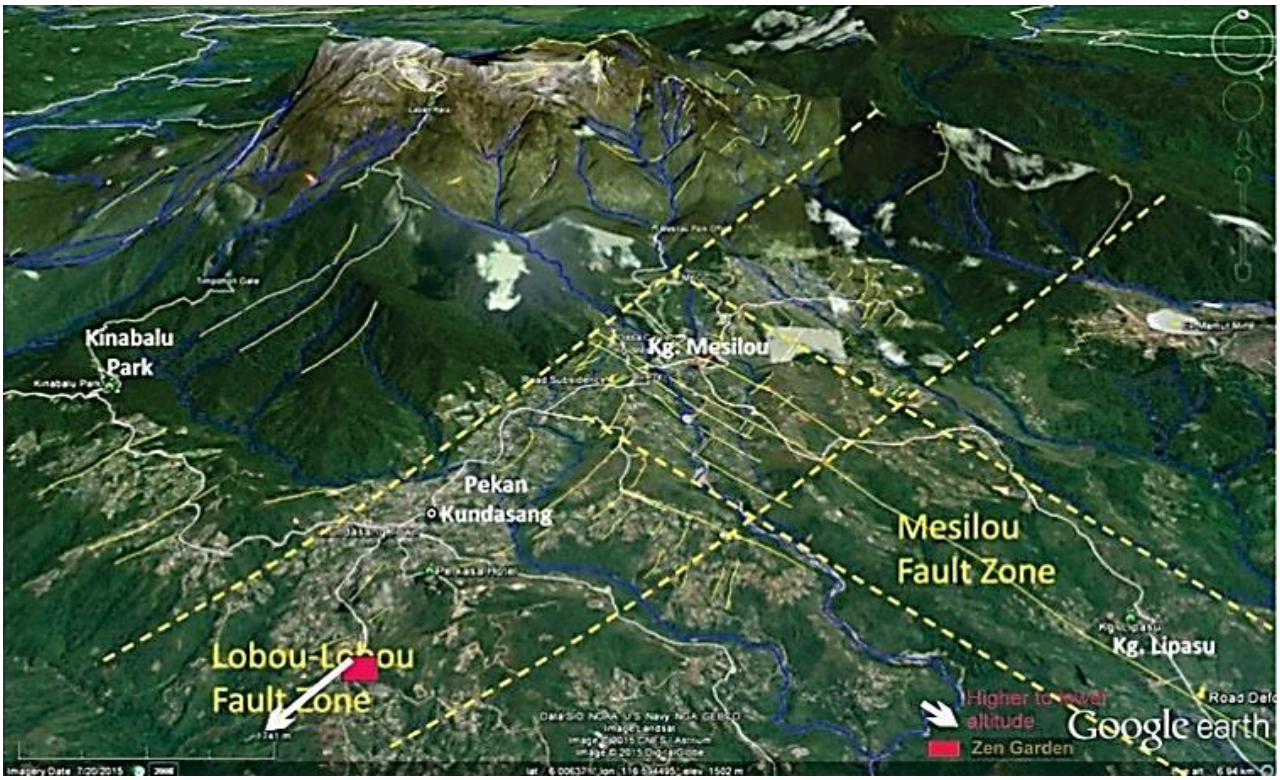

Figure 9 Normal fault scarp (in yellow) trending NE-SW across the Kundasang- Mesilou areas. These faults are grouped under the Lobou-Lobou Fault Zone. White arrows show driving force direction). Adapted from Ismail Abd Rahim et al. (2015).

In the 2011 Zen Garden Resort landslides, the rainfall is only 37 mm, and it was unable to bring the soil (Colluvium) into field capacity condition. But, according to Figure 5, there was 100 mm of rainfall thirteen days before the event and prolonged moderate to occasional heavy rainfall for four (4) months. Then, the field capacity may be achieved during that event. The slope material (Colluvium) was saturated and resisting force was decreased then landslides occur.

The thickness of Colluvium in the studied slope varies from 10-20m (Figure 10). The rainfall intensity during that event is only 1.54 mm/hrs. which is far from the suggested values (rainfall intensity of 3 to 4 mm/hr.) for the formation of a perched water table. But the daily rainfall ranges from 0.5 to 4.85 mm/hrs. for several days before the event may cause the water to percolate into colluvium and exceed the rate of seeping into bedrock. This condition forms a temporary perched water table in the Colluvium, and a downslope seepage force develops within the Colluvium. Excess pore pressures develop, the Colluvium becomes buoyant, the resisting forces are decreased, and landslides will occur (Turner, 1996; Kesseli, 1943).

Permeability contrasts within the bedrock may result in artesian conditions (Turner & Schuster,1996). The water contains Colluvium (dark brown) and bedrock units (dark green), and artesian (dark brown greenish color) conditions are shown in Figure 10.

This artesian condition was causing the water flow to concentrate within the Colluvium by the differences in permeability within both the Colluvium and the bedrock (Ellen, 1988) and facilitated landslides to occur.

Water table

The underground water table in the study area is high due to the natural surface erosion for the slope equilibrium process after the old landslide phenomena (refer to Figures 4B & 4C). The barren surface increased and the Colluvium deposits formed along the sliding surface. Rainwater was infiltrated freely by the barren area to increase water recharge, while soft Colluvium deposit is actively eroded and lowered at the surface level. These in turn will generally raise the water table in the slope areas.

The seismic profile in Figure 10 also shows the thin Colluvium deposit and high-water table of less than 20m depth. This high-water table will allow fast saturation conditions and reactivation or/ and creation of sliding plane, sliding process or landslide.

Artificial Causing Factors

The artificial causes are related to excavation of the slope or its toe, cut and fill activity, subterranean erosion, irrigation or water leakage from utilities, and vegetation removal or deforestation.

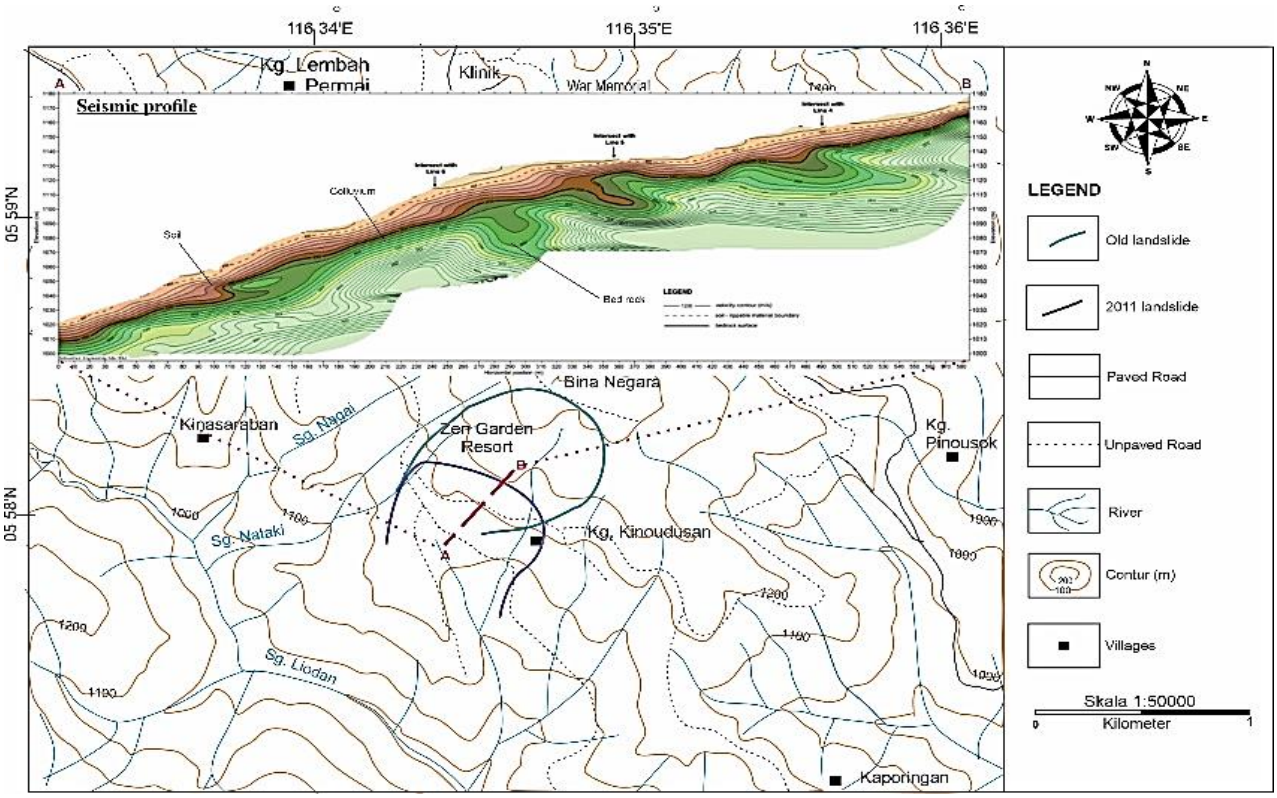

Figure 10 Seismic profile showing bed rock (Trusmadi formation), colluvium and soil. The 10-20m thick colluvium deposit can reach field capacity condition and perched water table. The dark brown and green show the contrast in permeability between colluvium deposit and

Excavation of the slope or its toe

The purpose of excavating the slope and slope toe is to stabilize and protect slopes as well as provide accessibility. The slope face is normally excavated for optimum slope angle, to reduce erosion, infiltration, and weathering rates, and to control surface water (Photo 3). But improper excavation will result in causing slope failures. Such as inaccurate optimum slope angle, improper berm drains, infiltration, and surface water controls.

Slope toe excavation was conducted to provide facilities for the resort itself or local residence surroundings (Photo 4). But improper excavation on slope toe has caused slope failure due to loss of or reduction of resisting force for slope forming materials.

Photo 3 Slope excavations. Construction of optimum slope angle, terrace, berm drain and shotcrete to increase resisting forces.

Cut and fill

There are about two square kilometers have been cut and filled to design and build the facilities in Zen Garden Resort (Figure 11). The cut and fill materials on the original ridge topography area may also contribute to weakening the ground foundation in a long-term condition since water flow, soil, and rock condition were already disturbed and altered. These activities altered the slope faces and drainage patterns in that area. The slope cutting has risen the rate of weathering, erosion, and infiltration. These in turn were reducing the resisting force of the slope.

Filling the slope or an area such as a lower area, major, minor valleys or a reservoir into a flat area has been altering the natural environment, drainage pattern, or types (Photo 5A). These alterations were normally causing blockage and inappropriate recharge and discharge of water into the drainage system or reservoir (Photo 5B). These cut and fill activities have changed water balance or equilibrium then increasing the driving force on the slope face.

Photo 4 Construction of minor roads at slope toe for the accessibility of the surrounding residents.

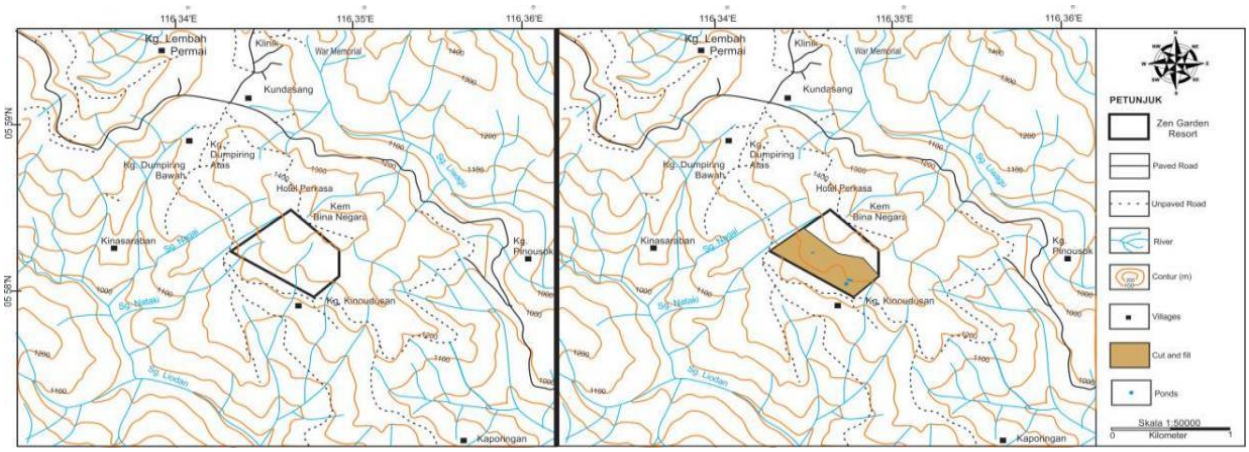

Figure 11 Zen Garden Resort landslide area and cut and fill section. Some rivers were filled and altered for this development.

Photo 5 A- Evidence of old drainage channel and landslide which has been cut (for foundation and building) and filled (red circle) and alteration of natural drainage by the construction of concrete drainage (yellow square). B- filling activity and changing natural drainage channel into the culvert.

Subterranean erosion

Subterranean drainage is a subsurface drainage system which is not seen from the surface. Normally subterranean drainage is made of PVC (Photo 6B) in various sizes or constructed of concrete (Photograph 6C). There is no landslide issue if this subterranean drainage is working. The problem is if the channel break or leakage (Photo 6A) then, subterranean erosion will occur. This leakage will erode the slope forming rock materials and finally reduce the resisting force.

Irrigation or water leakage from utilities

Kundasang is a highland area and doesn't have a proper water supply station except for collected from the natural spring water by Sabah Drainage and Irrigation Department, JPS. The activities or operation in Zen Garden Resort was conducted by using the water supply from JPS and collecting rainwater from Resort's personal tank. The photograph below shows the Resort water tank (in black color, Photo 7A) and irrigation system (Photo 7B)

The landslides become an issue if there is leakage in the tank and irrigation networks. This leakage will behave like rainwater that decreases the resisting force of rock-forming slope materials. The same condition will happen if a concrete ditch leaks by the occurrence of faults (Photo 7C).

Photo 6 Subterranean erosion. A- water leakage (red circle) due to broken channel or connection failure: B- subterranean drain (PVC) that is connected to the river; C- a small pond that is connected by the subsurface concrete drain. This pond is believed to be a small old river channel that fills and alters into a subterranean concrete ditch.

Photo 7 Water leakage from utilities. A- water tank to reserve water supply; B- part of irrigation or drainage system around this Resort; C- concrete ditch filled with water shows a fault (?) form fracture.

Deforestation/ Vegetation removal.

Deforestation or vegetation removal is a common practice by the local people for their own good. The Zen Garden Resort area was occupied by them for so long and just depended on agriculture. After some time, the area was developed for the Resort. Land clearance or vegetation removal was conducted but agricultural activity continued by the locals outside the Resort area.

Agricultural activity is still can be seen today (Photo 8). The land clearance has been causing the rate of erosion, weathering, and infiltration (runoff) to increase but reducing resisting force for slope forming rock material and contributing to landslides occurrence.

Photo 8 Vegetation removal or deforestation and planting activity by the locals.

CONCLUSIONS

The triggering and causal factors for the rotational clay slide of the 2011 Zen Garden Resort landslides are as follows:

i. Triggering factors are prolonged moderate to occasionally heavy rain.
ii. The causal factors are divided into natural and artificial sub-factors.
   - Natural sub-factors are tectonic uplift, weak materials, weathered materials, sheared or jointed materials, adversely oriented mass discontinuity or structural discontinuity, a contrast in permeability, and water table.
   - Artificial sub-factors are excavation of the slope or its toe, cut and fill, subterranean erosion/ piping, irrigation or water leakage from utilities, and deforestation or vegetation removal.

ACKNOWLEDGEMENT

This research was fully funded by grant No. SGA0076 & thanks to laboratory facilities of Geology Program, FSSA, UMS.

REFERENCES

Amy Natasha Arjali. 2021. Geologi am dan pemetaan tanah runtuh di Selatan Kundasang, Sabah, Malaysia. *B. Sc. (hons) Thesis*. Universiti Malaysia Sabah (unpublished).

Baba Musta, 2021. *Personal communication*.

Campbell, R. H. 1975. *Soil Slips, Debris Flows, and Rainstorms* in *the Santa Monica Mountains and Vicinity, Southern California. U.S.* Geological Survey Professional Paper 851, 51 pp.

Collenette, P., 1958. *The geology and mineral resources of Jesselton, Kinabalu area, North Borneo*. Geological Survey Department. Memoir **6**.

Cruden, D. M. & Lan, H. 2015. Using the Working Classification of Landslides to Assess the Danger from a Natural Slope. In: G. Lollino et al. (eds.), *Engineering Geology for Society and Territory* – Volume **2**, Springer International Publishing, Switzerland, pp. 3-12.

Ellen, S.D. 1988. Description and Mechanics of Soil Slip/ Debris Flows in the Storm. In: S. D. Ellen and G.E Wieczorek (eds.). *Landslides, Floods, and Marine Effects of the Storm of January 3-5, 1982, in the San Francisco Bay Region, California,* U.S. Geological Survey Professional Paper **1434**, pp. 63-112.

Hall, R., 2013. Contraction and extension in northern Borneo driven by subduction rollback. *Journal of Asian Earth Sciences*, 76, PP. 399-411.

Highland, L.M. & Bobrowsky, Peter, 2008. *The landslide handbook—A guide to understanding landslides*. Reston, Virginia, U.S. Geological Survey Circular 1325. 129 p.

Hungr, O., Leroueil, S. & Picarelli, L. 2014. The Varnes classification of landslide types, an update. *Landslides*, Volume 11, Issue **2**, pp 167–194.

Ibrahim Komoo & Lim, C.S., 2003. Kompleks Gelinciran Tanah Kundasang: Pemetaan Terperinci di Kawasan Sekolah Menengah Kebangsaan Kundasang. *Bulletin of the Geological Society of Malaysia*, 46, pp. 387-392.

IKRAM. 2011. Menjalankan kerja-kerja 'forensic geotechnical investigation', penyiasatan tapak (site investigation), ukur, reka bentuk cerun dan sistem perparitan termasuk penyediaan naskah meja tawaran (TTD) di km 5.5 jalan Samuruh Kinoundusan Ranau, Sabah (jalan negeri). *Technical report of JKR*.

Immas Jangok. 2021. Geologi am dan sifat jasad batuan Selatan Kundasang, Sabah, Malaysia. *B. Sc. (hons) Thesis*. Universiti Malaysia Sabah (unpublished).

Ismail Abd Rahim, Sanudin Tahir & Baba Musta. 2009. 'Lithological Unit Thickness' approach for determining Intact Rock Strength (IRS) of the heterogeneous Crocker Formation in CPSB Stone Quarry, Tamparuli. Borneo Science 25: 23-32.

Ismail Abd Rahim. 2011. Rock mass classification of the Crocker Formation in Kota Kinabalu for rock slope engineering purpose, Sabah, Malaysia. *PhD Thesis*, Universiti Malaysia Sabah, Kota Kinabalu, Sabah, Malaysia (Unpublished).

Ismail Abdul Rahim, Felix Tongkul, Mustaffa Kamal Shuib, Tajul Anuar bin Jamaluddin, Alexander Yan Sze Wah, Mohd Rozaidi Che Abas, Noraini Surip, Rozaina Binti Ismail, Mohd Nazan Awang, Ferdaus Bin Ahmad, Mohamad Bin Abd. Manap, Bailon Golutin, Henry Litong Among, Ledyhernando Taniou, Zaidi Daud, Roziah binti Che Musa, Zahid Ahmad, Rabieahtul Abu Bakar, Khamarrul Azahari Razak & Harry Benedick. 2015. *Remote sensing and field survey analysis of active fault in Malaysia.* Sciencefund Project No: 04-01-10-SF0201. Ministry of Science, Technology, and Innovation, Malaysia.

Jabatan Mineral & Geosains Malaysia (JMGM). 2012. Landslide phenomenon in Kundasang and Ranau. *Seminar Bencana Alam 2011 (BENCANA 2011)*. Universiti Malaysia Sabah, Kota Kinabalu.

Jacobson, G. 1970. Gunung Kinabalu area, Sabah, East Malaysia. *Malaysia Geological Survey Report no. 8*. Sarawak Government Press, Kuching.

Jesus C, C, Sérgio C, Oliveira S, C, Sena C & Fernando Marques F. 2017. Understanding constraints and triggering factors of landslides: Regional and local perspectives on a drainage basin. *Geoscience.*

Kazmi D, Qasim , Harahap I, S, H, Baharom S, Imran M & Moin S. 2016. A Study on the Contributing Factors of Major Landslides in Malaysia. *Civil Engineering Journal* Vol. 2, No. 12, 669 – 678pp.

Kesseli, J.E. 1943. Disintegrating Soil Slips of the Coast Ranges of Central California. *Journal of Geology*, Vol. 51, No. **5**, pp. 342-352.

Novotný J. 2012. Landslide Causes and Triggering Mechanisms. Faculty of Science, Charles University, Prague, Czech Republic.

Sapin, F., Hermawan, I., Pubellier, M., Vigny, C. & Ringenbach, J.-C., 2013. The recent convergence on the NW Borneo Wedge—a crustal-scale gravity gliding evidenced from GPS. *Geophysical Journal International*, 193(2), PP. 549–556.

Taiwan Geoscience portal (2021). *What is the landslide triggering factors?* Central Geological Survey, MOEA. https:// twgeoref.moeacgs.gov.tw/ GipOpenWeb/ wSite/mp?mp=107 (retrieve on 3 August 2021)

Tjia, H. D. 2007. Kundasang (Sabah) at the intersection of regional fault zones of Quaternary age. *Geol. Soc. Malaysia Bull.* **53**, pp 59-66.

Tongkul, F. 2015. The 2015 Ranau Earthquake: Cause and Impact. *Sabah Society Journal*, Vol. 32, pp. 1-28.

Tongkul, F. 2017. Active tectonics in Sabah – seismicity and active faults. *Bulletin of Geological Society of Malaysia*, Vol. 64, pp. 27-36.

Turner, A. K. & Schuster, R. L. 1996. *Landslides: Investigation and Mitigation*. University of Michigan, National Academy Press. 673p.

BorneoScience
The Journal of Science & Technology
Volume 43 Issue 2 : Oct 2022
Online ISSN : 2231-9085 | ISSN : 1394-4339

GEOPHYSICS ELECTRICAL CHARACTERIZATION FOR IDENTIFICATION OF SEAWATER INTRUSION IN THE COASTAL AREA OF PAPAR, SABAH

Hardianshah Saleh[1], Siam Jia Quan[2], Muhammad Jaya Padriyamzah Bin Abdul Hamid[3]

[1]Faculty Science and Natural Resources, Universiti Malaysia Sabah.
[2]Faculty of Science and Computer Informatic, Universiti Teknologi PETRONAS.
[3]Wullesdorf Resources Sdn Bhd.

Received 9th Feb 2022; accepted 11th July 2022
Available online 1st Nov 2022
Doi: https://doi.org/10.51200/bsj.v43i2.4507

ABSTRACT. *Seawater intrusion is known to be a major problem that influences the quality of groundwater within coastal regions globally. The groundwater table within the coastal area is usually close to the ground surface due to low topography or human development activities such as land reclamation and man-made drainage systems that keep the water table at constant low level. Electrical resistivity method is one of the geophysical methods that has been extensively used to investigate seawater intrusion due to the high electrical conductivity contrast produced by saline water. Papar, Sabah is located at the west coastal region of Sabah and is generally formed by Crocker formation and Quaternary alluvium. The sedimentary rock of Crocker Formation mainly consists of thick sandstone unit, interbedded sandstone, siltstone and shale unit and shale unit. A total of Five 2D electrical resistivity imaging (ERI) methods were carried to image and model the subsurface within the research area to investigate the possibility of seawater intrusion. The ERI results are also supported by four groundwater samples and detailed lithologies from the borehole. Interpretation of the results divided the research area into three main zones of seawater intrusion potentials. Zone 1 is considered the highest potential of seawater intrusion, Zone 2 interpreted as potential extended zone or mixing zones between seawater and fresh water and finally Zone 3 did not indicate any low resistivity or potential of seawater intrusion. The seawater intrusion map produced from this research initiated and divided the potential zones based on the occurrence of seawater in the subsurface.*

KEYWORDS. Geophysics, seawater intrusion, groundwater.

INTRODUCTION

Globally, seawater intrusion is known to be a major problem that influences the groundwater quality within coastal regions globally (Zakiyah Ainul Kamal *et al.*, 2020). The groundwater table within coastal areas is usually close to the ground surface due to low topography or human development activities such as land reclamation and man-made drainage systems that keep water tables at constant

low level (Jiao and Post, 2019; Giambastiani et al., 2020). Generally, the geological and hydrogeological properties of coastal aquifers systems are the key factors in controlling the occurrence and progression of saltwater intrusion (Carrera *et al.,* 2010 and Michael *et al.,* 2013).

External factors such as climate change and human activities also affect groundwater level, especially aquifers in the coastal region (Moser *et al.,* 2014; Green, 2016). Climate change will cause the changing of temperature and precipitation regimes, sea level rise, more frequent extreme weather events and coastal erosion (Norzaida *et al*., 2017). Changing in temperature and precipitation regimes could have certainly influenced the recharge rate for coastal aquifers and subsequently caused the saltwater intrusion in coastal wells (Griggs, G. & Reguero, 2021). A hot temperature could reduce the amount of rainfall and thus reduce the amount of freshwater input to the aquifer. Furthermore, warmer weather is likely to increase freshwater demand, which may lead to over pumping of the freshwater from aquifers. Combined with sea level rise, this change may bring more frequent and intense storm surges to coastal areas, leading to saltwater flooding around coastal wells (Van Biersal et al., 2007), besides seawater may seep into aquifers from the surface drainage systems. Human activities such as excessive groundwater pumping also contribute to seawater intrusion (e.g., Nawal and Kristine, 2017). This situation results in reducing the hydraulic head in the aquifer, subsequently slowing or stopping the seaward flow of freshwater, which allows seawater to move further inland (Khublalryn *et al.,* 2008).

The Papar coastal area has been developed as the agricultural land to grow plants such as paddy and coconut trees. Since the region is located on the West coast of Sabah, seawater intrusion could become the major threat towards the agricultural industry development which is experienced by many coastal areas in the world (e.g., Lam *et al*., 2021). Due to the high salt content in the soil, any seawater intrusion within this region would result in a loss of productivity and may make crop cultivation impossible (Tol, 2009). Evaluating and monitoring this situation should become the priority to sustain the groundwater quality as well as agricultural activities (e.g., Lee and Song, 2007).

Geophysical survey for seawater intrusion.

Electrical and electromagnetic techniques have been extensively used in hydrogeological investigations due to the relationship existing between the electrical and hydraulic properties of geological formation and containing fluid saturation (Stewart, 1982; Fitterman & Stewart, 1986; Duque *et al.,* 2008). The electrical resistivity method is one of the geophysical methods that has been extensively used to investigate seawater intrusion due to the high electrical conductivity contrast produced by saline water (e.g, Zakiyah Ainul Kamal *et al.,* 2020; Musta *et al.,* 2022). The technique consists of injecting the electric current into the ground through the electrodes (current electrodes) and measuring the potential difference via other electrodes (potential electrodes) (e.g, Hardianshah & Samsudin, 2016).

Direct quantitative interpretation of apparent electrical conductivity measurements is not easy because it is influenced by several factors, such as porosity, temperature, clay with high cation exchange capacity and concentration of dissolved electrolytes (McNeill, 1980). Thus, the interpretation based on electrical characterization requires in situ data such as geology bore log data

or outcrops observation in the field (e.g., Alajmi *et al.,* 2010).

Hydrogeology parameter of groundwater and salinity.

The pH of groundwater will vary depending on the composition of the rocks and sediments that surround the travel pathway of the recharge water infiltrating the groundwater. Groundwater chemistry will also vary depending on how long the existing groundwater is in contact with a particular rock. Groundwater can be classified based on its physical and chemical properties such as pH, salinity, total dissolved solid (TDS) and electric conductivity (EC). According to Tystsarin (1988) and Miller (2000) the water can be classified to acid sulphate drainage, most natural freshwaters, distilled reverse osmosis water, groundwater, most river water and seawater based on the pH values.

As a basic definition, salinity is the total concentration of all dissolved salts in water (Jain, 2014). Salts form ionic particles as they dissolve, each with a positive and negative charge. Thus, salinity is a strong contributor to conductivity (Hickin, 1995). There are many different dissolved salts that contribute to the salinity of water, the major ions in seawater are chloride, sodium, magnesium, sulfate, calcium, potassium, bicarbonate, bromide, Strontium, Boron and fluoride (Sudaryanto & Wilda, 2017). These ions are also present in inland freshwater such as river water, lake water and pond water but in much smaller amounts. According to Ohrel & Register (2006), the salinity of seawater ranges from 32 ppt to 37 ppt, freshwater is usually lower than 0.5 ppt, and brackish water ranges from 0.5 ppt to 17 ppt. However, the surface salinity of the ocean is more dependent on rainfall, especially areas around the equator and coast where rainfall is high, surface salinity values are lower than average and salinity indicated has a correlation with pH properties (modelled by Radke, 2002).

MATERIALS & METHODS

Investigation of subsurface model and identification of seawater intrusion require geological, geophysics method and hydrogeology input. Thus, this research was conducted by combining several methods and techniques from those fields. All the results were then correlated to produce robust interpretation and understanding regarding the potential of seawater intrusion within the study area.

Geological background of Papar, Sabah.

The Crocker formation dominated the region of West Coast Sabah, which also included the study area within Papar coastal region (**Figure 1**). Papar, Sabah region is generally formed by Crocker formation and Quaternary alluvium (Majeed *et al.*, 1994; Azfar Mohamed *et al*., 2016). Crocker Formation is used to describe the sedimentary rocks consisting of thick sandstone unit, interbedded sandstone, siltstone and shale unit (Jacobson,1970).

The Crocker Formation of Late Eocene to Early Miocene age is mostly concentrated in the western part of Sabah. The Crocker Formation consists mainly of clastic sediments of flysch type,

which were deposited in an elongated basin of abyssal depth (Collenete, 1958; Jacobson,1970). The sandstone unit is the thickest unit in the Crocker Formation. Individual layer thickness usually exceeds 4 meters and maximum thickness can reach up to 25 meters (**Figure 2a**). It is light grey coloured with grain size medium to coarse, and sometimes pebbly (**Figure 2b)**. Interbedded sandstone, siltstone and shale units are defined by an alternating sequence of sandstone, siltstone and shale of variable thickness and ratio. The shale unit is generally composed of grey and red types of shale. The grey variety is occasionally calcareous. It is usually interlayered with siltstone or very fine grain sandstone (**Figure 2c**). While the Quaternary alluvium (**Figure 2d**) is restricted to low land area, coastal areas and riverbank. It mainly consisted of deposited alluvial sediments on river terraces and floodplains and beaches (Majeed *et al*., 1994).

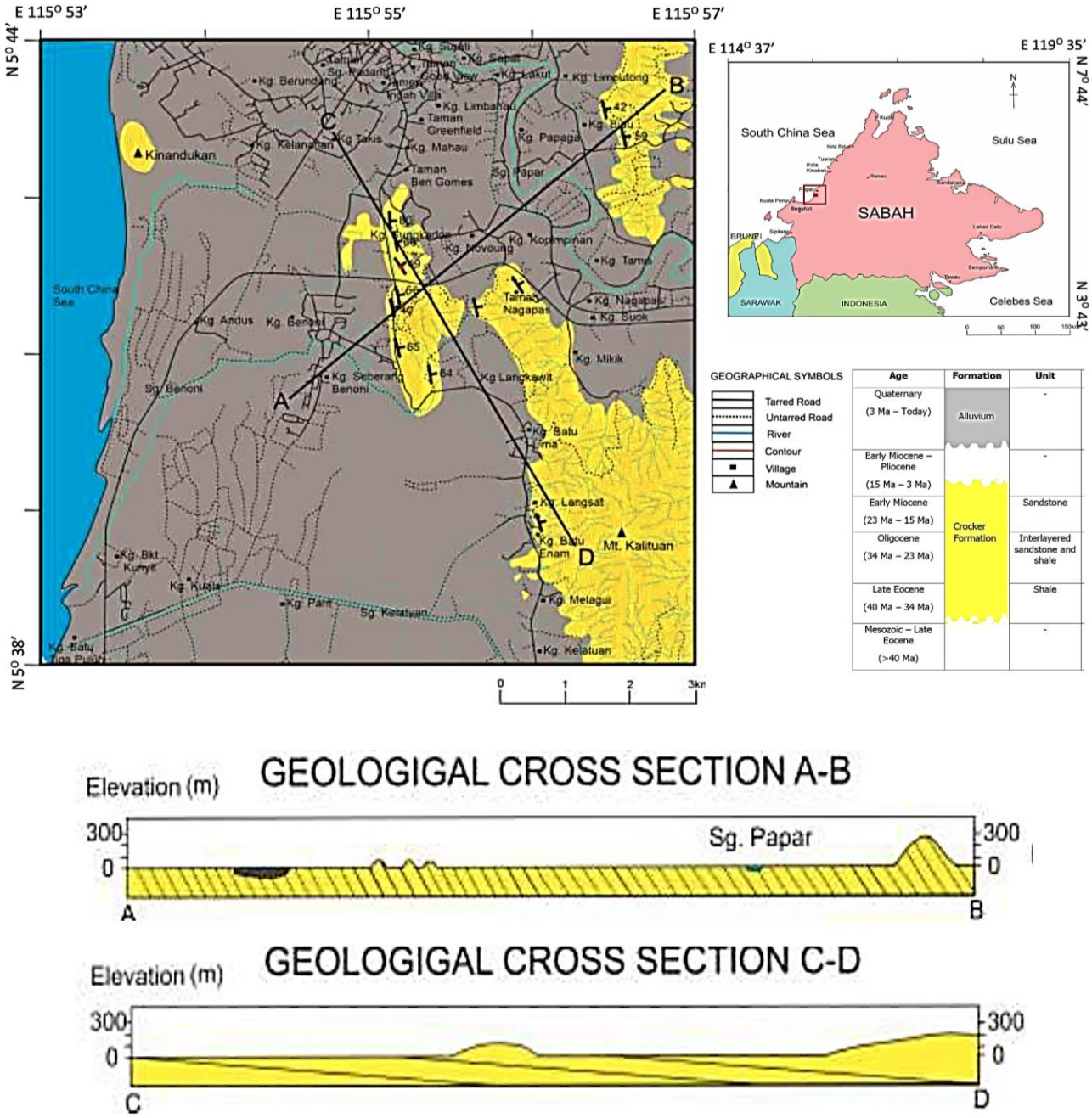

Figure 2. Geological map for the research area.

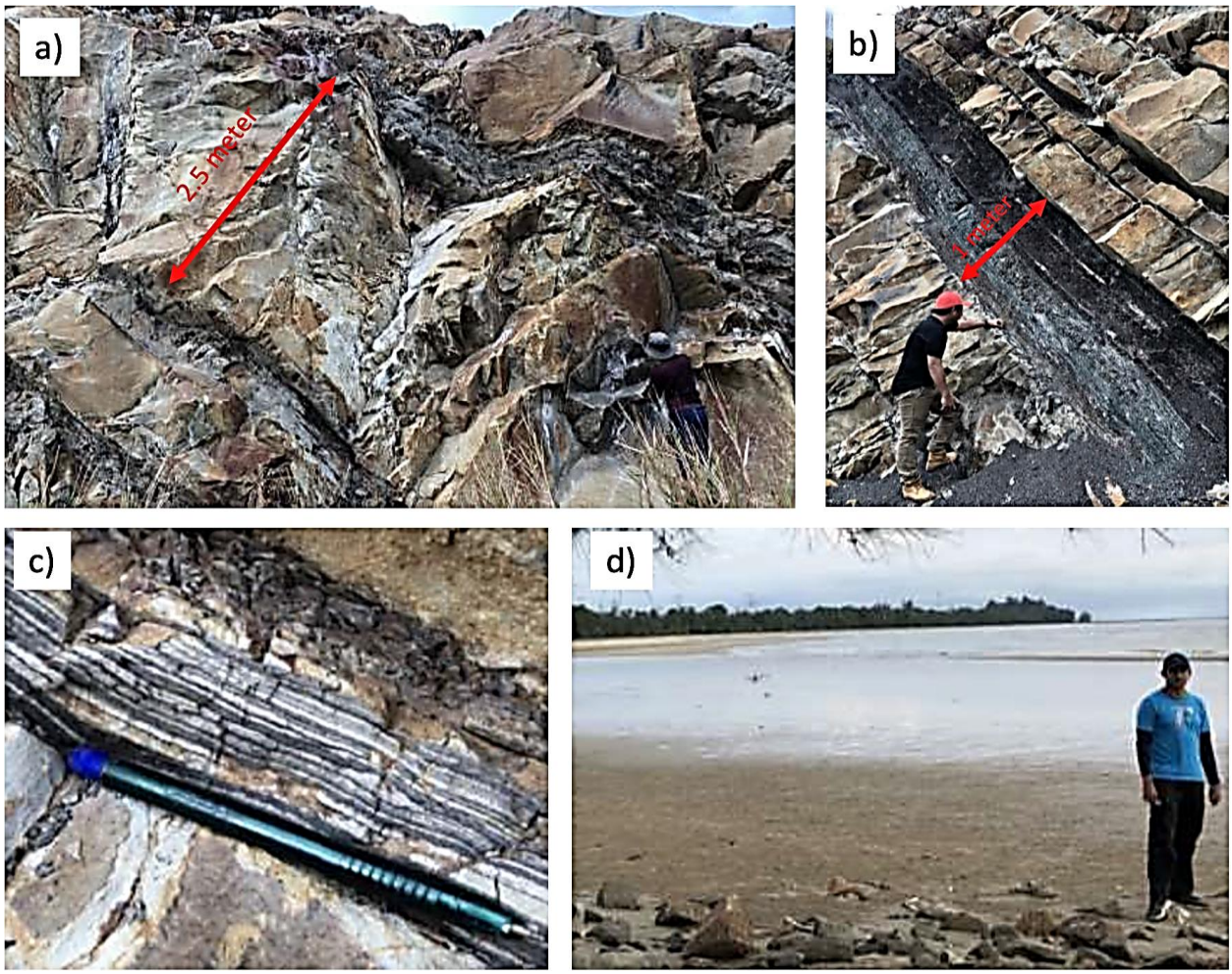

Figure 2. Typical Crocker formation and alluvium quaternary within the study area.

Electrical Resistivity Imaging, ERI survey.

Five 2D electrical resistivity imaging (ERI) methods were carried out to image and model the subsurface within the research area to investigate the possibility of seawater intrusion (**Figure 3**). The ERI survey was carried out using ABEM Terrameter LS which connected to stainless steel electrodes with a constant spacing via two or four multicore cables. The ERI survey carried out on all survey points is using 5m electrode spacing which has a total length survey of 200 meters when involving two multicore cables and 400 meters when involving 4 multicore cables. The 200 meters could acquire up to 33 meters of information, while 400 meters gives 80 meters depth of information.

In this studied the Wenner and Schlumberger arrays of electrodes, were used to acquire resistivity data. The Wenner array gives better horizontal resolution, while Schlumberger gives a better depth of information for the same maximum electrode spacing (**Figure 4**). Technically, the Wenner configuration requires 190 data points or resistivity values to model the subsurface. Four electrodes were selected to measure each of these data points, where two electrodes become current electrodes (C1 & C2) to inject current to the ground while another 2 electrodes as potential (PI & P2) to measure electrical potential of the ground. The Schlumberger array using 61 electrodes via four multi-core cables (400 meter) will require 800 of data points. Similarly, two current electrodes (C1 & C2) and two potentials (PI & P2) were used to inject current to the ground and measure current potential. The resistivity values were calculated based on Ohm's Law equation V=IR, resistivity (R)

can be obtained by dividing potential difference (V) to current (I). The resistivity values for subsurface for each datum point are calculated automatically based on the acquisition configuration and stored in the main computer of ABEM Terrameter LS system. The measured resistivity value is then inverted by using RES2DInv to produce a subsurface model (Griffith & Baker, 1993). This 2D subsurface model then correlates with the in-situ data to produce subsurface interpretation for the study area.

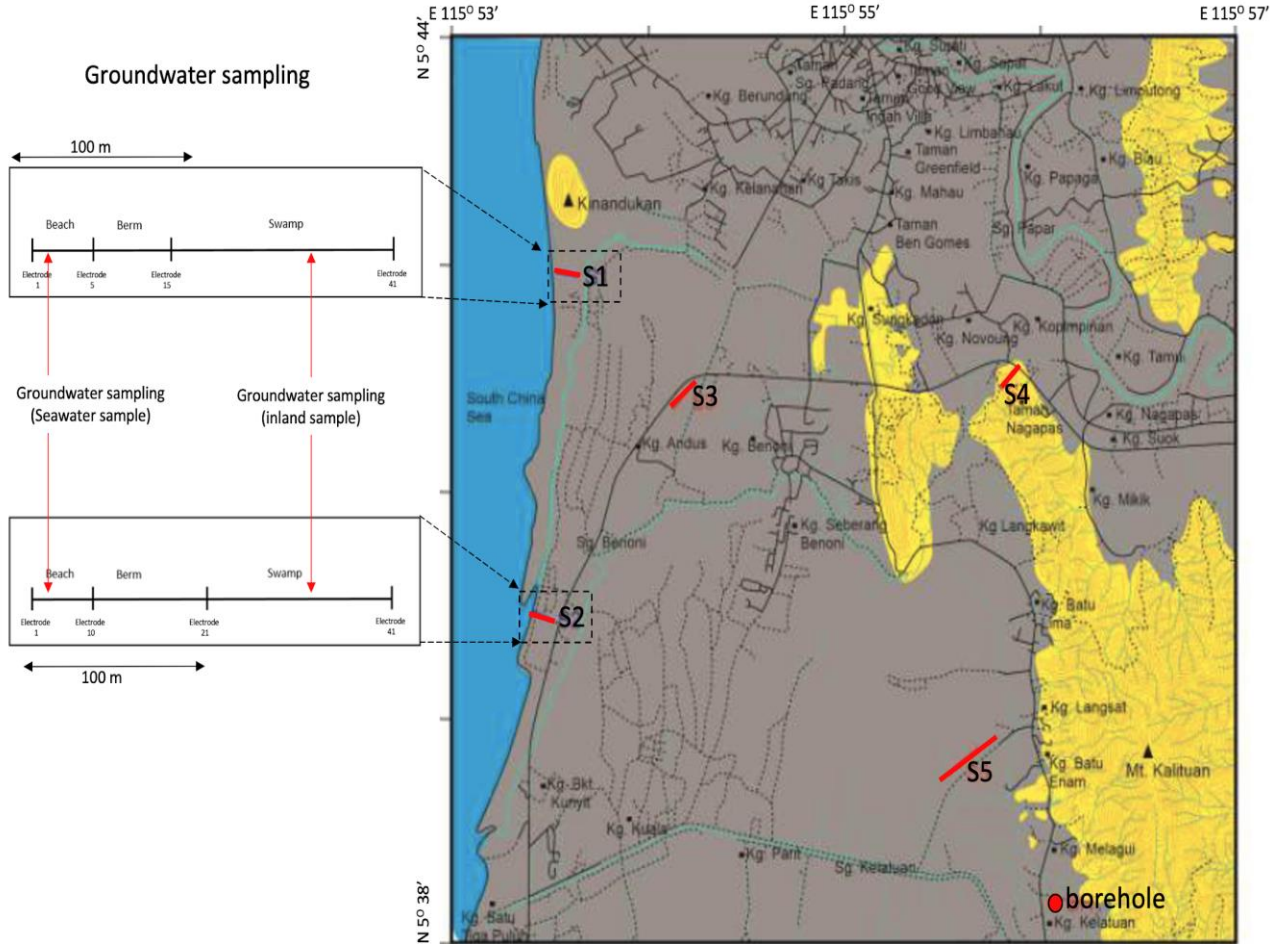

Figure 3. The location of Electrical Resistivity Imaging, ERI survey, groundwater sampling and bore hole.

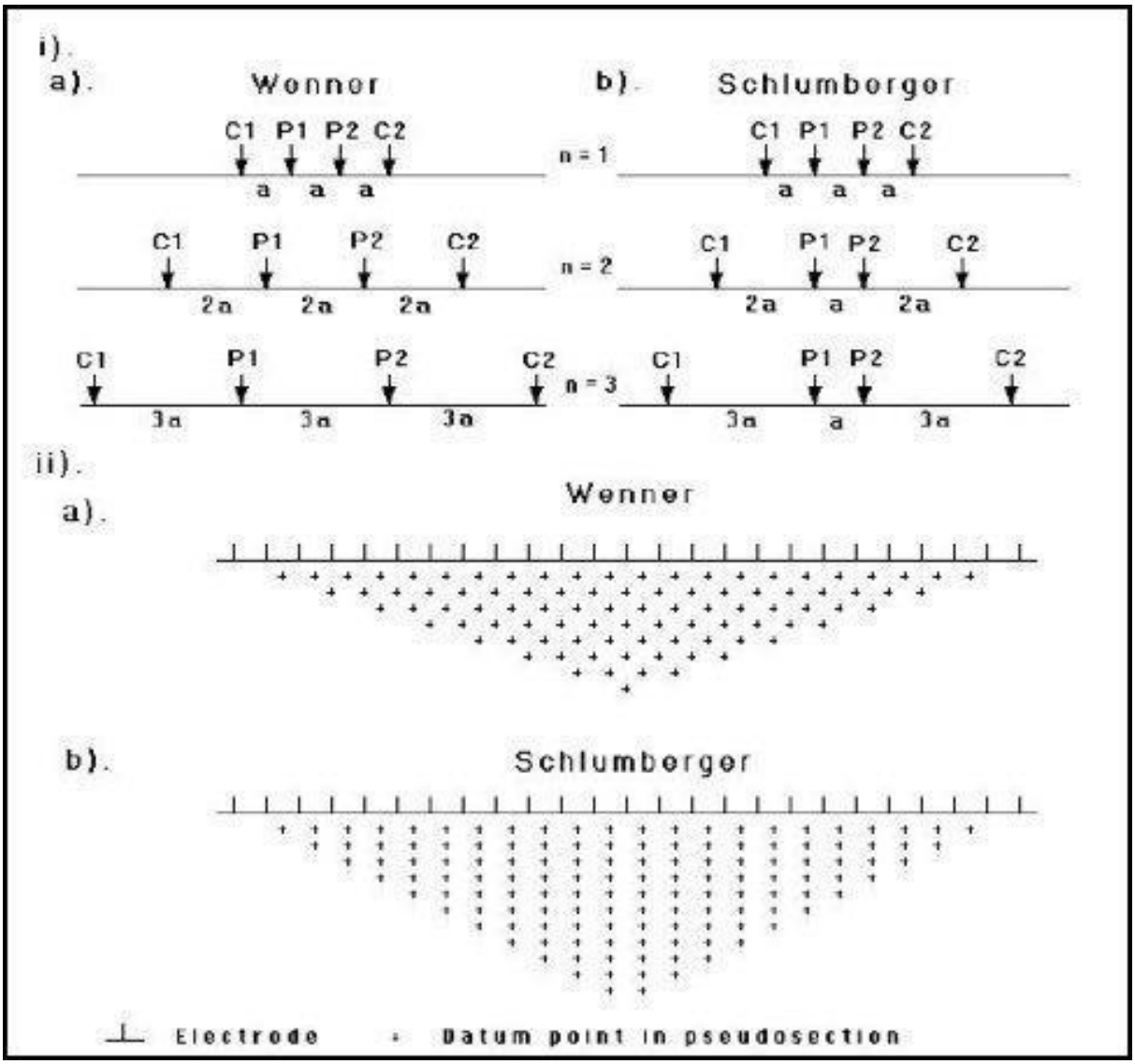

Figure 4. Comparison of ERI data acquisition by using Wenner and Sclumberger configuration (Loke, 1999; Basri *et al.*, 2019)

Physical properties of soil & rock formation.

Borehole data with 79.5 meter of depth (**Table 1**) which is located at Kampung Kelatuan, Papar is used and correlated to interpret the subsurface. It reached depth from 0 meter until 1 meter is unconsolidated fine sand and brown in colour due to high organic matter. From 1 meter until 9.5 meter is consolidated white colour fine sand while for 9.5 meter until 10 meter is consolidated medium grained white colour sand. Next is black shale layer from a depth of 10 meter until 20 meter. At 20 meter to 30 meter depth, there is grey-colored sandstone interlayered with shale or mudstone. At the end, 30 meter until 79.5 meter depth, are shale layers that are dark grey in colour and hard to penetrate. It is interlayered with sandstone layers or other shale layers.

Table 1. Description of subsurface materials from borehole data (Mohd. Kamal, 2011)

Layer	Depth (m)	Lithology
1	0 – 1.0	Unconsolidated brown colour sand
2	1.0 – 9.5	Consolidated white colour fine grained sand
3	9.5 – 10.0	Consolidated white colour medium grained sand
4	10.0 – 20.0	Black shale
5	20.0 – 30.0	Interlayered sandstone and shale unit (sandstone dominated)
6	30.0 – 79.5	Interlayered sandstone and shale unit (mudstone dominated)

Groundwater properties analysis

Two groundwater samples were taken from each of stations S1 and S2 by hand auger (Figure 4). One groundwater sample was taken at the first electrode of the geophysical survey, which is near the shoreface, while the second groundwater sample was collected more inland, which is located between electrodes 30 to 41 or within 150 to 200 meters from the shoreface. Physical properties of the groundwater sample such as pH, salinity, conductivity and total dissolved solid (TDS) were measured in the laboratory by using pH meter and Mettler Toledo Duo pH/ion/conductivity meter.

RESULTS & DISCUSSION

A total of five ERI survey lines with four groundwater analyses were conducted within the research area. Station S1 and S2 have additional groundwater samples from the shoreline and inland to correlate with the ERI results. While stations S5 rely on the borehole data that acquire near this station.

Electrical Resistivity Imaging, ERI results.

The first station is located near the shore face within Telinting Beach. The 200 m of total length survey gave 33.8 m depth of data acquisition. The results indicated that the resistivity value ranged from 0.03 Ωm up to 8 Ωm (**Figure 5a**). While for induced polarization, the chargeability is ranging up to 108.59 msec (**Figure 5b**). Based on ERI results and observation on the field, the subsurface interpreted build up is dominated by unconsolidated sand. The resistivity values are mainly controlled by the salinity and saturation level of seawater since the survey stations were located up to the seashore. Resistivity readings between 0.03 Ωm and 2.73 Ωm are interpreted as fully saltwater saturated sand. For resistivity values range from 5.09 Ωm until 9.47 Ωm which is partially seawater saturated sand for the vadose zone at beach area and low saline water saturated sand at swamp area. For contours with resistivity readings ranging from 17.6 Ωm until 212 Ωm, it is interpreted as sand with different water saturation level. The higher the resistivity the drier the sand.

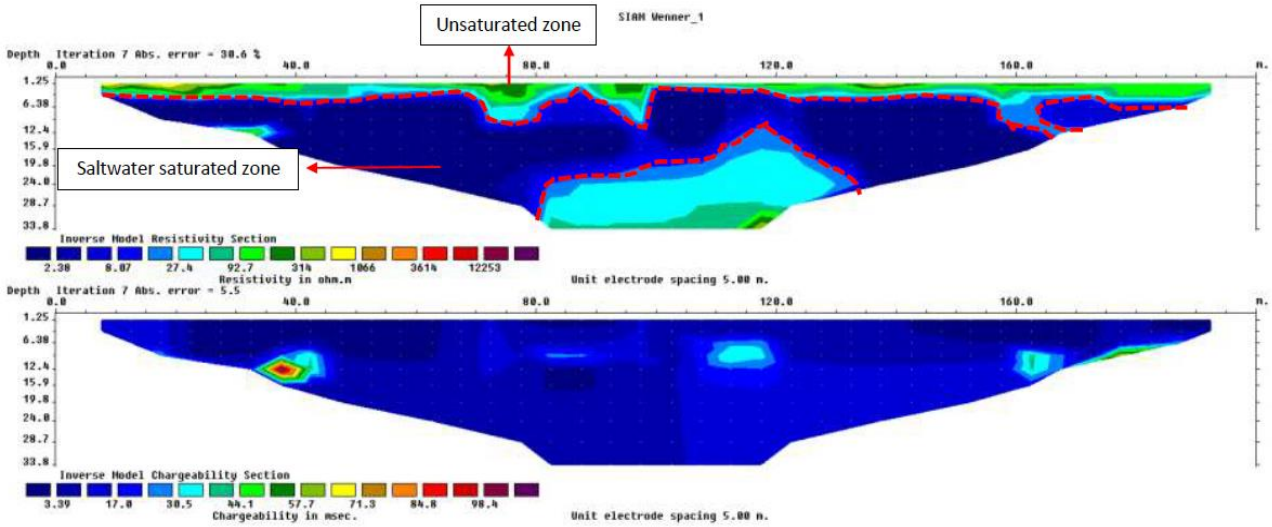

Figure 5. a) Resistivity and b) chargeability value for subsurface of station S1

The ERI results at Station S2 acquired depth of subsurface information up to 33.8 meter from the surface (**Figure 6**). The resistivity reading ranges from 0.18 Ωm up to 247.5 Ωm (**Figure 6a**). While induced polarization indicated the maximum of 49.1 msec (**Figure 6b**). The collected resistivity and induced polarization data are used to correlate with the lab analysis data for subsurface interpretation. The beach area consists of sand particles while swamp areas consist of clay particles (see Lambiase *et al*., 2008). In this area, resistivity readings are mainly controlled by the salinity and saturation level of seawater and soil material. Resistivity readings between 0.22 Ωm and 2.87 Ωm are interpreted as a fully sea water saturated sand layer at the left part of the cross-section. Although the salinity of the water sample collected at the swamp area is low, the resistivity values remain low at the middle right part of the cross-section. This is because soil particles of swamp consist of clay particles with higher cation exchange capacity and high conductivity (Adegoke *et al.,* 2016). This explanation is also supported by the induced polarization cross-section, which shows sudden increase in chargeability values at the right part and indicates the presence of clay layer. For resistivity values range from 4.38 Ωm until 10.2 Ωm is partially seawater saturated sand at the beach area, for contour with resistivity readings range from 15.7 Ωm until 130.9 Ωm is sand with different level of water saturation, the higher the resistivity the drier the sand.

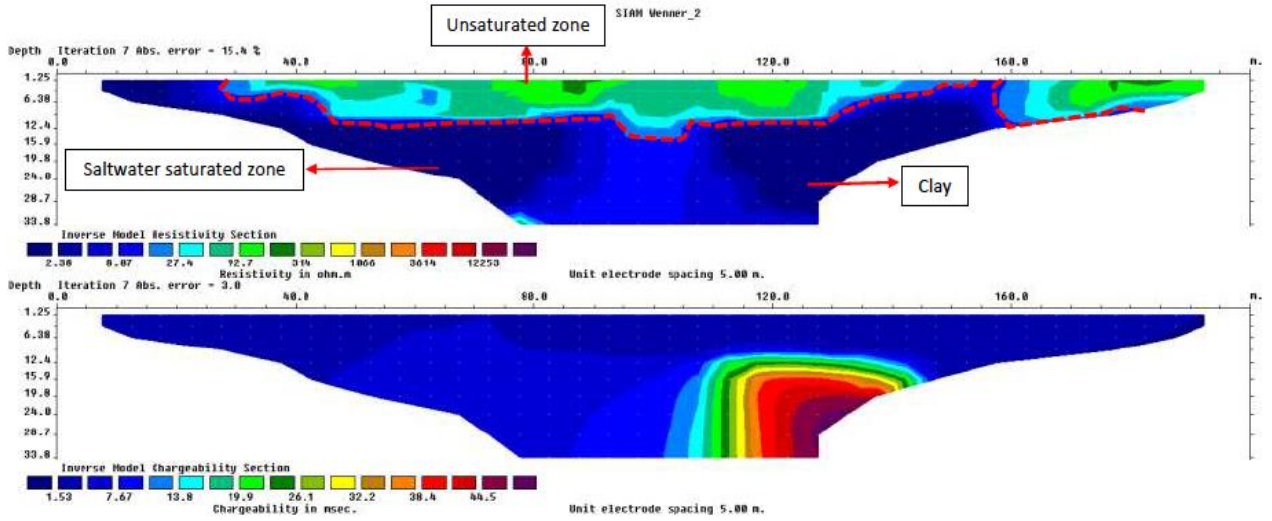

Figure 6. a) Resistivity and b) chargeability value for subsurface of station S2

Station S3 is located at Kampung Benoni, adjacent to a stream. Electrode array used in the electrical resistivity imaging survey for station 3 is Schlumberger array, 4 cable sets with 5 meter electrode distance which makes the total survey line distance is 400 meter with maximum depth of information up to 87.2 meter from the surface. Lowest resistivity reading collected is 0.60 Ωm and the highest is 463.14 Ωm. (**Figure 7**). According to the resistivity cross-section, topsoil consists of sand with different levels of water saturation, the shallower the depth the drier the sand. It has resistivity values ranging from 24.7 Ωm until 463.14 Ωm. Sudden decrease in resistivity around 3 meter depth indicates the level of the water table. Down in the groundwater, the resistivity of water at depth from 12.4 meter until 33.7 meter has relatively lower readings, 0.73 Ωm – 2.36 Ωm and indicates the presence of saltwater (Nassir *et al.*, 2000; Song *et al.*, 2007; Chafouq *et al.*, 2016). Start from depth of 33.7 meter, the resistivity for the saturated zone increased to 3.49 Ωm – 16.7 Ωm indicating salinity level of underground water decrease as depth increases which potentially indicate the appearance of Crocker formation that overlain by the alluvium.

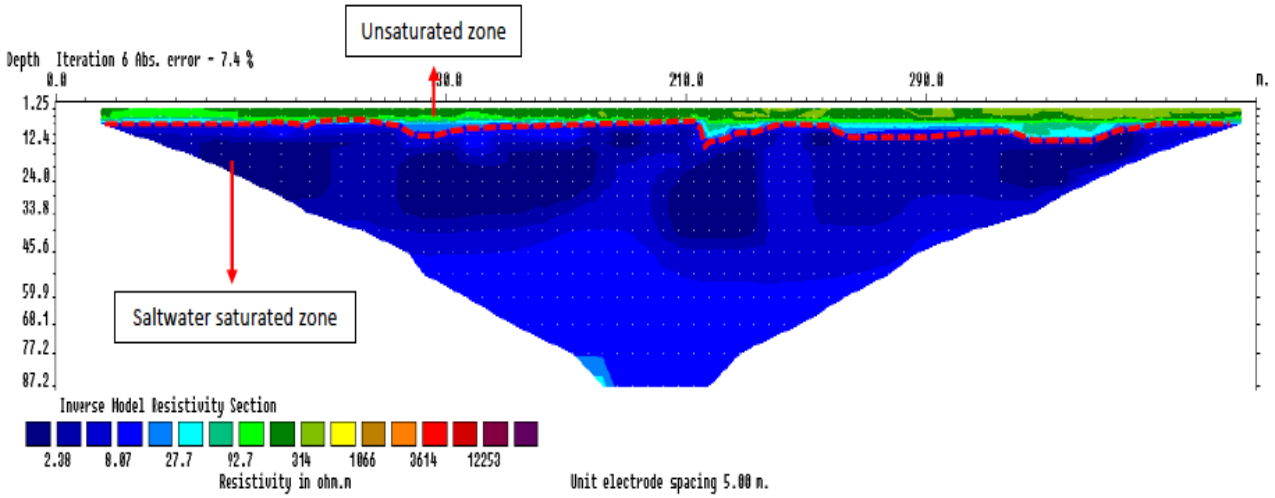

Figure 7. Resistivity (ERT) value for subsurface of station S3

Station S4 is located at Kampung Nagapas with a total distance for survey line is 200 meter with depth of data up to 26.2 meter. Lowest resistivity reading recorded is 1.75 Ωm and the highest is 56370.00 Ωm. An outcrop was found at station 4, it shows interbedded sandstone and shale layers and geological structures such as fault and fold (Majeed Faizal *et al.*, 1995; Lambiase *et al.*, 2008). The resistivity cross-section (**Figure 8**) indicates topsoil of this area reached up to 12.4 meter deep and has lower resistivity value. Resistivity values with the range 1.75 Ωm -14.9 Ωm are interpreted as clayey soil while for resistivity values range from 27.7 Ωm until 314.4 Ωm are known as sandy soil (Hardianshah & Abdul Rahim, 2013). Changing in resistivity horizontally for topsoil indicates weathered interlayered shale and sandstone layers which is the same as the rock layers in the outcrop. Down in the depths, the resistivity values increase, 578.9 Ωm – 56370.0 Ωm as the presence of Crocker Formation bedrock. The lower the weathering grade of the bedrock, the higher the resistivity.

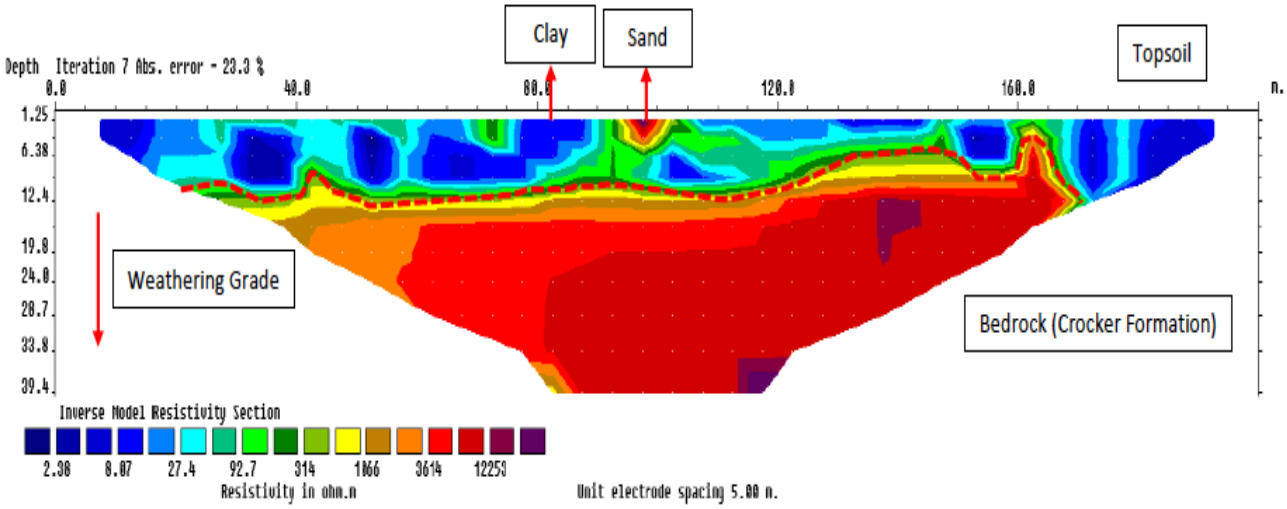

Figure 8. Resistivity (ERT) value for subsurface of station S4

Station S5 located at Kampung Langsat was conducted by using Schlumberger configuration that involved 4 multicore cable which makes the total survey line distance 400 meter. Since the maximum survey line is greater than the previous survey line, ERI results in this station can acquire deeper subsurface information up to 87.2 meter from the surface. The results for station S5 (**Figure 9**) indicate the lowest resistivity reading is 0.09 Ωm and the highest resistivity value up to 1125.90 Ωm.

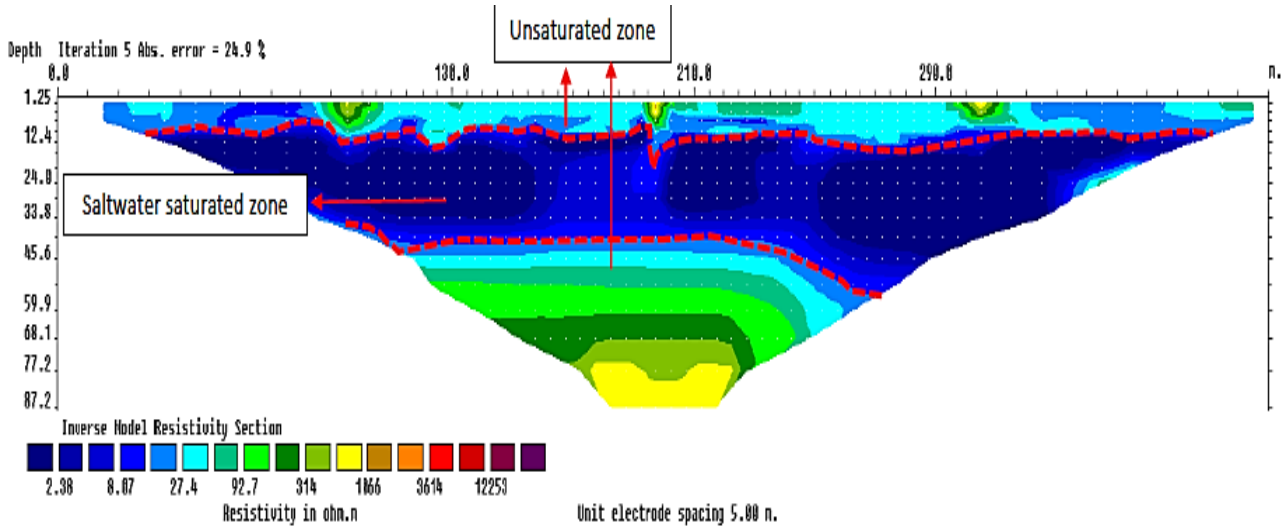

Figure 9. Resistivity (ERT) value for subsurface of station S5

Groundwater analysis from the shoreline region.

Table 2 shows the salinity analysis for water samples collected at stations 1 and 2. The salinity for seawater samples was 28.57 ppt and 16.57 ppt for station 1 and 2 respectively. The salinity values obtained are lower than average due to the rainy season and horizontal stratification of seawater salinity. In horizontal stratification, salinity of seawater increases towards the sea. While for the inland water sample in station S1 indicates the value of salinity is 0.70 ppt. Based on classification

by Ohrel and Register (2006), this water type is categorized as brackish water. Therefore, the area can be categorized as a transition zone between seawater and freshwater and known as saltwater swamp or it was a freshwater swamp originally and intruded by the seawater. The salinity for swamp water collected in station 2 is 0.10 ppt which means the water table zone is free from saltwater pollution.

Table 2. Salinity and pH for groundwater samples at station S1 and S2

Station	Groundwater sample	Average Salinity (ppt)	Average pH
S1	Seawater	28.57	7.73
	Inland	0.7	3.22
S2	Seawater	28.57	7.67
	Inland	0.10	5.04

Table 3. Conductivity for groundwater samples at station S1 and S2

Station	Groundwater sample	Average conductivity (S/cm)
S1	Seawater	0.464
	Inland	1.34×10^{-3}
S2	Seawater	0.027
	Inland	0.21×10^{-3}

The potential of seawater intrusion zones based on geoelectrical characterization.

Based on the interpretation ERI results from five stations (**Table 4**) and water sample analysis, the study area is divided into three main zones of seawater intrusion potentials (**Figure 10**). Zone 1 is considered the highest potential of seawater intrusion as indicated by the ERI results from stations S1 and S2. The appearance of seawater within the subsurface for both stations was confirmed by pH and salinity measured from water samples from these stations.

Table 4. Summary of ERI subsurface interpretation.

Survey Station	Resistivity range (Ωm)	Interpretation	Water table elevation (m)
S1	0.03 – 2.73	Saltwater saturated sand	6.0
	5.09 – 9.47	Brackish water saturated sand	
	17.60 – 999.80	Low saline water saturated sand – dry sand	
S2	0.18 – 2.87	Saltwater saturated sand, saltwater saturated clay	10.0
	4.38 – 10.20	Freshwater saturated clay	
	15.70 – 247.50	Partially freshwater saturated sand – dry sand	
S3	0.60 – 2.36	Saltwater saturated sandstone	10.0
	3.49 – 16.70	Brackish water saturated sandstone	
	24.70 – 463.14	Partially freshwater saturated sand – dry sand	
S4	1.75 – 14.90	Clay	N/A
	27.70 – 324.40	Sand	
	578.90 – 56370.00	Bedrock (Crocker Formation)	

S5	0.09 – 5.92	Saltwater saturated sandstone	12.4
	10.30 – 53.90	Partially saturated mud dominated, Interlayered sandstone and shale unit	
	93.70 – 1125.90	Dry sand, sandstone	

The existence of low resistivity (less than 3 Ωm) extended inland (Zone 2) as indicated and detected within station 3 and 5. This zone is interpreted as a potential extended zone or mixing zones between seawater and freshwater. There are a few parameters that may cause the appearance of low resistivity, such as the existence of clay (Long *et al.,* 2012). The survey area for station S1, S2, S3 and S5 are located within the alluvium which is dominated by clay materials that may cause this low resistivity. Furthermore, based on the resistivity results from stations S1, S2, S3 and S5, the quaternary alluvium deposits within the research area potentially formed an unconfined aquifer system that allow the saline and brackish water to move further inland. Besides, there are many drainages systems (natural and man-made) within the alluvium that may have contributed to this situation. Station S5 is approximately 5.8 km from the coastline, proving saltwater moves far enough inland. Though saltwater is a naturally occurring process, it can also be influenced by human activity in Papar. Overpumping of groundwater for plantation, industry or domestic use can reduce the recharge of fresh groundwater and cause saltwater intrusion. However, saltwater intrusion in Papar due to over-pumping of groundwater has not yet been verified.

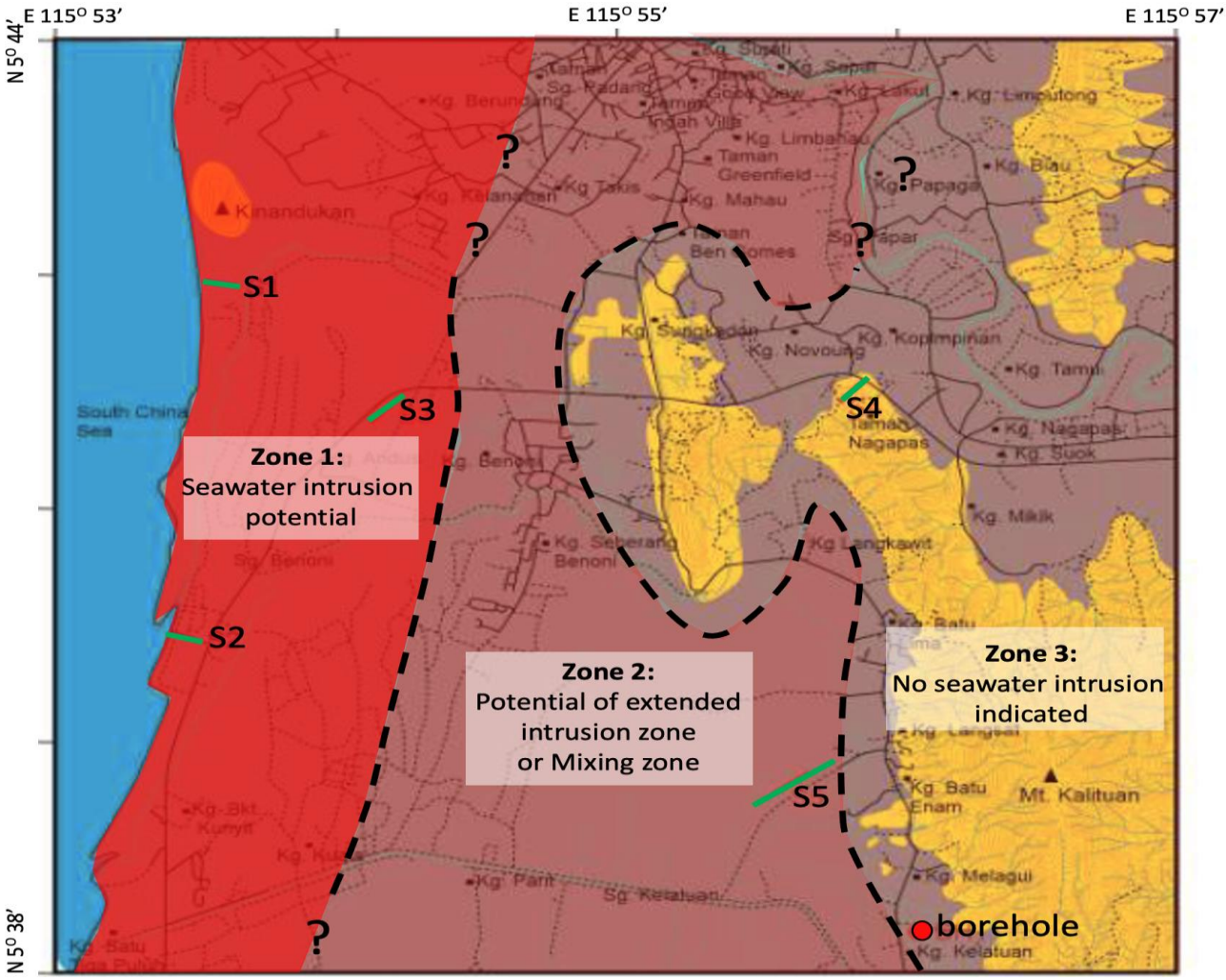

Figure 10. The seawater intrusion potential map.

Station S4 that located on the Crocker formation did not indicate any low resistivity, which also marked as Zone 3 in the Figure 13. The alluvium deposits slightly reach within this zone due to higher topography land (more than 20 m from MSL). This also may suggest that the unconfined aquifer system that build up by the alluvium quaternary did not continuation towards the aquifer system that may formed within the thick sandstone layer in the Crocker formation.

CONCLUSION & SUGGESTION

Correlation of ERI surveys and groundwater analysis gives the subsurface model within the research area. Very low resistivity values ranging from 0.03 Ωm until 6.00 Ωm detected within the subsurface and interpreted as the potential occurrence of seawater intrusion. There are a few parameters that may cause the appearance of low resistivity, such as the existence of clay. The survey area for station S1, S2, S3 and S5 are located within the alluvium which is dominated by clay materials that may cause this low resistivity. This should be able to be justified by using IP data as shown in Station 1 and 2, but unfortunately, due to instrument limitation, IP data is unable to be acquired for Station 3, 4 and 5. Thus, this needs to be confirmed by comprehensive hydro-chemical analysis and to justify whether this low resistivity is influenced by the seawater intrusion itself or the influence of clay mineral from the rock formation or alluvium deposits. Besides, many small channels (natural and man-made) within the alluvium area may transport seawater or brackish water from the shoreline towards the mainland. The subsurface model indicated three apparent zones within the area. Zone 1 indicated the highest potential for seawater intrusion, while Zone 2 indicated mixing zones that also indicated extended potential for seawater intrusion. High topographical areas that are higher than alluvium deposits did not indicate the potential of seawater intrusion.

The seawater intrusion map produced from this research initiated and divided the potential zones based on the occurrence of seawater in the subsurface. While some improvements need to be made to produce robust and detailed mapping such as additional the numbers of ERI survey lines and monitoring well among the proposed zones. This will provide a better image or idea of the condition of seawater intrusion and identify the absolute border between seawater, freshwater and mixing zone precisely.

ACKNOWLEDGEMENT

This research was supported by the University Malaysia Sabah with Project Code SGA0053-2019. All the geophysical survey has been done using the instrumentation owned by the Faculty of Science and Natural Resources (Fakulti Sains dan Sumber Alam, FSSA), Universiti Malaysia Sabah, Kota Kinabalu, Sabah, Malaysia. The laboratory work also has been done in the facilities of FSSA.

REFERENCE

Adegoke, J.A., Egbeyele, G. & Akinyemi, O.D. 2016. Effect of CEC of clay on thermal conductivity. *Malaysian Journal of Science*, Vol. 35 (2), Pp. 107-116.

Al-Ajmi, Hussain & Hinderer, Matthias & Keller, Martin & Rausch, Randolf & Blum, Philipp & Bohnsack, Daniel. 2010. The Role of Outcrop Analogue Studies for the Characterization of Aquifer Properties. *International Journal of Water Resources and Arid Environments.* **1(1)**: 48-54, 2011ISSN 2079-7079

Azfar Mohamed, Abdul Hadi Abd Rahman & Mohd Suhaili Ismail. 2016. Sedimentary Facies of the West Crocker Formation North Kota Kinabalu-Tuaran Area, Sabah, Malaysia. *IOP Conf. Ser.: Earth Environ. Sci*. **30** 012004

Basri, Kasbi & Wahab, Norhaliza & Abu Talib, Mohd Khaidir & Zainorabidin, Adnan. (2019). Sub-surface Profiling Using Electrical Resistivity Tomography (ERT) with Complement from Peat Sampler. *Civil Engineering and Architecture*. **7**. 7-18. 10.13189/cea.2019.071402.

Chafouq, D.; Mandour, A.E.; Elgettafi, M.; Himi, M.; Bengamra, S.; Lagfid, Y.; Casas, A. 2016. Assessing of saltwater intrusion in Ghiz-Nekor aquifer (North Morocco) using electrical resistivity tomography. *Near Surf. Geosci*, Pp.1–6

Carrera, J., Hidalgo, J. J., Slooten, L. J., & V zquez-Su, E. 2010. Computational and conceptual issues in the calibration of seawater intrusion models. *Hydrogeology Journal*, **18**: 131-145.

Collenette, P. 1958. *The Geology and Mineral Resources of the Jesselton- Kota Kinabalu Area, North Borneo*. W.J.Chater, Government Printer.

Duque, C., Calvache, M. L., Pedrera, A., Rosalees, W. M. & Chicano, M.L. 2008. Combined time domain electromagnetic soundings and gravimetry to determine marine intrusion in a detrital coastal aquifer (Southern Spain). *Journal of Hydrology*, 536-547.

EPA. 2014. Sediments. In Water: Pollution Prevention & Control. Retrieved from http://water.epa.gov/polwaste/sediments/).

Fitterman, D.V., Stewart. M.T. 1986. Transient electromagnetic sounding for groundwater. *Geophysics*, **51(4)**: 995-1005.

Giambastiani BMS, Macciocca VR, Molducci M, Antonellini M. Factors Affecting Water Drainage Long-Time Series in the Salinized Low-Lying Coastal Area of Ravenna (Italy). Water. 2020; 12(1):256. https://doi.org/10.3390/w12010256.

Green T.R. 2016. Linking Climate Change and Groundwater. In: Jakeman A.J., Barreteau O., Hunt R.J., Rinaudo JD., Ross A. (eds) *Integrated Groundwater Management*.

Griffiths, D. and R. Barker, 1993. Two-dimensional resistivity imaging and modelling in areas of complex geology. *Journal of applied Geophysics,* 1993. 29(3-4): p. 211-226.

Griggs, G. & Reguero, B.G. 2021. Coastal Adaptation to Climate Change and Sea-Level Rise. *Water*, **13**, 2151. https://doi.org/10.3390/w13162151

Hardianshah, S. & Abdul Rahim, S. 2013. Geo-electrical resistivity characterization of sedimentary rocks in dent peninsular, lahad datu, sabah. *Borneo Science*, **32**.

Hickin, E. J. (Ed.). 1995. *River Geomorphology*. Chichester: Wiley.

Jacobson, G. 1970. Gunong Kinabalu area, Sabah, Malaysia. *Geological Survey Malaysia. Report 8*.

Jain C.K. 2011. Salinity. In: Singh V.P., Singh P., Haritashya U.K. (eds) *Encyclopedia of Snow, Ice and Glaciers. Encyclopedia of Earth Sciences Series*. Springer, Dordrecht. https://doi.org/10.1007/978-90-481-2642-2_461.

Jiao, J., & Post, V. 2019. Impact of Land Reclamation on Coastal Groundwater Systems. In *Coastal Hydrogeology* (pp. 255-282). Cambridge: Cambridge University Press. doi:10.1017/9781139344142.009.

Kanagaraj G, Elango L, Sridhar SGD and Gowrisankar G. 2018. *Environmental Science and Pollution Research*, **25**. 8989.

Khublaryan, M.G., A.P. Frolov, and I.O. Yushmanov. 2008. Seawater intrusion into coastal aquifers. *Water Resources*, **35(3)**: 274–86.

Lam, Y., Winch, P.J., Nizame, F.A. Broaduss-Shea, E.T., Harun, M.G.D & Surkan, P.J. 2021. Salinity and food security in southwest coastal Bangladesh: impacts on household food production and strategies for adaptation. *Food Sec*, **2021**. https://doi.org/10.1007/s12571-021-01177-5.

Lambiase, J.J., Tzong, T.Y., William, A.G., Bidgood, M.D., Brenac, P., and Cullen, A.B., 2008, The West Crocker formation of northwest Borneo: A Paleogene accretionary prism, *ln* Draut, A.E., Clift, p.D., und Scholl, D.W., eds., Formation and Applications of the Sedimentary Record in Arc Collision Zones: *Geological Society of America Special* paper 436, p. l7 l-184, doi: 1 0.1 1 30/2008.2436(08).

Lee, Jin-Yong & Song, Sung-Ho. 2007. Evaluation of groundwater quality in coastal areas: Implications for sustainable agriculture. *Environmental Geology*. **52**. 1231-1242. 10.1007/s00254-006-0560-2.

Loke, M., 1992. *Electrical imaging surveys for environmental and engineering studies. A practical guide to 2-D and 3-D surveys*.

Long, M., Donohue, S., L'Heureux, J-S., Solberg, I-L., Rønning, J-S, Limacher, R., O'Connor, P., Sauvin, G., Rømoen, M. and Lecomte, I. 2012. Relationship between electrical resistivity and basic geotechnical parameters for marine clays. *Canada Geotech. J.* Vol. 49, Pp.1–11.

Majeed Faisal, Shariff A.K. Omang & Sanudin HJ. Tahir. 1994. Geology of Kota Kinabalu and its implications to groundwater potential. *Bulletin Geol. Soc. Malaysia*, **38**, 11-20.

McNeill J. D. 1980. *Survey Interpretation Techniques*. Geonics, Ltd., Misissauga, Canada, Technical Note TN-5.

Michael, H. A., Russoniello, C. J., & Byron, L. A. 2013. Global assessment of vulnerability to sea-level rise in topography-limited and recharge-limited coastal groundwater systems. *Water Resources Research*, **49**: 2228-2240.

Miller, G.T. 2000. Living in the Environment, Brooks/Cole Publishing Company, Pacific Grove. Haines, Skyring, Stephens, Papworth (2001) Managing Lake Wollumboola's Odour Problem. Proc. 11th NSW Coastal Conference, Newcastle 13-16 November 2001.

Mohd. Kamal. 2011. Kimanis power plant field subsurface exploration log. STL Geotechnical Engineering Sdn. Bhd. Unpublished report.

Moser, S. C., M. A. Davidson, P. Kirshen, P. Mulvaney, J. F. Murley, J. E. Neumann, L. Petes, and D. Reed, 2014: Ch. 25: Coastal Zone Development and Ecosystems. Climate Change Impacts in the United States: The Third National Climate As-sessment, J. M. Melillo, Terese (T.C.) Richmond, and G. W. Yohe, Eds., U.S. Global Change Research Program,579-618. Springer,Cham.

Musta, B., Asat, M.A., Ling, S.Y. & Saleh, H. 2022. Geophysical Investigation and Geochemical Study of Sediment along the Coastal Area in Kota Belud Sabah, Malaysia. *Journal of Physics: Conference Series*, **2165 (1).**

Nawal Alfarrah and Kristine Walraevens, 2017. Groundwater Overexploitation and Seawater Intrusion in Coastal Areas of Arid and Semi-Arid Regions. *Water*, **10**, 143; doi:10.3390/w10020143.

Nassir, A.S.S. Loke, M.H. Lee, C.Y & Nawawi, M.N.M. 2000. Salt-water intrusion mapping by geoelectrical imaging surveys. *Geophys. Prospect*, Vol. 48, 647–661.

Norzaida Abas, Zalina Mohd Daud, Norazizi Mohamed & Syafrina Abdul Halim, 2017. Climate change impact on coastal communities in Malaysia. *Journal of Advanced Research Design*. **33**. 1-7.

Ohrel, R. and Register, K. 2006. *Volunteer Estuary Monitoring: A Methods Manual*. U.S. Environmental Protection Agency (EPA), Office of Wetlands, Oceans and Watersheds, The Ocean Conservancy.

Radke, L.C. 2002. Water allocation and critical flows: potential ionic impacts on estuarine organisms. *Proceedings of Coast to Coast 2002 – "Source to Sea",* Tweed Heads, pp. 367-370.

Song, S.H.; Lee, J.Y.; Park, N. 2007. Use of vertical electrical soundings to delineate seawater intrusion in a coastal area of Byunsan, *Korea. Environ. Geol*, Vol. 52, Pp. 1207–1219

Stewart. M.T. 1982. Evaluation of Electromagnetic Methods for Rapid Mapping of Salt-Water Interfaces in Coastal Aquifers. *Groundwater*, **20 (5)**: 538-545.

Sudaryanto and Wilda Naily. 2018. Ratio of Major Ions in Groundwater to Determine Saltwater Intrusion in Coastal Areas. *IOP Conf. Ser.: Earth Environ. Sci*. **118** 012021.

Tol, R.S.J. 2009. Economics of Sea Level Rise, Editor(s): John H. Steele, Encyclopedia of Ocean Sciences (Second Edition), Academic Press, Pages 197-200, ISBN 9780123744739, https://doi.org/10.1016/B978-012374473-9.00774-8.

Van Biersel, T.P., D.A. Carlson, and L.R. Milner. 2007. Impact of hurricane storm surges on the groundwater resources. *Environ Geol*, 53: 813–26.

Zakiyah Ainul Kamal, Mohd Syakir Sulaiman, Muhammad Khairul Hakim, Thilageswaran, Anis Syahira, Zahidi Hamzah and Mohammad Muqtada Ali Khan. 2020. Investigation of Seawater Intrusion in Coastal Aquifers of Kelantan, Malaysia using Geophysical and Hydrochemical Techniques. *IOP Conf. Ser.: Earth Environ. Sci*. 549 012018.

BorneoScience
The Journal of Science & Technology
Volume 43 Issue 2 : Oct 2022
Online ISSN : 2231-9085 | ISSN : 1394-4339

RECOVERY OF USED LUBRICATING OIL BY GLACIAL ACETIC ACID WITH TWO DIFFERENT ACTIVATED CARBONS

S. M. Anisuzzaman[1,2]* and Mohammad Hafiz Jumaidi[2]

[1]Energy Research Unit (ERU),
[2]Chemical Engineering Programme, Faculty of Engineering,
Universiti Malaysia Sabah, 88400 Kota Kinabalu, Sabah, Malaysia.

*Corresponding author: anis_zaman@ums.edu.my

Received 23rd June 2022; accepted 11th July 2022
Available online 1st Nov 2022
Doi: https://doi.org/10.51200/bsj.v43i2.4510

ABSTRACT: *Recovery of used lubricating oil (ULO) generally comprises cleaning, drying, and adsorption in order to eliminate water, sludge, and impurities. As the ULO is one of the hazardous wastes generated in various industrial and automotive industries, it should not be used or disposed of in ways that are harmful to the environment. The main purpose of this study was to investigate the effectiveness of two different types of activated carbons (ACs) which are coconut AC (CAC) and rice husk AC (RHAC) in recovering the ULO. Glacial acetic acid was used in the acid treatment as it does not react with the base oils, and the ACs were substituted with the clay used in the clay treatment. The recovered oil was analysed through analytical characterizations, which are Fourier transform infrared spectroscopy (FTIR),* ultraviolet-visible *(UV-vis) spectroscopy and atomic absorption spectrometry (AAS). FTIR analysis revealed that the properties of the untreated ULO samples improved by removing the carbonyl compounds. In terms of metal removal, RHAC had shown better performance than CAC as it gave low metal contents in AAS. The response surface methodology (RSM) was used to study the optimum process parameters that would maximise the efficiency of the process. There are two factors that were manipulated, which are the weight of adsorbent (A) and speed of mixing (B). For CAC, the optimum value of factors A was 4.00 g while the B was set to 524.89 rpm. Meanwhile, for RHAC, the optimum value of factors A was 2.29 g while the B was set to 4000 rpm. CAC has higher desirability with 0.83 compared to RHAC with 0.69.*

KEYWORDS: Acid clay treatment; activated carbon; optimization; response surface methodology; used lubricating oil

INTRODUCTION

Lubricating oil (LO) is base oil mixed with additives to enhance their characteristics, which can be used to minimize wearing that is caused by physical friction [1]. During usage, the LO will undergo changes in terms of degradation, oxidation, and contamination, which make the lubricating oil ineffective for further application and need to be replaced [2]. Used lubricating oil (ULO) is a highly

hazardous waste that requires responsible management due to increasing quantities generated by automotive and industrial activities worldwide. It can cause a detrimental effect on the environment if it is not properly disposed of, handled, or treated [3,4]. Normally, ULO has high contaminants such as carbon residue, asphaltenic materials, heavy metals, water, and others [5]. Such pollutants can cause pollution to the environment to a large extent, where each volume can pollute not less than two hundred and fifty thousand volumes of water [6,7]. Developing countries have rapid urbanization and industrialization activity that has resulted in a large number of industrial wastes consisting of ULO. The percentage has been increasing throughout the years due to modernization and urbanization. It can be said that improper management of ULO can cause detrimental effects not just to the environment but also to humankind when it is not treated properly. Thus, in order to solve this problem, recovery of ULO can be one of the possible solutions [8-11]. Recovery of ULO has many advantages which include it is environmentally friendly, cost-effective and consumes lower energy in recycling.

Various treatment technologies are applied in order to recover and reclaim the ULO to its base oil form and remove contaminants [11-14]. Udonne [15] stated that acid clay method is the best method in recycling ULO. A comparative study had been conducted between different methods of recycling ULO. Acid- clay method using acetic acid is more effective compared to sulphuric acid in ULO recovery [16]. Hamawand *et al.* [16] concluded that acetic acid does not react chemically with the base oil compared to sulphuric acid, which reacts with base oil and might release sulphur dioxide to the atmosphere. However, the acid-clay method for the re-refining of ULO produces residual sludge which can pollute the soil and give low yield [17]. There are several research papers that use activated carbon (AC) in the treatment of the ULO [18,19]. According to a research conducted by Abdel-Jabbar *et al.* [5], they managed to recover the ULO by using various types of adsorbents such as date palm kernels powder, bentonite, and eggshell powder. The AC used in the treatment is a good material for the treatment of ULO, especially to reduce metal concentrations [18]. However, to date, the optimisation of the process parameters for ULO treatment by adsorption process using adsorbents is still lacking in much of the published literature.

Hence, the aim of this study was to recover oil from ULO and optimise the parameters to produce the high-quality base LO as well as to reduce the environmental impacts. In this study, there were two types of AC which are coconut AC (CAC) and rice husk AC (RHAC) used to recover the ULO. This study focused on the effectiveness of those ACs by characterizing the recovered oil and optimized the value for parameters in order to obtain the minimized value for both absorbances. The parameters such as weight of adsorbent and speed of mixing were optimized using the response surface methodology (RSM). Meanwhile, the responses that are being observed are the absorbance of fourier transform infrared spectroscopy (FTIR) and absorbance of ultraviolet-visible (UV-vis) spectroscopy.

MATERIALS AND METHODS

Materials

ULO samples (were collected from local car oil-change shops. The powdered CAC and RHAC had been obtained from Zhengzhou Zhongchuang Water Purification Material Co., Ltd, China. Glacial acetic acid (purity, 99.5%) for acid treatment was purchased from Sigma Aldrich. The recovered oil

was analysed through analytical characterizations, which are FTIR (Bruker INVENIO® R), UV-vis spectroscopy (Perkin Elmer LAMBDA™ 365) and atomic absorption spectrometry (AAS) (Hitachi Z-5000 Polarized Zeeman Flame/Graphite Furnace). Table 1 shows the physical characterization data for both ACs.

Table 1. Physical characterization data of powdered CAC and RHAC

Sl. no	Description	Unit	Detection result
1	Particle size	mesh	200
2	Iodine value	mg/g	700
3	Moisture	%	5
4	Ash content	%	5
5	Methylene blue	mg/g	90
6	Proportion	kg/m^2	500

Experimental procedure

Before undergoing acid clay treatment, it is important that moisture content be removed completely from the ULO. The ULO sample was heated up in the oven at 250ºC for approximately 1 h [20]. After that, the oil was allowed to cool down to room temperature before proceeding to the next step, filtration. The dehydrated oil was then filtered using a vacuum pump to remove any debris or impurities from the oil. In the acid treatment, 1 ml of glacial acetic acid was added into 10 ml of filtered oil followed up by heating and stirring using the hot plate under room temperature for about 1 h [16]. After that, the mixture was allowed to settle down for 24 h at room condition. The last step in acid treatment was to undergo centrifugation for 1 h in order to separate base oil from any contaminants. After acid treatment, AC treatment took place and 15 ml of the treated oil was mixed with 1 g, 2.5 g and 4 g of the AC. The same step was done for both ACs. The mixture of the adsorbent and the oil were heated up to 250ºC and centrifuged with different speeds of 500 rpm, 2300 rpm and 4000 rpm for 30 min [16]. The oil was filtered by using filter paper and the final oil recovered from the treatment was analysed.

FTIR analysis

FTIR analysis of the recovered oil was undergone in order to determine the functional groups. The range of FTIR used was in between 4000-400 cm^{-1}.

Concentration using UV-vis spectroscopy

UV-vis spectroscopy analysis of the recovered oil was undergone to determine concentration of oil sample. As the colour of treated LO remained dark, the absorbance of the treated EO was high as well. Treated oil samples (1 ml) were diluted with kerosene (10 ml) before being examined using a UV-vis spectrophotometer. Kerosene was selected because it is more suitable for mass spectrometric analysis [21].

Metal content analysis

Before the analysis, the recovered oil sample was heated to 60°C, stirred to ensure the homogeneity of the sample and was combined with ten volumes of kerosene (ratio 1:10) [22]. Metal concentrations were determined from the calibration curve obtained from standard solutions.

RSM modelling

RSM is known as a collection of mathematical and statistical techniques for empirical modelling. The main objective of RSM was to maximize the response that is influenced by various independent variables. The optimization was created using Design Expert 12 to evaluate the numerical accuracy and precision of the models developed. Performance evaluation apps are known as excellent indicators. In this study, a 3-level factorial design was applied. Other designs that are commonly used, for example Box-Behnken and central composite design (CCD) are usually used for more than two factors as the full factorial design needs more experimental runs than 3-level factorial. Before applying the RSM technique, it is necessary to select an experimental design to determine the courses that should be carried out within the experimental range being studied. There are two factors that were manipulated, which are the weight of adsorbent (A) and speed of mixing (B). The range of A was 1 g to 4 g for 15 ml of ULO while the range of B was 500 rpm to 4000 rpm [23]. Table 2 shows the model information used in RSM.

Table 2. Model information used in RSM

Factor	Units	Type	Coded low	Coded high
A	g	Numeric	-1 ↔ 1.00	1 ↔ 4.00
B	rpm	Numeric	-1 ↔ 500.00	1 ↔ 4000.00

RESULTS AND DISCUSSION

FTIR analysis

In this study, the virgin lubricating oil (VLO) was used as a reference to identify the effectiveness of the adsorption. Figure 1 shows the FTIR analysis of VLO and ULO.

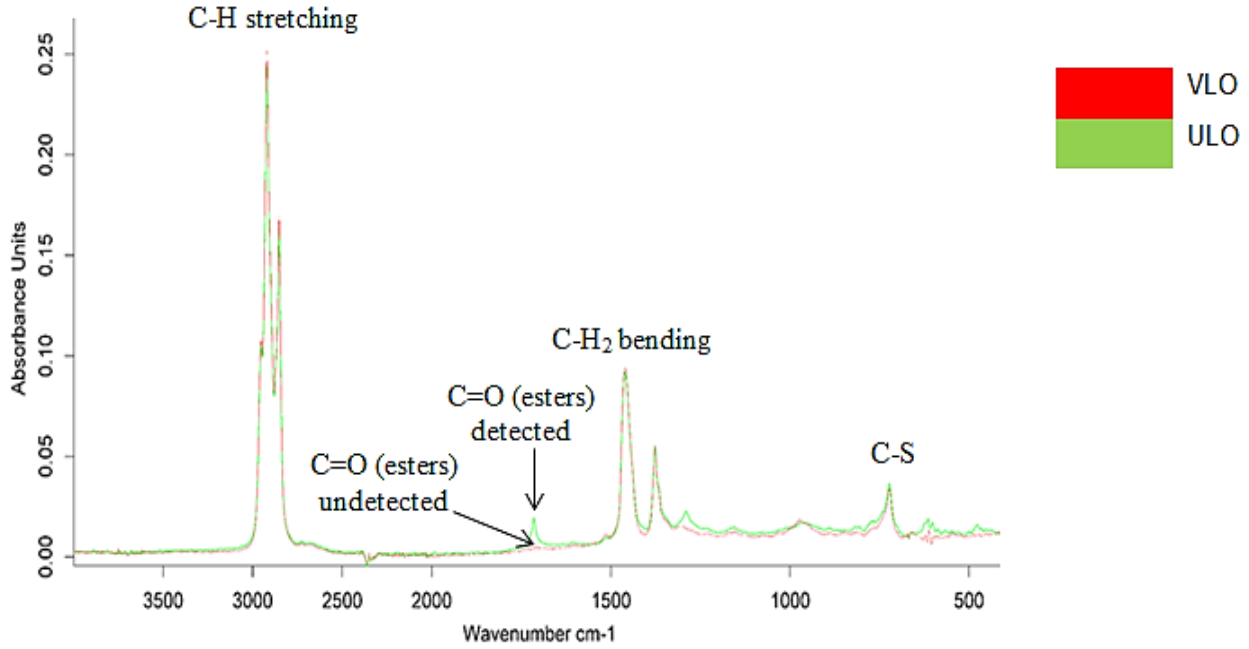

Figure 1. FTIR analysis of VLO and ULO

Table 3 shows the wavelengths of components that were found in VLO and ULO

Table 3. Wavelengths of components that were found in VLO and ULO

Sample	Wavelength (cm^{-1})				
	C-H stretching	C-H_2 bending	C=O (esters)	C-S	S=O stretching
VLO	2921.07 2852.46 1376.78	1460.13	UD	722.59	UD
ULO	2921.06 2852.47 1376.80	1460.35	1715.23	722.59	UD

Based on Figure 1 and Table 3, it was observed that the VLO contains C-H stretching with a wavelength at 2921.07 cm^{-1} , 2852.46 cm^{-1} and 1376.78 cm^{-1} whilst C-H_2 bending found at 1460.13 cm^{-1} and C-S was found at at 722.59 cm^{-1}. According to Timur [24], the LOs consist of long chain hydrocarbons. Other components such as carbonyl groups which are caused by oxidation were undetected (UD). Meanwhile for ULO, it also contains C-H stretching with a wavelength at 2921.06 cm^{-1}, 2852.47 cm^{-1} and 1376.80 cm^{-1} whilst C-H_2 bending is found at 1460.35 cm^{-1} and C-S group was found at at 722.59 cm^{-1}. However, the presence of carbonyl group at wavelength of 1715.23 cm^{-1} with higher absorbance units indicated that the ULO was being contaminated due to the oxidation**.** Based on a study conducted by Honda T and Sasaki [25], the causes of lubricating oil contamination are roughly classified into two types: the contamination caused by solid particles and oil oxidation products.

After undergoing acid clay treatment using the two different types of AC, it had improved the properties of the ULO by removing the carbonyl compound that was originally present in the ULO. However, S=O group was found in a few samples of oil that had been treated. Figure 2 shows FTIR analysis of treated ULO using CAC (samples A-M).

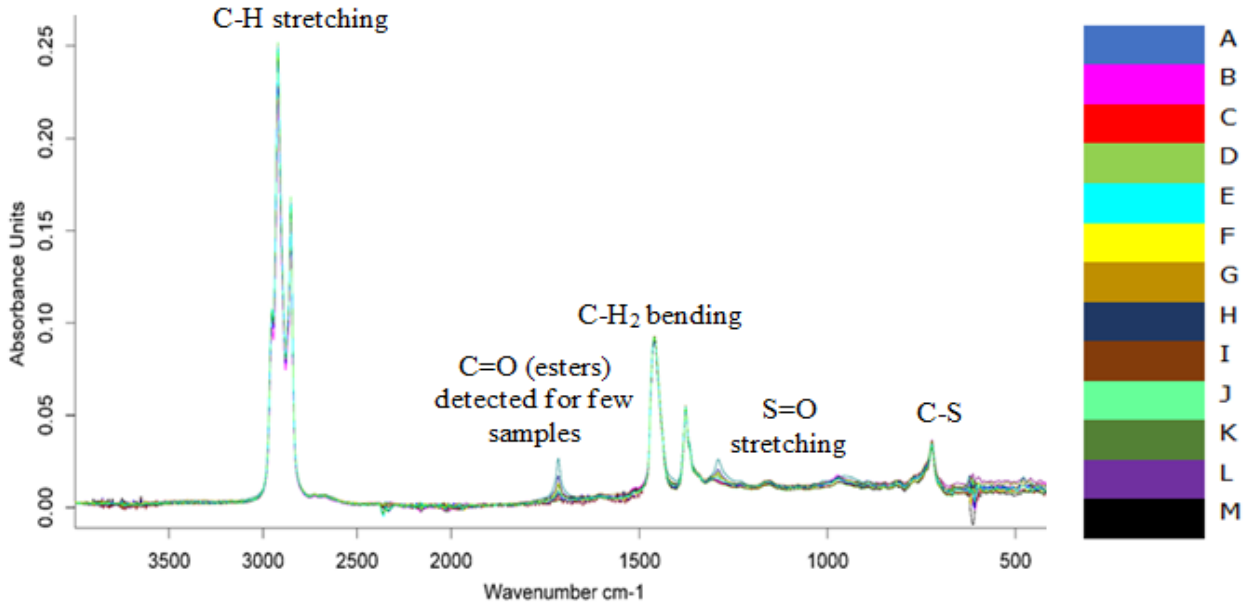

Figure 2. FTIR analysis of treated ULO using CAC

Table 4 shows wavelengths of components that were found in the treated ULO using CAC (samples A-M).

Table 4. Wavelengths of components that were found in the treated using CAC

Samples	Wavelength (cm^{-1})				
	C-H stretching	$C-H_2$ bending	C=O (esters)	C-S	S=O stretching
A	2921.08 2852.45 1376.59	1458.16	UD	722.29	UD
B	2921.12 2852.48 1376.75	1460.09	1715.23	722.69	1289.83
C	2921.12 2852.47 1376.73	1459.96	UD	722.23	UD
D	2921.14 2852.50 1376.76	1460.01	UD	722.37	UD
E	2921.17 2852.49 1376.78	1460.15	UD	722.25	UD
F	2921.20 2852.51 1376.77	1460.41	1714.94	721.98	UD
G	2921.13 2852.47 1376.74	1460.15	UD	722.20	UD
H	2921.19 2852.51 1376.74	1460.02	1715.29	722.19	1290.13
I	2921.11 2852.50 1376.63	1459.29	UD	722.13	UD
J	2921.03 2852.41 1376.63	1460.04	UD	722.07	UD
K	2921.12 2852.47 1376.77	1460.18	1715.36	722.18	1289.99
L	2921.17 2852.52 1376.80	1459.97	1715.27	721.85	1290.55
M	2921.15 2852.48 1376.67	1459.05	UD	722.35	UD

For CAC, samples B, F, H, K, and L were indicated the presence of the carbonyl group at 1715.23 cm^{-1}, 1714.94 cm^{-1}, 1715.29 cm^{-1}, 1715.36 $cm^{-1}$and 1715.27 cm^{-1}, respectively. The presence of S=O was also found in samples B, H, K and L at 1289.83 cm^{-1}, 1290.13 cm^{-1}, 1289.98 cm^{-1} and 1290.55 cm^{-1}. Figure 3 shows FTIR analysis of treated ULO using RHAC (samples A1-M1).

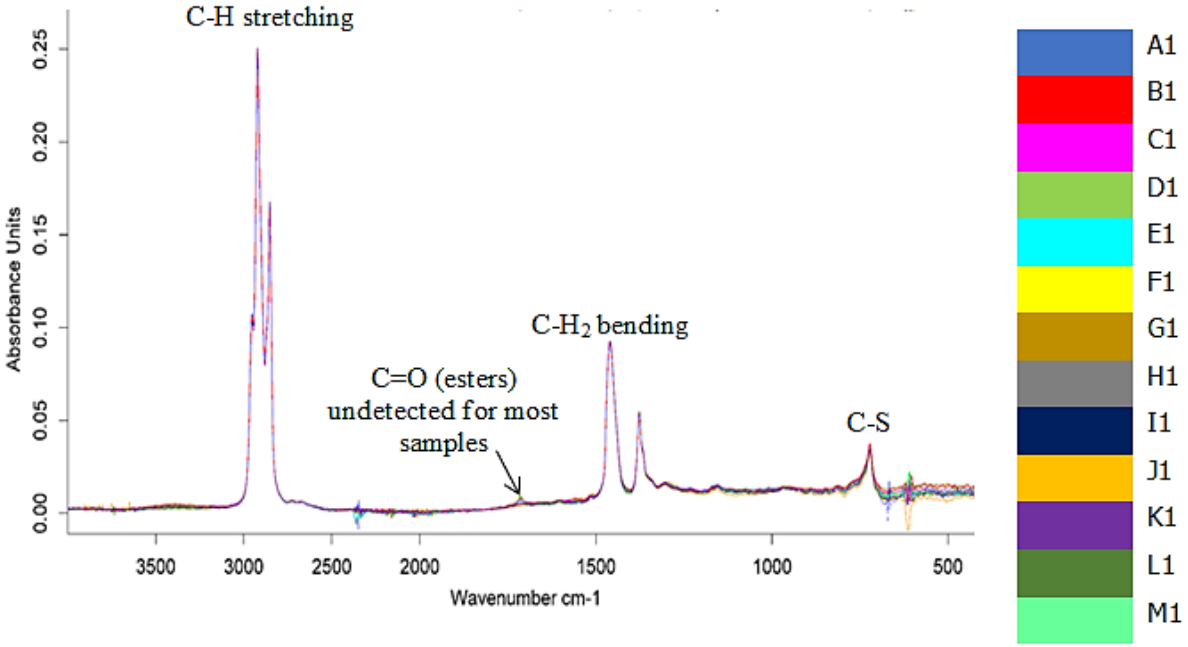

Figure 3. FTIR analysis of treated ULO using RHAC

Table 5 shows wavelengths of components that were found in the treated ULO using RHAC (samples A1-M1).

Table 5. Wavelengths of components that were found in the treated ULO using RHAC

Samples	Wavelength (cm^{-1})				
	C-H stretching	$C-H_2$ bending	C=O (esters)	C-S	S=O stretching
A1	2921.18 2852.49 1376.73	1460.08	UD	721.85	UD
B1	2921.13 2852.47 1376.72	1460.16	UD	722.04	UD
C1	2921.16 2852.47 1376.74	1460.24	UD	721.95	UD
D1	2921.13 2852.51 1376.76	1460.13	UD	722.03 609.88	UD

E1	2921.16 2852.49 1376.75	1460.20	1715.88	722.27 609.50	UD
F1	2921.20 2852.48 1376.74	1460.19	UD	722.32	UD
G1	2921.11 2852.46 1376.73	1460.14	UD	721.80	UD
H1	2921.12 2852.48 1376.71	1460.10	UD	722.13	UD
I1	2921.17 2852.51 1376.74	1460.24	UD	722.09 609.77	UD
J1	2921.14 2852.48 1376.72	1460.33	UD	722.19	UD
K1	2921.05 2852.46 1376.75	1460.42	UD	722.23	UD
L1	2921.15 2852.46 1376.73	1460.45	UD	722.29	UD
M1	2921.14 2852.52 1376.72	1459.87	1715.90	722.48	UD

Based on Figure 3 and Table 5, for RHAC, samples E1 and M1 indicated the presence of the carbonyl group at wavelength of 1715.88 cm^{-1} and 1715.90 cm^{-1}, respectively. Meanwhile, the presence of S=O was not found in the samples.

UV-vis spectroscopy analysis

Table 6 shows the absorbance values of LO samples analysed by UV-vis spectroscopy. The VLO peak identified at 665.1 nm was used to analyse the absorbance. As on Table 6, at peak of 665.1 nm, the absorbance VLO was 0.023 whilst for ULO was 3.427. This shows that ULO has higher absorbance which means the quantity of light that passes is high due to the high concentration and the colour of the oil is darker. It also can be observed that all the samples that have been treated showed lower absorbance than untreated ULO. It means the adsorption process managed to improve the colour of the treated samples. For oil treated by CAC (samples A-M), the highest absorbance can be obtained in sample I with 2.957 while the lowest absorbance is in sample 0.603. Meanwhile for oil samples treated with RHAC (samples A1-M1), the highest absorbance can be obtained is 2.582 in sample K1 and the lowest absorbance is in sample C1 with 0.857.

Table 6. Absorbance analysed using UV-vis spectroscopy

Samples	Peak = 665.1 nm Absorbance
VLO	0.023
ULO	3.427

Oil treated using CAC		Oil treated using RHAC	
Samples	Absorbance	Samples	Absorbance
A	0.603	A1	1.269
B	1.644	B1	1.873
C	1.308	C1	0.857
D	1.596	D1	0.902
E	1.361	E1	1.044
F	1.738	F1	0.949
G	2.024	G1	2.284
H	1.235	H1	1.076
I	2.957	I1	1.951
J	2.656	J1	2.387
K	2.769	K1	2.582
L	0.976	L1	1.806
M	1.246	M1	1.193

AAS analysis

Table 7 shows the metal content found in the VLO, untreated ULO and ULO samples after being treated using CAC and RHAC. Table 7 shows that in the VLO, no metal content such as Pb, Cu and Fe was found, while for untreated ULO all of these metals were obtained. For oil samples treated using CAC, no Pb content was found, meaning the metal was fully absorbed by the ACs (Table 7). Meanwhile, for metal Cu, there was a decrease after being treated. Even samples D, I, and M showed no Cu content. For Fe, the metal content only showed a slight decrease after being treated. Only one sample E showed no Fe content. For oil samples treated using RHAC, metal content of Pb was fully absorbed after being treated (Table 7). Meanwhile, for metal Cu, it experienced a significant decrease after being treated. Samples B1, G1, I1 and J1 showed no metal content of Cu. For metal Fe, the metal content also showed a significant decrease after being treated.

Table 7. Metal content found in LO samples

Samples	Metal content (ppm)		
	Pb	Cu	Fe
VLO	0.0000	0.0000	0.0000
ULO	0.0121	0.3680	4.1623

Oil treated using CAC				Oil treated using RHAC			
	Pb	Cu	Fe		Pb	Cu	Fe
A	0.0000	0.0954	0.2964	A1	0.0000	0.1174	1.1766

B	0.0000	0.1613	0.6338	B1	0.0000	0.0000	0.4431
C	0.0000	0.1503	2.1156	C1	0.0000	0.0132	1.0813
D	0.0000	0.0000	3.2600	D1	0.0000	0.0570	1.4261
E	0.0000	0.0845	0.0000	E1	0.0000	0.0680	1.4847
F	0.0000	0.0351	1.0739	F1	0.0000	0.0516	1.3600
G	0.0000	0.0077	2.5300	G1	0.0000	0.0000	0.8319
H	0.0000	0.1009	1.4114	H1	0.0000	0.0680	0.6045
I	0.0000	0.0000	3.1406	I1	0.0000	0.0000	0.6045
J	0.0000	0.0241	2.6931	J1	0.0000	0.0000	0.7365
K	0.0000	0.1448	3.0305	K1	0.0000	0.0516	1.0373
L	0.0000	0.1229	1.3820	L1	0.0000	0.0132	0.7952
M	0.0000	0.0000	2.4217	M1	0.0000	0.1174	1.2500

Optimization of experimental design by using RSM

The Table 8 and Table 9 represent the sets of experiments in the model run in Design Expert 12 for CAC and RHAC, respectively. Both the tables also show the responses obtained after experiments had been conducted.

Table 8. Set of experiments in the RSM model for CAC

Run	Factor 1 (A)	Factor 2 (B)	Response 1 (FTIR)	Response 2 (UV-vis spectroscopy)
1	4	500	0.02951	0.603
2	2.5	2300	0.02252	1.644
3	2.5	4000	0.0163	1.308
4	4	4000	0.01446	1.596
5	4	2300	0.01315	1.361
6	1	2300	0.01233	1.738
7	2.5	2300	0.01145	2.024
8	2.5	500	0.01110	1.235
9	2.5	2300	0.00199	2.957
10	2.5	2300	0.00198	2.656
11	1	4000	0.00099	2.769
12	1	500	0.00098	0.976
13	2.5	2300	0.00097	1.246

Table 9. Set of experiments in the RSM model for RHAC

Run	Factor 1 (A)	Factor 2 (B)	Response 1 (FTIR)	Response 2 (UV-vis spectroscopy)
1	4	500	0.00055	1.269
2	2.5	2300	0.0001	1.873
3	2.5	4000	0.00101	0.857
4	4	4000	0.00178	0.902
5	4	2300	0.00171	1.044
6	1	2300	0.00192	0.949
7	2.5	2300	0.0008	2.284
8	2.5	500	0.00092	1.076
9	2.5	2300	0.00043	1.951
10	2.5	2300	0.00041	2.387
11	1	4000	0.00048	1.582
12	1	500	0.00046	1.806
13	2.5	2300	0.00089	1.193

Optimization of experimental design using RSM for CAC

The statistical analysis of this experiment was dependent on the analysis of variance (ANOVA). The analysis was done by studying the p- value, $R^2$and adjusted R^2 [26, 27]. The statistical analysis was tabulated based on the ANOVA variance analysis.

Effect of parameters on the absorbance of FTIR for CAC

After analysis had been conducted, the suggested modelling technique was a linear model for the absorbance of FTIR. After applying the developed model using the previously defined data, the following pre-model has been obtained. Equation (1) shows the final equation for absorbance of FTIR in terms of actual factors.

$$R = 0.031657 - 0.005704 \times A - 2.98713 \times 10^{-6} \times B \quad (1)$$

Where R represents absorbance of FTIR for CAC; A represents weight of adsorbent, g; B represents speed of mixing, rpm

Regression coefficients and ANOVA for the predicted response surface model shows in Table 10.

Table 10. ANOVA for the absorbance of FTIR for CAC

Source	Sum of Squares	Mean Square	F-value	p-value	
Model	0.0006	0.0003	7.93	0.0086	significant
A	0.0004	0.0004	11.55	0.0068	
B	0.0002	0.0002	4.31	0.0645	
Residual	0.0004	0.0000			
Lack of fit	0.0001	0.0000	0.4138	0.8398	not significant
Pure error	0.0002	0.0001			
Cor total	0.0010				

Standard deviation	0.0062	R^2	0.6134
Mean	0.0106	Adjusted R^2	0.5361
C.V. %	58.21	Predicted R^2	0.3831
	Adequate precision		9.3062

Based on Table 10, it was observed that the calculated model F-value of 7.93 (as it is desirable to have the biggest value) which implies the model is significant [21]. However, to specify that model terms are significant, p-value should be less than 0.05. p-value less than 0.05 indicate model terms are significant (Table 10). Behera *et al.* [28] stated that the larger the F-value and the lower the p-value implies that the model is significant. There is only 0.86% chance that an F-value this large could occur due to noise. In this case only factor A is regarded as a significant model term. The lack of fit F-value of 0.4138 implies that the lack of fit is not significant relative to the pure error. There is an 83.98% chance that a Lack of Fit F-value this large could occur due to noise. Non-significant lack of fit is good as the model needs to be fitted. The 'Predicted R^2' of 0.3831 is in practical agreement with the 'Adjusted R^2' of 0.5361 with a difference of less than 0.2. Adequate precision measures the signal to noise ratio. A ratio greater than 4 is desirable. The ratio of 9.306 indicates an adequate signal. This model can be used to navigate the design space. Besides, the lower standard deviation portrays that a good model that gives a good value between predicted and actual value of the response [28]. Figure 4 shows the interactions between each component in a three-dimensional group based on ANOVA.

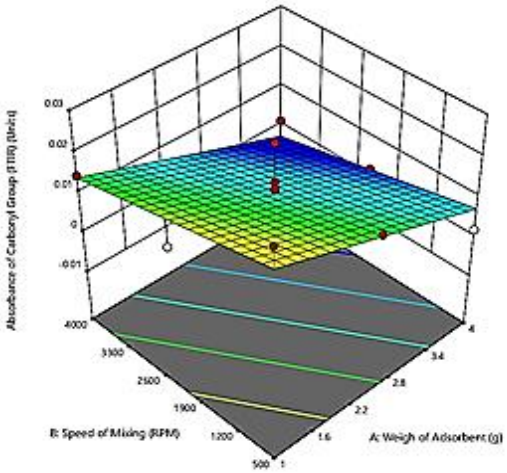

Figure 4. Variations in output experimental design with factors A and

Based on Figure 4, it illustrates the factors that affect the absorbance of FTIR for CAC. For factor A, as it is increased, the absorbance of the FTIR decreases. Meanwhile for factor B, the pattern was the same with factor A. Thus, it was found that with higher weight of adsorbent and speed of mixing, the absorbance of FTIR can be decreased.

Effect of parameters on the absorbance in UV-vis spectroscopy for CAC

Equation 2 shows the final equation for the absorbance in UV-vis spectroscopy in terms of actual factors

$$S = 1.60482 - 0.213667 \times A + 0.000277 \times B \quad (2)$$

Where S represents absorbance of UV-vis spectroscopy; A represents weight of adsorbent, g and B represents speed of mixing, rpm

Regression coefficients and ANOVA for the predicted response surface model shows in Table 11.

Table 11. ANOVA for the absorbance in UV-vis spectroscopy for CAC

Source	Sum of squares	Mean square	F-value	p-value	
Model	2.03	1.01	2.44	0.1371	not significant
A	0.6163	0.6163	1.48	0.2510	
B	1.41	1.41	3.39	0.0952	
Residual	4.15	0.4150			
Lack of fit	2.16	0.3607	0.7262	0.6548	not significant
Pure error	1.99	0.4966			
Cor total			6.18		

Standard deviation	0.6442	R^2	0.3279
Mean	1.70	Adjusted R^2	0.1935
C.V. %	37.87	Predicted R^2	-0.0121
	Adequate precision		5.2021

Table 11 shows that the F-value and p-value are 2.44 and 0.1371, respectively. These values clearly indicated that the model is not significant. There is a 13.71% chance that an F-value this large could occur due to noise. The lack of fit F-value of 0.7262 implies that this value is not significant relative to the pure error. The negative 'Predicted R^2" implies that the overall mean may be a better predictor of the response than the current model. In some cases, a higher order model may also predict better. Adequate precision was 5.2021 which indicate an adequate signal. Since it is higher than 4, thus this model can be used to navigate the design space. Figure 5 shows the interactions between each component in a three-dimensional group based on ANOVA.

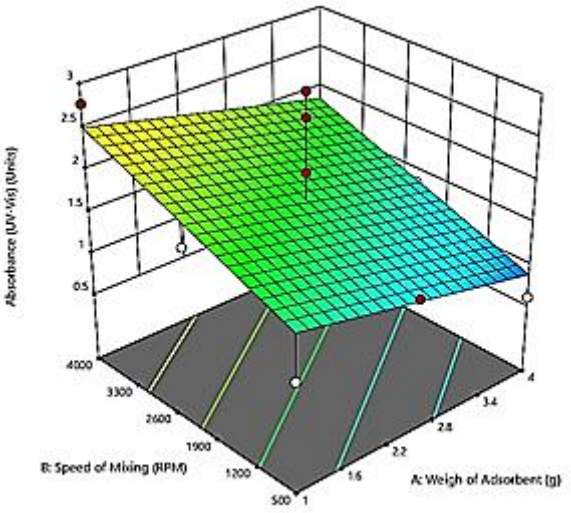

Figure 5. Variations in output experimental design with factors A and B

Based on Figure 5, it illustrates the factors that affect the absorbance of UV-vis spectroscopy. For factor A, as it is increased, the absorbance decreases. However, for factor Y, the pattern is not the same with factor A as the speed of mixing increases, the absorbance significantly increases. Thus, it can be concluded that with a higher weight of adsorbent and with lower speed of mixing, the absorbance in UV-vis spectroscopy can be decreased. According to Hussanin and Kamakar [29], the absorbance should be lower as the concentration of LO decreases, the absorbance should be decreased indicating that the oil is less deteriorated.

Effect of parameters on the absorbance of FTIR for RHAC

Equation 3 shows the final equation for absorbance of FTIR in terms of actual factors

$$R = 0.001990 - 0.001450 \times A + 2.08561 \times 10^{-7} \times B + 1.1356 \times 10^{-7} \times A \times B + 0.000265 \times A^2 - 8.1079 \times 10^{-11} \times B^2 \quad (3)$$

Regression coefficients and ANOVA for the predicted response surface model shows in Table 12.

Table 12. ANOVA for the absorbance of FTIR for RHAC

Source	Sum of squares	Mean square	F-value	p-value	
Model	1.869E-06	3.738E-07	1.18	0.4047	not significant
A	2.254E-07	2.254E-07	0.7127	0.4265	
B	2.993E-07	2.993E-07	0.9463	0.3631	
Residual	2.214E-06	3.162E-07			
Lack of Fit	1.802E-06	6.007E-07	5.84	0.0607	not significant
Pure Error	4.117E-07	1.029E-07			
Cor Total	4.083E-06				

Standard deviation	0.0006	R^2	0.4578
Mean	0.0009	Adjusted R^2	0.0705
C.V. %	63.79	Predicted R^2	-2.5141
	Adequate precision		4.0155

Table 12 shows that the F-value and p-value are 1.18 and 0.4047, respectively. These values clearly indicated that the model is not significant. There is a 40.47% chance that an F-value this large could occur due to noise. The lack of fit F-value of 5.84 implies that there is a 6.07% chance that a lack of fit F-value this large could occur due to noise. The negative 'Predicted R^2' implies that the overall mean may be a better predictor of the response than the current model. In some cases, a higher order model may also predict better. The ratio of 'Adequate precision' is 4.0155 which imply an adequate signal. Since the ratio is greater than 4, thus this model can be used to navigate the design space. Figure 6 shows the interactions between each component in a three-dimensional group based on ANOVA

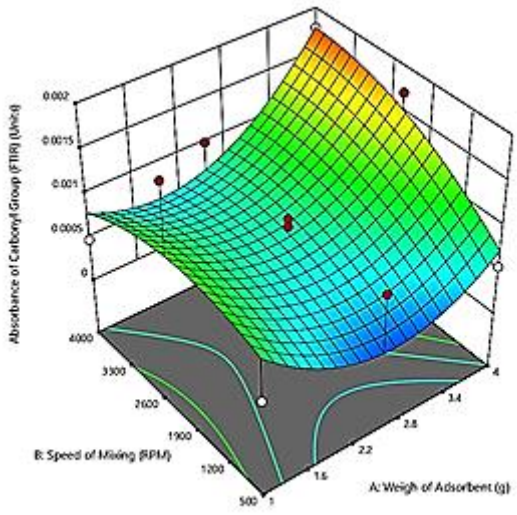

Figure 6. Variations in output experimental design with factors A and B

Based on Figure 6, it illustrates the factors that affect the absorbance of FTIR. For factor A, as it is increased, the absorbance of the FTIR decreases but only up to 2.5 g weight of adsorbent and then it increases back. Meanwhile for factor B, the pattern is vice versa with factor A whereas the speed of mixing increases, the absorbance of the FTIR also increases up until 2300 rpm and then it shows slightly decreases as the speed of mixing increases. Thus, it has found that there is a certain point that needs to be chosen in order to decrease the absorbance of the FTIR.

Effect of parameters on the absorbance of UV-vis spectroscopy for RHAC

Equation 4 shows the final equation the absorbance of UV-vis spectroscopy in terms of actual factors

$$S = 1.80555 - 0.124667 \times A - 0.000076 \times B \quad (4)$$

Regression coefficients and ANOVA for the predicted response surface model are shown in Table 13.

Table 13. ANOVA the absorbance of UV-vis spectroscopy for RHAC

Source	Sum of squares	Mean square	F-value	p-value	
Model	0.3158	0.1579	1.14	0.3569	not significant
A	0.2098	0.2098	1.52	0.2458	
B	0.1060	0.1060	0.7680	0.4014	
Residual	1.38	0.1380			
Lack of Fit	0.8908	0.1485	1.21	0.4449	not significant
Pure Error	0.4891	0.1223			
Cor Total			1.70		

Standard deviation	0.3715		R^2	0.1862
Mean	1.32	Adjusted R^2		0.0235
C.V. %	28.12	Predicted R^2		-0.2281
		Adequate precision		3.5850

Table 13 shows that the F-value and p-value are 1.14 and 0.3569, respectively. These values clearly indicated that the model is not significant. There is a 35.69% chance that an F-value this large could occur due to the noise. The lack of fit F-value of 1.21 implies the lack of fit is not significant relative to the pure error. There is a 44.49% chance that a lack of fit F-value this large could occur due to noise. The negative 'Predicted R^2' implies that the overall mean may be a better predictor of the response than the current model. In some cases, a higher order model may also predict better. The ratio of 'Adequate precision' is 3.5850 which implies an inadequate signal. Since the ratio is not greater than 4, this model should not be used to navigate the design space. Figure 7 shows the interactions between each component in a three-dimensional group based on ANOVA

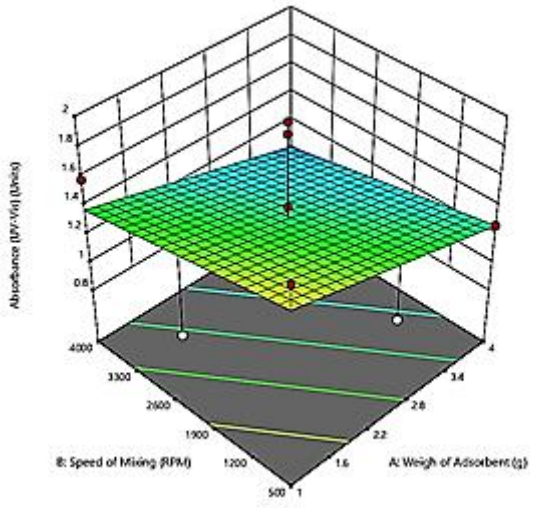

Figure 7. Variations in output experimental design with factors A and B

Based on Figure 7, it illustrates the factors that affect the absorbance of UV-vis spectroscopy. For factor A, as it is increased, the absorbance slightly decreases. Meanwhile for factor B, the pattern is the same with factor A whereas the factor B increases, the absorbance decreases. Thus, it can be concluded that with higher weight of adsorbent and speed of mixing, the absorbance in UV-vis spectroscopy can be decreased.

Comparison of optimization between CAC and RHAC

In this model the objective of optimization was to determine the best operating parameters that can be used to decrease both of the absorbance values of the ULO. Table 14 shows the comparison of optimization value of the factors between CAC and RHAC. Numerical method was conducted in order to determine optimum operating parameters. The goal for absorbance of FTIR and absorbance in UV-vis spectroscopy was being minimised as the values to be lowered. For CAC, the optimum value of factors A was 4.00 g while B was set to 524.89 rpm. Meanwhile, for RHAC, the optimum value of factors A was 2.29 g while B was set to 4000 rpm.

Table 14. Comparison of optimization value of the factors between CAC and RHAC

	CAC	RHAC
Name	Optimization value	Optimization value
A	4.00	2.29
B	524.89	4000
Absorbance of FTIR	0.05	0.01
Absorbance of UV-vis spectroscopy	0.90	1.22
Desirability	0.83	0.69

As Table 14 shows, RHAC produced the lowest value for absorbance of carbonyl group while CAC produced the lowest value of absorbance in UV-vis spectroscopy. CAC has higher desirability with 0.83 compared to RHAC with 0.69.

CONCLUSION

In conclusion, acid-clay treatment was proven in treating and improving the properties of ULO. The ULO could be best recovered with acid-clay treatment using the AC, as it is able to improve the quality of the ULO which is comparable with VLO. In terms of metal removal, RHAC had shown better performance than CAC as it gave low metal contents in AAS. This study also optimized the value for parameters in order to obtain the minimized value for both absorbances. For CAC, the optimum value of the factors is that A was 4.00 g while B was set to 524.89 RPM. Meanwhile, for RHAC, for factors A and B were 2.29 and 4000 rpm, respectively. CAC has higher desirability with 0.83 compared to RHAC with 0.69.

ACKNOWLEDGEMENTS

The authors pay their sincere gratitude to Universiti Malaysia Sabah (UMS) for providing necessary research facilities to accomplish this study.

REFERENCES

Moura, L. G. M., Assunção Filho, J. L. and Ramos, A. C. S. (2010) Recovery of used lubricant oils through adsorption of residues on solid surfaces. *Braz. J. Petroleum Gas,* **4(3),** 91–102.

Josiah, P. N. and Ikiensikimama, S. S. (2010) Effect of desludging and adsorption ratios on recovery of low pour fuel oil (LPFO) from spent engine oil. *Chem. Eng. Res. Bull.,* **14(1),** 25–28.

Osman, D. I., Attia, S. K. and Taman, A. R. (2018) Recycling of used engine oil by different solvent. *Egypt. J. Pet.,* **27(2),** 221–225.

Diphare, M., Muzenda, E., Pilusa, T. J. and Mollagee, M. (2013) A comparison of waste lubricating oil treatment techniques. 2nd International Conference on Environment, Agriculture and Food Sciences, (ICEAFS'2013), Kuala Lumpur, Malaysia, 106–109.

Abdel-Jabbar, N. M., Al Zubaidi, E. A. H. and Mehrvar, M. (2010) Waste lubricating oil treatment by adsorption process using different adsorbents. *Int. J. Chem. Biol. Sci.,* **3(2),** 70–73.

Udonne, J. D. and Bakare, O. A. (2013) Recycling of used lubricating oil using three samples of acids and clay as a method of treatment. *Inter. Arch. App. Sci.,* **4(2),** 8–14.

Rahman, M. M., Siddiquee, T. A., Samdani, S. and Kabir, K. B. (2008) Effect of operating variables on regeneration of base-oil from waste oil by conventional acid-clay method. *Chem. Eng. Res. Bull.,* **12,** 24–27.

Anisuzzaman, S. M., Abang, S., Krishnaiah, D. and Azlan, N. A. (2019) Removal of used motor oil from water body using modified commercial activated carbon. *Malays. J. Chem.c* **21(1),** 36–46.

Aljabiri, N. A. (2018) A comparative study of recycling used lubricating oils using various methods. *J. Sci. Eng.,* **5(9),** 168–177.

Shaikh, R. and Mahanwar, P. (2018) Reclamation of used engine oil using polymeric flocculants. *Int. J. Chem. Sci.,* **16(2),** 1–14.

Omolara, A. M., Olurotimi, A. D., Olatunji, G. O. (2015) Regeneration of used lubricating engine oil by solvent extraction process. *Int. J. Energ. Env. Res.,* **3(1),** 1–12.

Kamal, A. and Khan, F. (2009) Effect of extraction and adsorption on refining of used lubricating oil. *Oil Gas Sci. Technol. - Rev. IFP,* **64(2),** 191–197.

Rincon, J., Cañizares, P. and García M. T. (2007) Regeneration of used lubricant oil by ethane extraction. *J Supercrit. Fluid.,* **39(3),** 315–322.

Hamad. A., Al-Zubaidy, E., Fayed, M. E. (2005) Used lubricating oil recycling using hydrocarbon solvent. *J Environ Manage.,* **74(2),** 153–159.

Udonne, J. D. (2011) A comparative study of recycling of used lubrication oils using distillation, acid and activated charcoal with clay methods. *J. Petroleum Gas Eng.,* **2(2),** 12–19.

Hamawand, I., Yusaf, T. and Rafat, S. (2013) Recycling of waste engine oils using a new washing agent, *Energies,* **6(2),** 1023–1049.

Shakirullah M., Ahmad I., Khan M. A., Ishaq M., Rehman H. and Saeed, M. (2006) Spent lubricating oil residues as new precursors for carbon. *Fuller. Nanotub. Car. N.,* **14(1),** 39–48.

Riyanto, T. A. A. and Juliantydjawi, D. P. (2018) The effect of treatment with activated carbon on the metal content in reuse of lubricating oil waste. *MATEC Web of Conferences,* **154 (01018),** 1-5.

Bhaskar, T., Uddin, A., Muto, A., Sakata, Y., Omura, Y., Kimura, K. and Kawakami, Y. (2004) Recycling of waste lubricant oil into chemical feedstock or fuel oil over supported iron oxide catalysts. *Fuel,* **83(1),** 9–15.

Emam, E. A. and Shoaib, A. M. (2012) Re-refining of used lube oil , II- by solvent/clay and acid/clay-percolation processes. *ARPN J. Eng. Appl. Sci.,* **2(11),** 1034–1041.

Osman H. (2019) Model Prediction and optimization of waste lube oil treated with natural clay. *Processes,* **7(10),** 729–743.

Mekonnen, H. A. (2014) Recycling of used lubricating oil using acid-clay treatment process, M. Sc. thesis, Addis Ababa University, Addis Ababa Institute of Technology (AAiT), 1–71.

Oladimeji, T. E., Sonibare, J. A., Omoleye, J. A., Adegbola, A. A. and Okagbue, H. I. (2018) Data on the treatment of used lubricating oil from two different sources using solvent extraction and adsorption. *Data Brief,* **19,** 2240–2252.

Timur A. (2017) Reclamation of used lubricating oils using magnetic nanoparticles and caustic soda; M. Sc. thesis; Department of materials science and engineering, Graduate school of engineering and science, Bilkent university; 1–81.

Honda T and Sasaki A. (2018) Development of a turbine oil contamination diagnosis method using colorimetric analysis of membrane patches. *J. Adv. Mech. Des. Syst. Manuf.,* 12(4) 1–8.

Bono, A., Krishnaiah, D. and Rajin, M. (2008) Products and process optimization using response surface methodology, Universiti Malaysia Sabah Press, Kota Kinabalu, Sabah, Malaysia.

Bono, A., Anisuzzaman, S. M. and Ding, O. W. (2014) Effect of process conditions on the gel viscosity and gel strength of semi-refined carrageenan (SRC) produced from seaweed (Kappaphycus alvarezii*). J King Saud Univ Eng Sci.,* **26(1),** 3–9.

Behera, S. K., Meena, H., Chakraborty, S. and Meikap, B. C. (2018) Application of response surface methodology (RSM) for optimization of leaching parameters for ash reduction from low-grade coal. *Int. J. Min. Sci. Technol.,* **28(4),** 621–629.

Hussain, K. and Karmakar, S. (2014) Condition assessment of transformer oil using UV-Visible spectroscopy; Power Systems Conference (NPSC), Eighteenth National, IEEE, 1–5.

BorneoScience
The Journal of Science & Technology
Volume 43 Issue 2 : Oct 2022
Online ISSN : 2231-9085 | ISSN : 1394-4339

ADSORPTION OF 2,4-DICHLOROPHENOL (2,4-DCP) ONTO ACTIVATED CARBON DERIVED FROM COFFEE WASTE

S M Anisuzzaman[1], Collin G. Joseph[2,*], Mintshe Tan[2]

[1]Chemical Engineering Programme, Faculty of Engineering,
Universiti Malaysia Sabah, 88400 Kota Kinabalu, Sabah, Malaysia.
[2]Industrial Chemistry Programme, Faculty of Science and Natural Resources,
Universiti Malaysia Sabah, 88400 Kota Kinabalu, Sabah, Malaysia.

[*]Corresponding author: collin@ums.edu.my

Received 23rd June 2021; accepted 11th July 2022
Available online 1st Nov 2022
Doi: https://doi.org/10.51200/bsj.v43i2.5106

ABSTRACT. *In this study, activated carbons (ACs) were prepared from coffee waste via a two-stage self-generated atmosphere method after impregnation by zinc chloride ($ZnCl_2$). The effect of impregnation ratio (IR) on the physicochemical properties and adsorption capacity for 2,4-dichlorophenol (2,4-DCP) was studied. Characterizations of the generated ACs were carried out to determine the percentage of yield, moisture and ash contents, pH, surface chemistry studies and morphological attributes. The results showed that the yield of AC decreased from 41.16% to 37.12% with the increase in IR. As for moisture and ash contents, the percentage values ranged from 4.18% to 6.16% and 9.73% to 10.34% respectively. Meanwhile, the AC samples were slightly acidic with pH values varying between 6.06 and 6.56. The adsorption capacity increased from 16.8 mg/g for AC1 to 21.72 mg/g for AC4. The AC produced with an IR of 4:1 (AC4) had the highest adsorption capacity of 2,4-DCP, which was 21.72 mg/g. The maximum Brunauer, Emmett and Teller (BET) surface area of the best produced AC4 was found to be 951.10 m^2/g, which is by far the highest achieved in comparison with other coffee waste-derived ACs reported in the literature. N_2 adsorption-desorption graph showed a Type I isotherm, indicating that the AC4 was a microporous solid with chemisorption properties. Langmuir isotherm model was found to be a better fit for the adsorption data when compared to the Freundlich isotherm model. Pseudo-second order kinetic model was best described for the kinetic of 2,4-DCP adsorption. This proved that 2,4-DCP adsorption by AC4 was a chemisorption process.*

KEYWORDS: Activated carbon, two-stage activation, 2,4-dichlorophenol, coffee waste, adsorption

INTRODUCTION

Chlorophenols are one of the pollutants of emerging concern commonly found in polluted water. This is because chlorophenols are widely used in chemical industries as pesticides, petroleum

refineries process, wood preservation, and bleaching process in the pulp and paper industry. Chlorophenols have been categorized as hazardous materials since they are carcinogenic, mutagenic, and teratogenic. Moreover, phenolic compounds (PCs) properties may contribute to rapid absorption through contact with nasal, oral, eye or skin and dermal contact. Chlorophenols can permeate through human skin and a sufficient dose of chlorophenols can cause liver damage, chronic bronchitis, cough, and even death [1,2]. The removal of chlorophenols from the environment is crucial because of their structural stability and persistence in the environment and to prevent the exposure of chlorophenols to living organisms [3-5]. Due to their toxicity, phenols have been included in the Malaysian government's list of priority contaminants. According to National Water Quality Standards for Malaysia, the phenol compounds should be less than 10 mg/l in water surface. Consequently, the removal or biodegradation/bioconversion of PC from wastewater is necessary before it is released into water bodies. Numerous research studies have been conducted to develop sustainable technology in the PCs contaminated industrial effluents [6-9].

Adsorption technology has gained some attention in PCs containing wastewater treatment processes since it is versatile in design, simple operation, and effective regeneration of adsorbents via desorption [10-12]. Moreover, this technology is also able to extract PC at low concentrations [13]. However, the quality of the adsorption mechanism was highly reliant on the adsorbent material used in the process. In wastewater treatment, the removal of various pollutants using activated carbon (AC) has been proven to be faster than other chemical and physical methods, such as biological treatment, photochemical treatment, and electrochemical oxidation [14-16]. AC is a highly porous material with an amphoteric character on its surface. Besides that, AC has high mechanical strength, thermo-stability, adequate pore size distribution, and low acid/base reactivity [17-20]. However, commercial AC is produced from expensive precursor materials; its usage has been narrowed. Hence, cheaper precursor materials such as agricultural waste have been utilised to produce AC [21-22].

One precursor material that has been used to generate AC in many studies is coffee waste [23-29]. Coffee waste is the solid residue of the coffee bean after the flavour had been extracted to make coffee beverages. Coffee waste is utilised as precursor material because a great quantity of coffee waste is produced annually since coffee is one of the essential agricultural commodities in the world. Besides that, recycling the coffee waste to produce AC is environmentally friendly due to coffee waste needing large amounts of oxygen for degradation. Furthermore, coffee provides a waste-to-wealth opportunity in which a low-cost AC can be produced from it. Its low ash content and high availability make it an ideal precursor for producing AC [27-29].

Therefore, in this study, coffee waste as precursor material was used to prepare the AC with different impregnation ratios (IR) of zinc chloride ($ZnCl_2$) to precursor using two-stage chemical activation under a self-generated atmosphere for the removal of 2,4-Dichlorophenol (2,4-DCP) in the aqueous medium. The initial concentration of chlorophenols, adsorbent dosage, and solution pH were varied in batch adsorption test to study the adsorption of chlorophenols by AC. The AC was characterised by utilizing moisture and ash content test, Fourier-transform infrared (FT-IR) spectroscopy, and scanning electron microscopy (SEM).

MATERIALS AND METHODOLOGY

Chemicals and instruments

The chemicals utilised in this study were zinc chloride ($ZnCl_2$) from EMSURE®, methanol (CH_3OH) from Fisher Scientific UK, 2,4-dichlorophenol (2,4-DCP), hydrochloric acid (HCl), and sodium hydroxide (NaOH) from Sigma-Aldrich. All chemicals were used without further purification. The instruments used in this study were FT-IR spectrometer (Thermo Nicolet Nexus 670 FTIR, Thermo Scientific), muffle furnace (CWF 1200, CARBOLITE), scanning electron microscope (SEM) (JSM-5610 LV, JEOL), and Ultraviolet–visible (UV-Vis) spectrophotometer (Agilent Cary 60 UV-Vis, Agilent Technologies).

Preparation of coffee waste

Coffee waste was employed as the precursor material for the preparation of AC and was obtained from the local restaurants in Kota Kinabalu, Sabah, Malaysia. The coffee waste was washed with hot water to remove dust, impurities, and water-soluble substances. Then, it was rewashed with distilled water and dried in an oven for 24 h at 110^{o}C to reduce the moisture content of coffee waste [29]. The dried coffee waste was stored in a desiccator to prevent moisture uptake.

Preparation of AC

A two-stage self-generated atmosphere method was used to prepare the AC from dried coffee waste. The precursor was semi-carbonized (first stage), and then subjected to an activation process (second stage) after impregnating the semi-carbonised char with $ZnCl_2$. $ZnCl_2$ was used for the impregnation process as the prepared AC will have a great surface area, and more micropores but lesser mesopores [30]. Both semi-carbonization and activation were done in a self-generated atmosphere. Self-generated atmosphere is the atmosphere that consists of the volatile matter which is generated from the pyrolysis process. The dried coffee waste was divided into 5 batches and labelled as AC1, AC2, AC3, AC4, and AC5 respectively. These samples were weighed using an electronic balance and the weight of each sample was recorded as W_o (g). Then, these samples were put into the muffle furnace and semi-carbonised at 300^{o}C for 1 h under self-generated atmosphere[31]. After the semi-carbonisation process, the samples were left in the muffle furnace to cool down to room temperature and kept in a desiccator.

Activation process

The AC1 was agitated with the $ZnCl_2$ solution at an IR of 1:1 at 85^{o}C using a hot plate and stirred with a magnetic bar until the solution in the beaker was completely dried. After that, AC1 was activated in the muffle furnace at 500^{o}C for 2 h under a self-generated atmosphere and left to cool down to room temperature [31]. The resulted AC1 was boiled with 0.01M hydrochloric acid (HCl) for 1 h and washed thoroughly with hot distilled water to remove the residual $ZnCl_2$ until the washing solution reached pH 6 – 7. Finally, AC1 was dried in the oven at 110^{o}C for 24 h. The dried AC1 was weighed, and its weight was recorded as W_{DAC}(g). These procedures were repeated for AC2 – AC5 of which the $ZnCl_2$ was added in the ratio of 2:1, 3:1, 4:1, and 5:1 respectively. Table 1 showed the semi-carbonisation and activation conditions of AC1 – AC5.

Table 1. Semi-carbonisation and activation conditions of AC1 – AC5

Samples	Semi-carbonisation		Activation		
	Time (h)	Temperature (°C)	IR ($ZnCl_2$:AC)	Time (h)	Temperature (°C)
AC1	1	300	1:1	2	500
AC2	1	300	2:1	2	500
AC3	1	300	3:1	2	500
AC4	1	300	4:1	2	500
AC5	1	300	5:1	2	500

Determination of percentage of yield

The percentage of yield was calculated based on the equation 1.

$$Percentage\ of\ yield\ (\%) = \frac{W_f}{W_i}\ x\ 100\% \quad (1)$$

where, W_f is the initial mass of the dry impregnated sample; W_i is the he final mass of the sample after activation process is complete

Determination of moisture and ash contents

In order to determine the moisture content, 1 g of AC1 was weighed in a tarred petri dish with cover. Then, AC1 in the tarred petri dish was dried in the oven at 145 - 155°C for 3 h with the cover removed. The sample was covered and left to cool to room temperature. The cooled AC1 was weighed immediately. These steps were repeated for AC2 – AC5. The moisture content was calculated through equation 2.

$$Moisture\ content\ (\%) = \frac{Initial\ weight\ (g) - Final\ weight\ (g)}{Initial\ weight\ (g)}\ x\ 100\% \quad (2)$$

In the determination of ash content, the crucible was heated in a muffle furnace for 1 hour at 650 ± 25°C and weighed after it was cooled. The dried AC1 from the moisture content test was put into the crucible and weighed before heating in a muffle furnace at 650 ± 25°C from 3 - 16 h until the carbon was completely burnt. The sample was left to cool to room temperature and weighed immediately. These steps were repeated for AC2 – AC5. The ash content was calculated by equation 3.

$$Ash\ content\ (\%) = \frac{Weight\ of\ the\ sample\ after\ ash\ process}{Weight\ of\ the\ sample\ before\ ash\ process}\ x\ 100\% \quad (3)$$

Determination of pH

1 g of dried AC1 was put into a 250 ml Erlenmeyer flask and 100 ml of hot distilled water was poured into the same flask. The mixture was boiled gently for 15 minutes and the AC1 in the mixture was filtered out using vacuum filtration. The filtrate was collected and cooled to 50 ± 5°C. The pH of the filtrate was measured using the pH meter. These procedures were repeated for AC2 – AC5.

Surface chemistry studies

The surface chemistry was studied using FT-IR spectroscopy. A small amount of coffee waste, AC samples, and KBr powder were firstly dried in oven at 110^{o}C for 24 h. Then, the coffee waste and AC samples were crushed into powder form and mixed with KBr respectively. After that, the mixture was made into a transparent disc and tested with a FT-IR spectrometer. The FT-IR spectroscopy was carried out under room temperature in the wavenumber range from 4000 cm^{-1} to 400 cm^{-1} with 2 cm^{-1} resolution.

Morphological studies

The morphology of coffee waste and AC were investigated utilising SEM method. The AC samples were sieved to get the granular form. After that, a small amount of coffee waste and granular AC samples were dried for 24 h at 110^{o}C in an oven before analyse using SEM.

Chlorophenols adsorption experiment

The adsorption equilibrium and adsorption kinetics studies were performed using batch adsorption method. The effects of initial concentration, adsorbent dosage, and solution pH on the 2,4-DCP adsorption of AC with the highest adsorption capacity of 2,4-DCP were studied.

Preparation of 2,4-DCP Solution

The λ_{max} of 2,4-DCP is 280nm. In order to prepare 1000 mg/l of the 2,4-DCP solution, 1 g of 2,4-DCP powder was weighed and dissolved using 10 ml of methanol in a beaker. Then, the solution was diluted in a 1000 ml volumetric flask. A magnetic bar was put into the volumetric flask and the solution was stirred on a hot plate for 1 hour. After that, the desired concentration of the 2,4-DCP solution was prepared from the 1000 mg/l of 2,4-DCP solution through the dilution method.

Adsorption capacity test

The AC samples (AC1 – AC5) were sieved to get the granular form AC. 0.5 g of granular AC samples and 600 ml of 20 mg/l 2,4-DCP solution were put into a beaker. The mixture was stirred using a hot plate and magnetic bar for 3 hours at room temperature. The AC samples were filtered out and the 2,4-DCP uptake at equilibrium was analysed using the UV-Vis spectrophotometer. The objective of this test was to find an AC sample with the largest adsorption capacity of 2,4-DCP for the following procedures. The 2,4-DCP uptake at equilibrium was calculated by equation 4.

$$Q_e = \frac{(C_i - C_e)V}{W} \quad (4)$$

where, Q_e (mg/g) is the 2,4-DCP uptake at equilibrium, C_i and C_e (mg/l) are the liquid-phase concentration of 2,4-DCP at initial and equilibrium respectively, V(l) is the volume of the solution, and W (g) is the mass of AC used.

Effect of initial concentration

In order to study the effect of initial concentration on the 2,4-DCP adsorption, different concentrations (5, 10, 15, and 20 mg/l) of 2,4-DCP solution were prepared in volumetric flasks. 600 ml of each of the 2,4-DCP solutions was poured into 4 beakers respectively. Next, 0.5 g AC was added into the beakers separately. The beakers were placed on a hot plate and stirred using a magnetic

bar for 3 h and then the AC was filtered out. The 2,4-DCP uptake at equilibrium was analysed using the UV-Vis spectrophotometer and calculated using equation 4.

Effect of Adsorbent Dosage

0.1, 0.3, and 0.5 g of AC were added respectively into 3 beakers which contained 600 ml of 2,4-DCP solution with a concentration of 20 mg/l . The mixture was stirred for 3 h and the 2,4-DCP adsorption capacity was analysed using the UV-Vis spectrophotometer and calculated using equation 4. In addition, the percentage of removal was determined from equation 5.

$$Percentage\ of\ removal\ (\%) = \frac{(C_i - C_e)}{C_i} x100\% \quad (5)$$

Effect of Solution pH

600 ml of 20 mg/l 2,4-DCP solution was poured into an Erlenmeyer flask. The pH of the 2,4-DCP solution was altered to 3, 7, and 9 by adding HCl and NaOH solutions with different concentrations (0.01 M and 0.1 M). After that, 0.5 g of AC samples were added into the Erlenmeyer flasks that contain 2,4-DCP solution with different pH respectively. The mixture was stirred for 3 h using a hot plate and magnetic bar. Then, the sample solutions were filtered using 0.45 µm polytetrafluoroethylene (PTFE) syringe filter and put into a quartz cuvette. The residual concentration of 2,4-DCP was determined through a UV-Vis spectrophotometer.

Adsorption kinetics studies

600 ml of 20 mg/l 2,4-DCP solution and 0.5 g of AC sample were added into a beaker. The mixture was agitated utilising a hot plate and a magnetic bar for 200 min. The aqueous samples were taken at every 10 min for UV-Vis spectrophotometer analysis [43]. The 2,4-DCP uptake at time t, Q_t (mg/g) was calculated by equation 6.

$$Q_t = \frac{(C_i - C_t)V}{W} \quad (6)$$

where C_i is the initial adsorbate concentration at given time (mg/l); C_t is the equilibrium adsorbate concentration at given time (mg/l); V (l) is the volume of the solution, and W (g) is the mass of AC used.

The adsorption kinetics of AC on chlorophenols was evaluated through pseudo-first-order, pseudo-second-order and intraparticle diffusion models. The equations of pseudo-first order, pseudo-second order and intraparticle diffusion models are as bellows respectively.

$$ln\ ln\ (Q_e - Q_t) = -K_1 t + ln\ ln\ Q_e \quad (7)$$

where, Q_t is the amount of adsorbate adsorption at time (mg/g); K_1 is the Pseudo-first order adsorption rate constant (hr^{-1}); t the is mixing time (hr); Q_e is the amount of adsorbate adsorption at equilibrium (mg/g)

$$\frac{t}{Q_t} = \frac{t}{Q_e} + \frac{1}{K_2 Q_e^2} \quad (8)$$

where, Q_t is the amount of adsorbate adsorption at time (mg/g); K_2 is the Pseudo-second order adsorption rate constant (g/mg.hr); t is the Mixing time (hr); Q_e is the amount of adsorbate adsorption at equilibrium (mg/g)

$$Q_t = k_{id} t^{1/2} + a \quad (9)$$

where k_{id} (mg/g $min^{1/2}$) is the intraparticle diffusion rate constant, a (mg/g) is a constant in the intraparticle diffusion model, which reflects the significance of the boundary layer or mass transfer effect.

Adsorption isotherms studies

The equilibrium data was fitted to the Langmuir and Freundlich isotherm models to show the most suitable correlation for the adsorption system. The equations of Langmuir and Freundlich isotherm models are listed in equations 10 and 11 correspondingly.

$$\frac{C_e}{Q_e} = \frac{C_e}{Q_{max}} + \frac{1}{K_L Q_{max}} \quad (10)$$

where, Q_{max} is the maximum monolayer adsorption capacity (mg/g); K_L is the Langmuir isotherm constant (mg/l); C_e is the Equilibrium adsorbate concentration (mg/l); Q_e is the amount of adsorbate adsorption at equilibrium (mg/g)

$$In\ Q_e = In\ K_f + \frac{1}{n} In\ C_e \quad (11)$$

where, Q_e is the adsorption density at the equilibrium solute concentration (mg adsorbate/g adsorbent); C_e is the equilibrium concentration of adsorbate in solution (mg/l); K_f *i*s the Freundlich adsorption capacity constant (mg/g); n is the adsorption intensity (mg/g)

RESULTS AND DISCUSSION

The physical appearance of washed and dried coffee waste was slightly different from the raw coffee waste. The surface of washed and dried coffee waste was less shiny and had shrunk slightly due to the loss of moisture content from the coffee waste. After the semi-carbonisation and activation processes, the brownish-black coffee waste had changed into fragile black AC. Furthermore, the AC had lost its original coffee fragrance. The prepared AC samples (AC1 – AC5) were characterised via the percentage of yield, moisture and ash contents, pH, surface chemistry and morphological studies.

Physical characterization

The yield, moisture and ash content percentage along with pH of AC1-AC5 are shown in Table 2.

Table 2. Percentage of yield, moisture and ash contents, and pH of AC1 – AC5

Samples	Yield (%)	Moisture content (%)	Ash content (%)	pH
AC1	41.16	4.56	9.73	6.18

AC2	40.61	4.18	9.88	6.06
AC3	38.16	5.22	9.96	6.36
AC4	37.35	6.16	10.17	6.56
AC5	37.12	5.01	10.34	6.54

Based on Table 2, the results showed that the yield of AC decreased from 41.16% to 37.12% with the increase in IR. The decrease in yield was due to the formation of mesopore in AC which is induced by the $ZnCl_2$. As the IR increased to above 1:1, the initial function of $ZnCl_2$ during activation which is the inhibition of volatile matter would be lost. During activation, the volatile matters will be discharged from the carbon surface since their movement through the pore passages will not be inhibited [32]. Consequently, the pores will start to widen and collapse due to the increased pyrolytic decomposition as IR is further increased [46]. This in turn leads to the weight loss in the precursor at the activation stage.

As can be seen from Table 2, the moisture contents of five AC samples were ranged from 4.18% to 6.16%. AC2 had the lowest moisture content, 4.18% whereas AC4 had the highest moisture content, 6.16%. In comparison, the moisture contents of AC1 – AC5 were slightly lower than in the previous study carried out by Boonamnuayvitaya *et. al.* [28] in which the moisture contents ranged from 5.36% to 12.63%. The moisture in AC was due to the uptake of moisture in the atmosphere. This result indicated that IR does not influence the moisture content of AC.

From the outcome obtained, it was proven that the ash content of AC was increased with the increasing IR. This is because more inorganic compounds are formed and more carbon atoms are consumed as IR is increased. AC1 recorded the lowest ash content, 9.73% and AC5 recorded the highest ash content, 10.34%. On the other hand, the ash contents of AC1 – AC5 was higher than other ACs that were prepared from different precursors. For instance, the ash content of AC prepared from the grape stalk in 1:1 IR was 1.16%.

The prepared AC samples (AC1 – AC5) were found to be slightly acidic as seen in Table 2. AC2 had the lowest pH value which was 6.06, whereas AC4 had the highest pH value which was 6.56. The acidic character of AC samples indicated that their surface contains more oxygen-containing groups (carboxylic, anhydrides, lactones, and phenols) than oxygen-free Lewis sites, carbonyls, pyrone, and chromene-type structures. Besides that, the acidic wash utilised HCl also contributed to this outcome. The pH values obtained were found to be compatible with the research of Namanea *et. al.* [29] in which their AC made from the coffee ground by $ZnCl_2$ activation had pH of 6.36.

Surface chemistry studies of AC

The FT-IR spectra of coffee waste and AC1 – AC5 are shown in Figure 1. The FT-IR spectrum of coffee waste showed a broad band at 3443.76 cm^{-1} which was attributed to -OH stretching vibration from carboxyls, phenols or alcohols. The band at 2927.56 cm^{-1} was corresponded to C-H stretching vibration and generally indicated the presence of an alkane group. Moreover, the peak at 2353.62 cm^{-1} indicated the C≡C stretching and the peak at 1645.98 cm^{-1} indicated the C=C stretching vibration from alkenes or C=O stretching vibration from aldehydes, ketones, carboxylic acids or esters. The band at 1383.44 cm^{-1} was resulted from C-H bending of methyl group or C-N stretching from amines

or amides. Furthermore, the C-O stretching from alcohols, ethers, carboxylic acids or esters produced a peak at 1067.49 cm^{-1} and the peak at 671.45 cm^{-1} was assigned to C-H out-of-plane bending in benzene derivatives or C-Cl stretching vibration.

On the other hand, the FT-IR spectra of AC1 – AC5 generally demonstrated a similar pattern. The broad band at 3452 cm^{-1} – 3417 cm^{-1} indicated the –OH stretching vibration, the band at 2367 cm^{-1} – 2349 cm^{-1} was attributed to C≡C stretching vibration and the band at 1628 cm^{-1} – 1614 cm^{-1} was assigned to C=C stretching vibration. Furthermore, the peak at 1387 cm^{-1} – 1383 cm^{-1} was attributed to C-H bending, the peak at 1103 cm^{-1} – 1089 cm^{-1} indicated the C-O stretching vibration, and the peak at 675 cm^{-1} – 671 cm^{-1} was assigned to C-H out-of-plane bending.

As compared with the FT-IR spectrum of coffee waste, there were missing peaks observed in the spectra of AC1 – AC5. The most significant observation was the disappearance of the peak at 2927.56 cm^{-1} as shown in Figure 1. This may be due to the decomposition of cellulose, hemicelluloses, and lignin, as well as the elimination of hydrogen in the coffee waste after activation process [33,34].

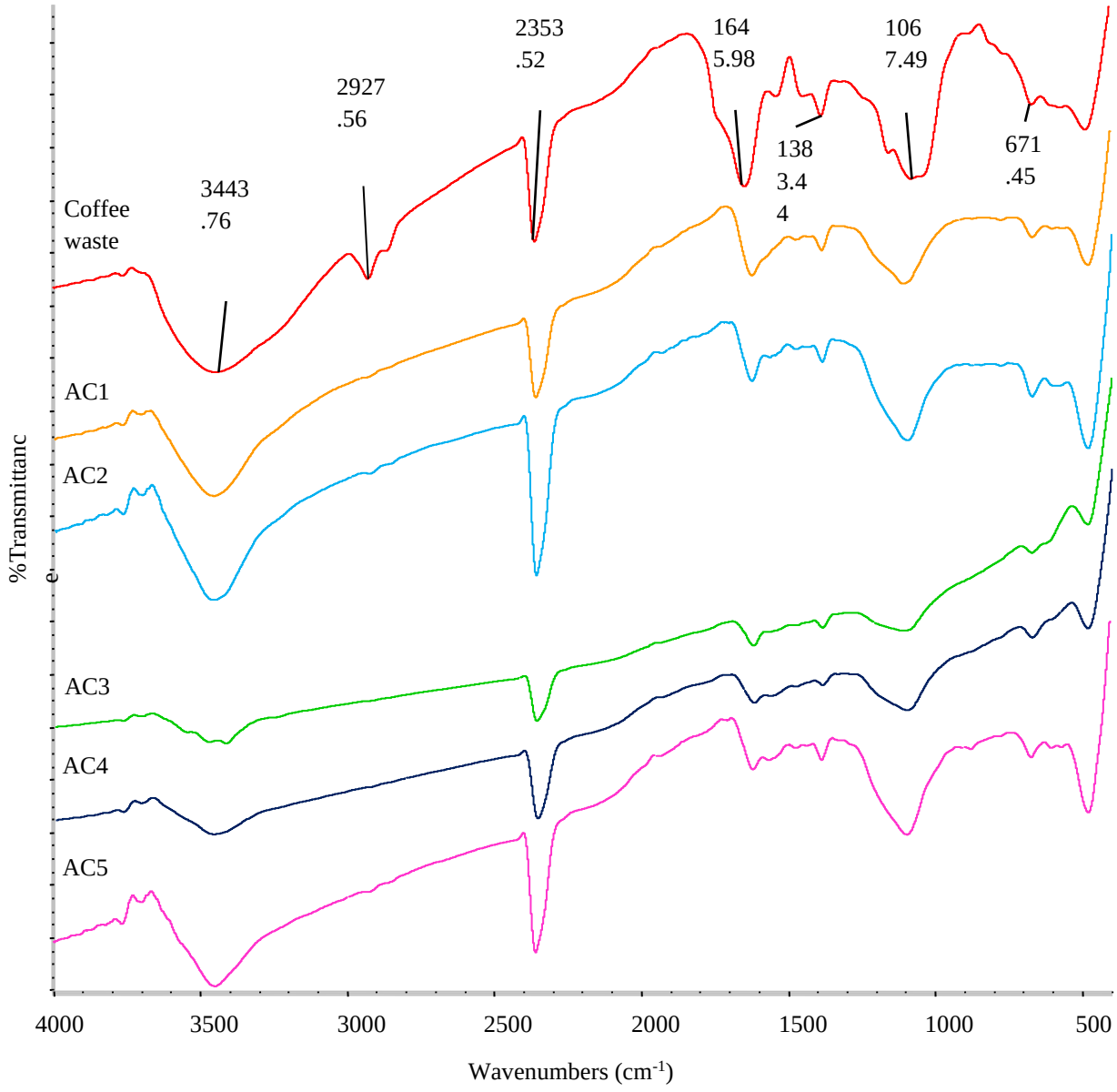

Figure 1. FT-IR spectra of coffee waste and AC1 – AC5.

Table 3 summarizes the peak identification of FTIR spectra on coffee waste and AC1 – AC5 samples.

Table 3. Peak Identification of FTIR spectra on coffee waste and AC1 – AC5

Sample	Band position (cm^{-1})	Possible Functional Group
Coffee waste	3443.76	-OH stretching
	2927.56	C-H stretching
	2353.62	C≡C stretching
	1645.98	C=C stretching
	1383.44	C-H bending
	1067.49	C-O stretching
	671.45	C-H out-of-plane bending
AC1 – AC5	3452 – 3417	-OH stretching
	2927.56	Undetected
	2367 – 2349	C≡C stretching
	1628– 1614	C=C stretching
	1387 cm^{-1} – 1383	C-H bending
	1103 cm^{-1} – 1089	C-O stretching
	675 cm^{-1} – 671	C-H out-of-plane bending

Morphological studies of AC

Scanning electron microscopy (SEM) was used to study the morphological structure of the prepared AC (Figure 2). The observation proved that different IR of $ZnCl_2$ can give different surface morphology to the produced AC. The surface structure of AC1 and AC2 comprised of cavities and pores of different shapes and sizes as shown in Figure 2 (b) and Figure 2 (c). Meanwhile, AC3 appeared to have a honeycomb-like structure as illustrated in Figure 2 (d). The morphology of AC4 which was observed from Figure 2 (e) showed that it had many cracks and irregular pores. Furthermore, irregular pores also existed for the morphology of AC5 as seen from Figure 2 (f). These pore structures are formed from the evaporation of $ZnCl_2$ and volatile matters during the activation process, leaving behind the voids which is formerly occupied by them [30,35].

In comparison, the rough and highly folded surface of coffee waste (Figure 2 a) was changed to AC1 – AC5 with a porous surface (Figure 2 (b-f)) after activation by $ZnCl_2$. This further verifies that $ZnCl_2$ is an activating agent. Besides that, the morphology of AC1 and AC2 showed smoother surfaces and had fewer voids than other AC samples. Although AC4 did not have a regular pore structure like AC3, it had more crevices and smaller pores compared to AC3. Meanwhile, AC5 had larger and crooked pores with the absence of small pores compared to AC4. Additionally, from the micrograph, it is evident that the pores of AC5 were starting to collapse compared to others AC samples. These indicate that increasing IR would generate AC with more pores but eventually, the pores would collapse because of the intense chemical attack by $ZnCl_2$.

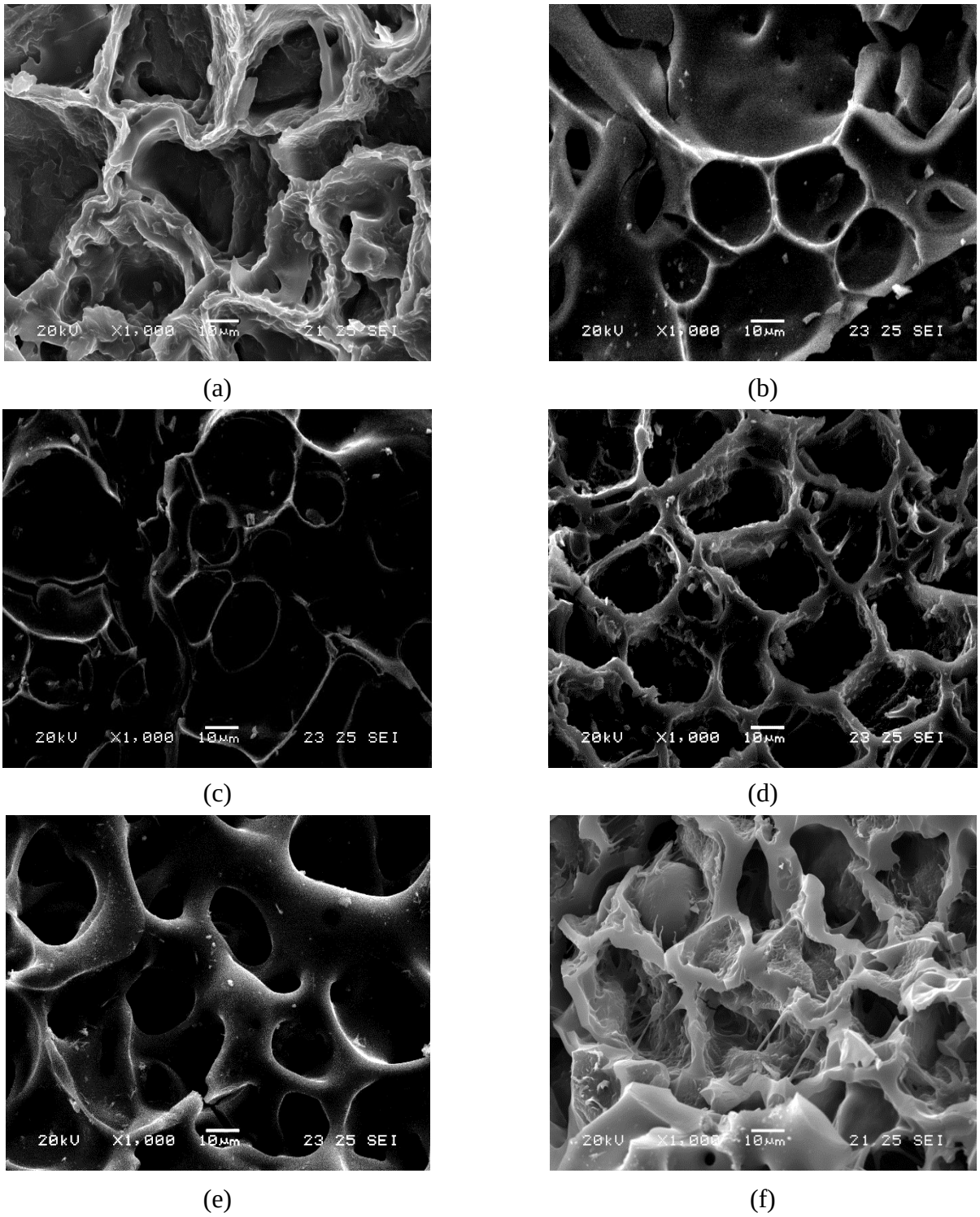

Figure 2. SEM micrographs (x1000 magnification) of (a) coffee waste (b) AC1 (c) AC2 (d) AC3 (e) AC4 (f) AC5

Specific surface area and pore-distribution

AC4 was selected for surface area and pore distribution analysis. The maximum Langmuir surface area of 951.10 m^2/g and the average pore diameter of 23.25 Å are comparable with other researchers' findings [36,37]. Table 4 represents the porous and surface characteristics of AC3.

Table 4. Surface area, pore volume and pore size of AC4

Surface area	
Langmuir surface area, m^2/g	$9.511x10^2$
BJH method cumulative adsorption surface area, m^2/g	$1.329x10^3$
BJH method cumulative desorption surface area, m^2/g	$1.325x10^3$
Pore volume	
BJH method cumulative adsorption pore volume, cc/g	0.4748
BJH method cumulative desorption pore volume, cc/g	0.4685
Pore size	
Average pore diameter, Å	23.25
BJH method adsorption pore diameter (mode), Å	8.870
BJH method desorption pore diameter (mode), Å	9.164

Figure 3 shows N_2 adsorption isotherm for coffee waste. N_2 adsorption-desorption graph showed a Type I isotherm, indicating that the AC4 was a microporous solid with chemisorption properties.

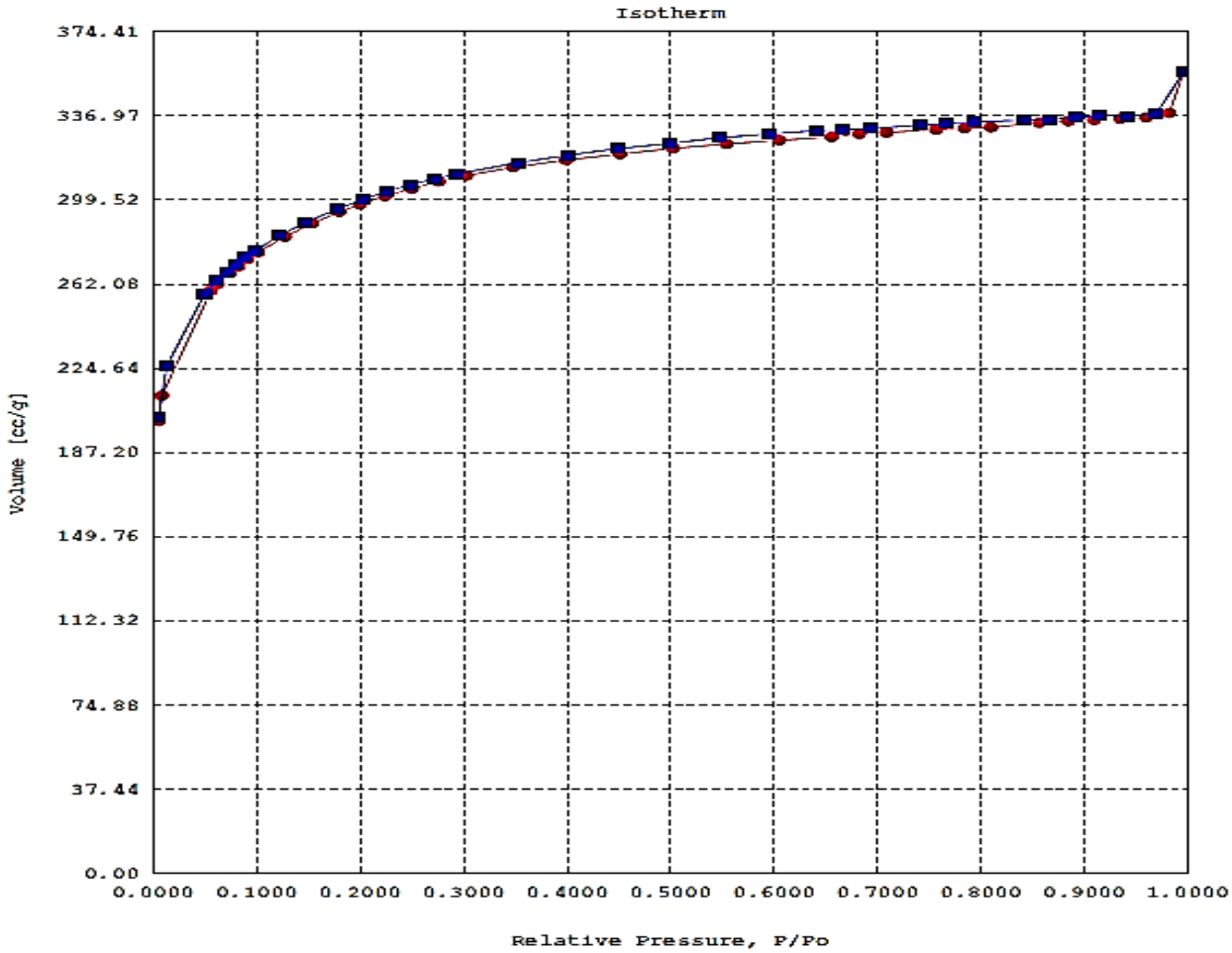

Figure 3. N_2 adsorption isotherm for coffee waste

Adsorption capacity test

The 2,4-DCP adsorption capacity test indicated that an increase in the IR would increase the adsorption capacity of AC. The adsorption capacity increased from 16.8 mg/g for AC1 to 21.72 mg/g for AC4. This is due to the development of micropore and mesopore of AC which increased proportionally with the IR. In consequence, the larger the number of pores, the higher the 2,4-DCP adsorption capacity of AC. This result proved that AC4 had the highest adsorption capacity which was compatible with the SEM micrograph of AC4 (Figure 2e) that illustrated a large number of pores. However, the adsorption capacity for AC5 dropped to 20.40 mg/g, indicating that further increases in the IR will destroy the pores of AC and hence decrease the adsorption capacity. The AC4 was utilised in the following 2,4-DCP adsorption tests. Table 5 shows the adsorption capacity of AC1 – AC5.

Table 5. Adsorption capacity of AC1 – AC5.

Samples	Adsorption capacity (mg/g)
AC1	16.80
AC2	18.72
AC3	19.32
AC4	21.72
AC5	20.40

Effect of initial concentration

In the effect of initial concentration, the amount of 2,4-DCP adsorbed by AC4 increased as the initial concentration was increased as shown in Figure 4. When the initial concentration was increased from 5 mg/l to 20 mg/l , the amount of 2,4-DCP adsorbed increased from 5.76 mg/g to 21.6 mg/g. This is because more 2,4-DCP available for AC to adsorb and the higher initial concentration provides a greater driving force for the mass transfer between 2,4-DCP and AC. Therefore, the adsorption efficiency of AC4 also increased.

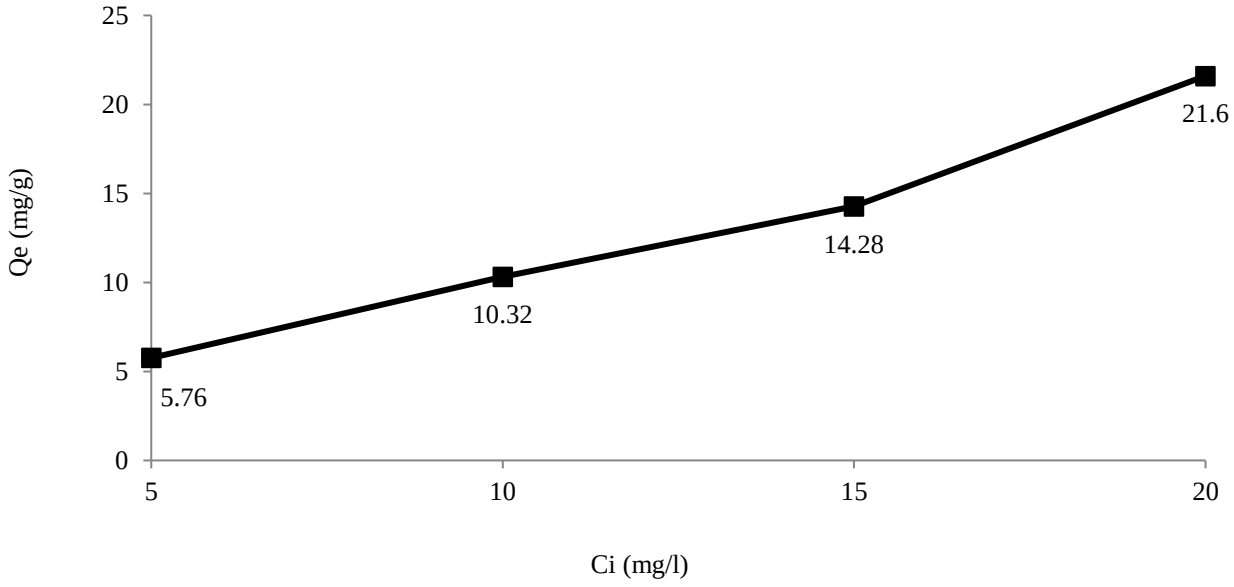

Figure 4. Amount of 2,4-DCP adsorbed, Q_e against initial concentration of 2,4-DCP

Effect of adsorbent dosage

The effect of adsorbent dosage on the removal of 2,4-DCP is presented in Figures 5 and 6. The amount of 2,4-DCP uptake decreased from 43.80 mg/g to 20.76 mg/g as the adsorbent dosage increased. This trend is due to the unsaturation of adsorption sites caused by the low concentration of adsorbate. There is also a that the large quantity of AC present would agglomerate and eventually cause decrement in the total surface area of AC. However, the removal percentage increased from 36.5% to 86.5% along with the increased adsorbent dosage. This is because more adsorption sites are available for the adsorption of 2,4-DCP and hence more 2,4-DCP molecules can be removed.

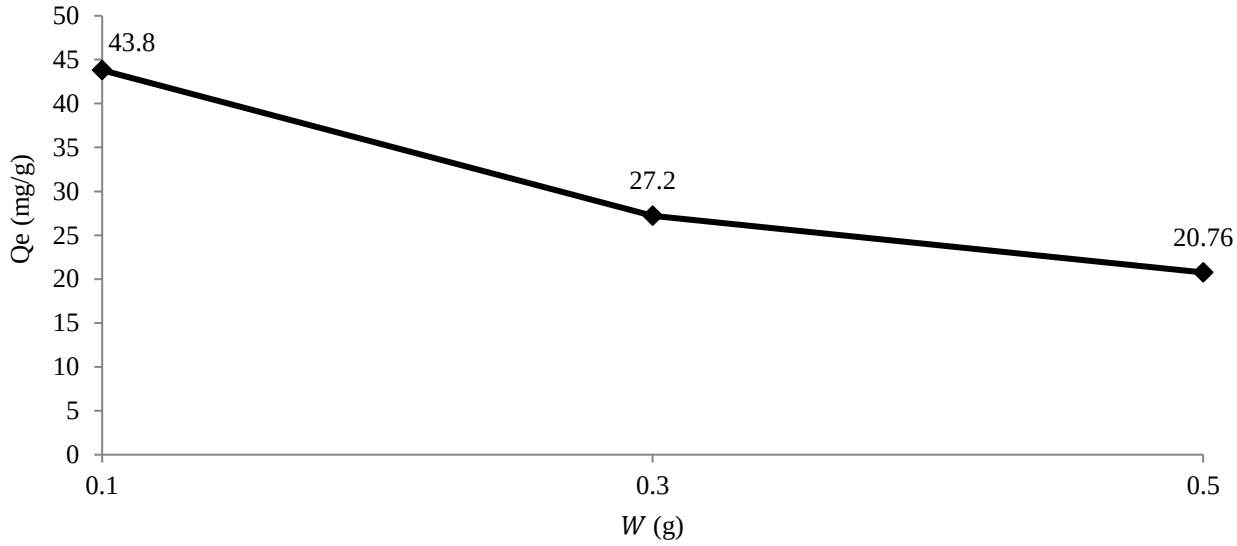

Figure 5. Amount of 2,4-DCP adsorbed, Q_e against mass of AC used

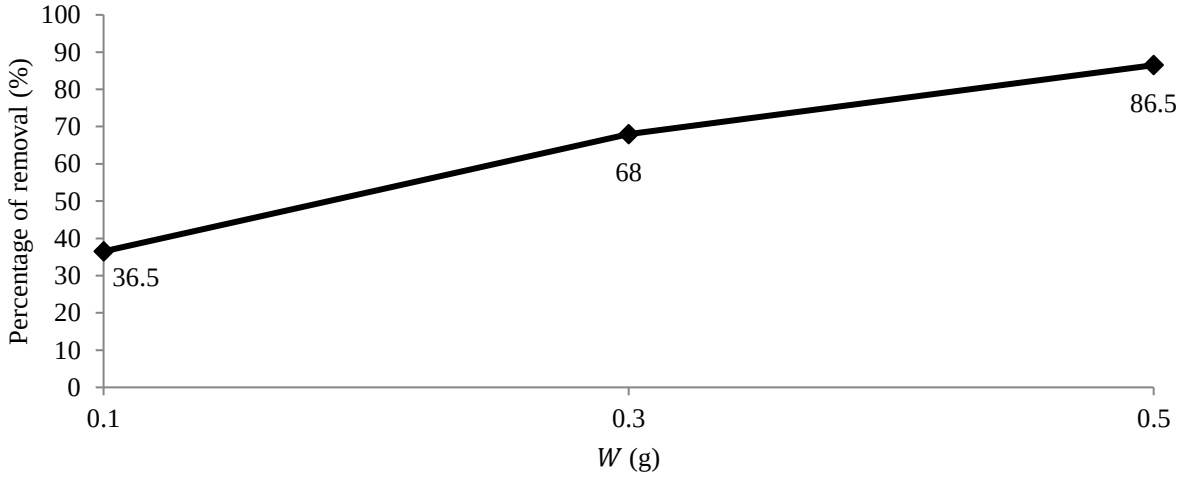

Figure 6. Percentage of removal against mass of AC used

Effect of solution pH

From Figure 7, the adsorption capacity decreases with an increase in the pH of the solution. In acidic pH (pH < pK_a of 2,4-DCP), the 2,4-DCP molecules exist in non-ionic form and the adsorption sites of AC are positively charged. This leads to the electrostatic attraction between the molecular form of 2,4-DCP and the adsorption sites. Therefore, an increase in the adsorption capacity of AC in low pH.

Alternatively, in basic pH (pH > pK_a of 2,4-DCP), the 2,4-DCP molecules dissociate into phenolate ions, while the surface functional groups of AC become neutral or negatively charged. This can cause electrostatic repulsion between phenolate ions and negatively charged adsorption sites, lowering adsorption capacity.

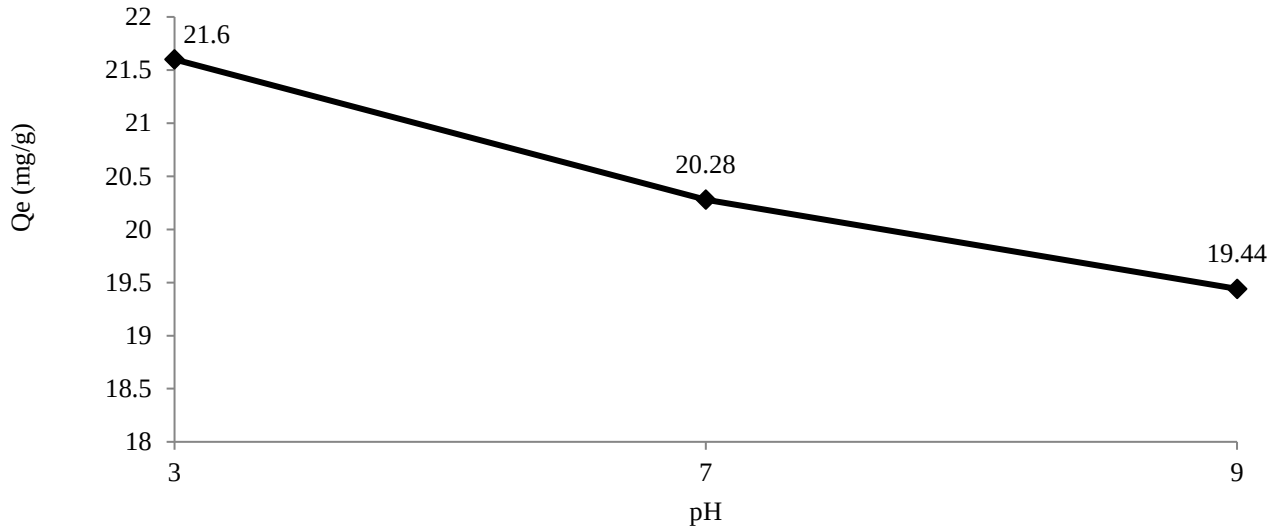

Figure 7. Amount of 2,4-DCP adsorbed, Q_e against pH.

Adsorption kinetics studies

The adsorption kinetics studies of 2,4-DCP onto AC4 were determined from the uptake analysis data. As shown in Figure 8, the amount of 2,4-DCP adsorbed by AC4 was increased rapidly for the first 20 min due to the many vacant adsorption sites present for the adsorption. However, after 20 min, the adsorption of 2,4-DCP became slower. This is because the adsorption sites are gradually saturated with the adsorbate molecules. At 180 min, the equilibrium was achieved in which the amount of 2,4-DCP adsorbed was 21.12 mg/g.

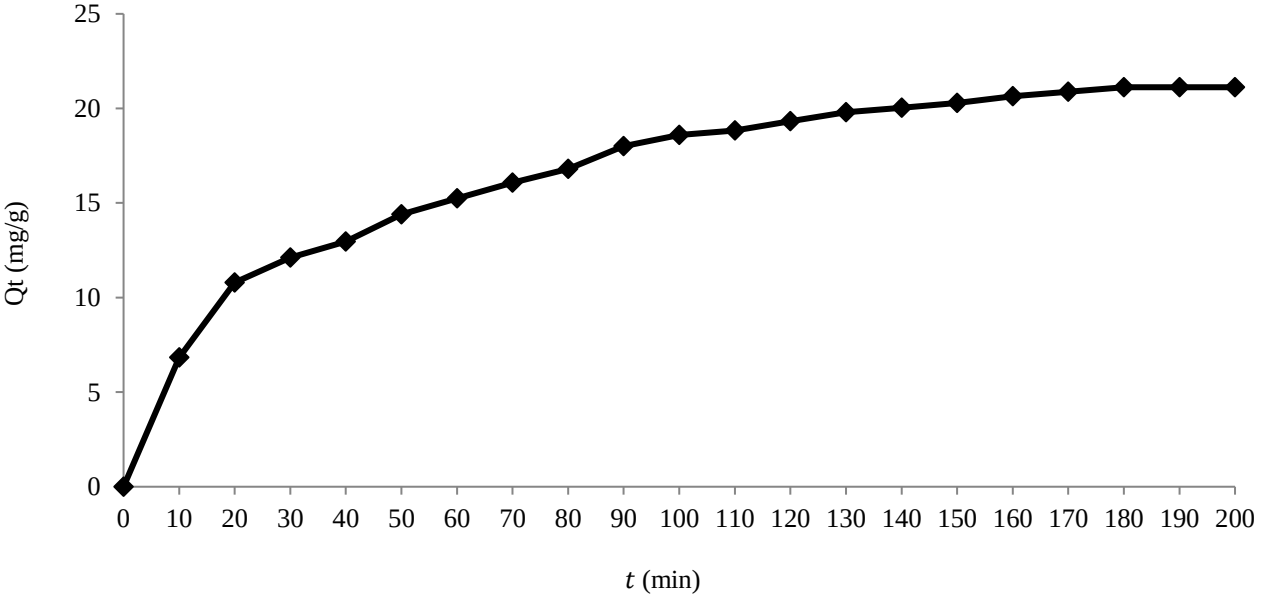

Figure 8. Amount of 2,4-DCP adsorbed at time t, Q_t against time

From the results demonstrated in Figure 9 (a,b), the adsorption kinetics of 2,4-DCP onto AC4 was best fitted into the pseudo-second order kinetic model with correlation coefficients, R^2 equals to 0.9971 which was more than the correlation coefficients of pseudo-first order kinetic model (R^2 = 0.9645). This verifies that chemisorption was the rate-controlling step which involves valence forces generated from the sharing and exchange of electrons between 2,4-DCP molecules and AC4 during the adsorption process. This result was in accordance with the previous research carried out on the adsorption of 2,4-DCP utilised AC prepared from palm pith [38].

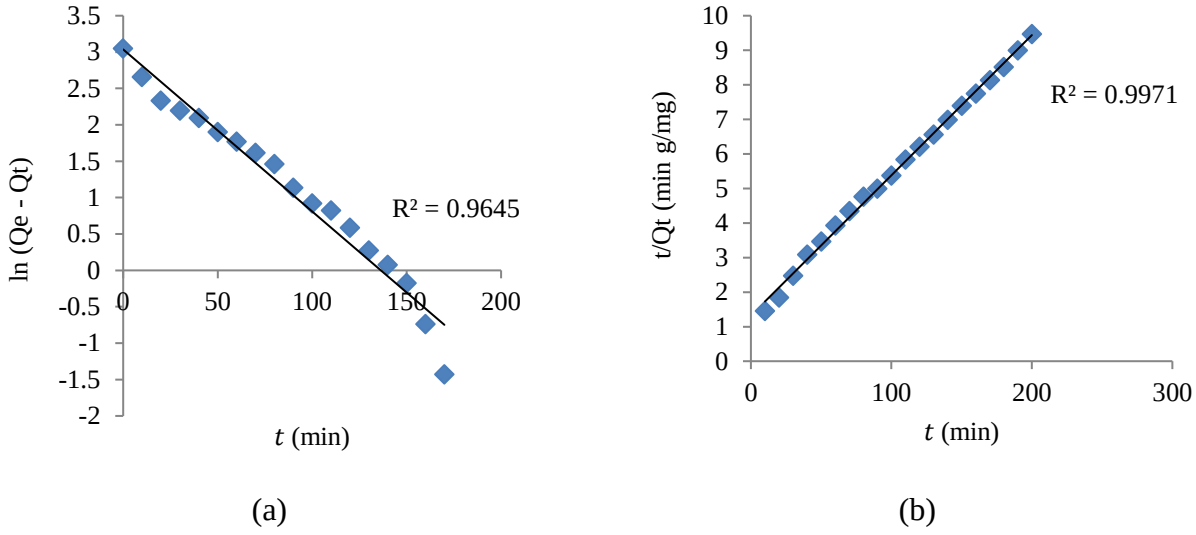

(a) (b)

Figure 9. Adsorption of 2,4-DCP onto AC4 (a) Pseudo-first order kinetic model (b) Pseudo-second order kinetic model

In order to understand the mechanism of 2,4-DCP adsorption by AC4, intraparticle diffusion kinetic model was applied. The plot shown in Figure 10 exhibited multi-linearity, indicating that the adsorption process can be divided into three stages (regions 1, 2, and 3). The sharper region 1 indicates the instantaneous adsorption or external surface adsorption. Region 2 with a smaller gradient signified the gradual adsorption stage where intraparticle diffusion was rate-limiting. As the intraparticle diffusion began to slow down, the final equilibrium stage was achieved (region 3). This was caused by the exceedingly low concentration of 2,4-DCP in the solution. On the other hand, intraparticle diffusion was not the rate-controlling step and there was some degree of boundary layer control as the linear lines did not pass through the origin [39]. From the intraparticle diffusion model equation, the thickness of boundary layer can be estimated through value a. The higher the value of a, the greater the boundary layer effect.

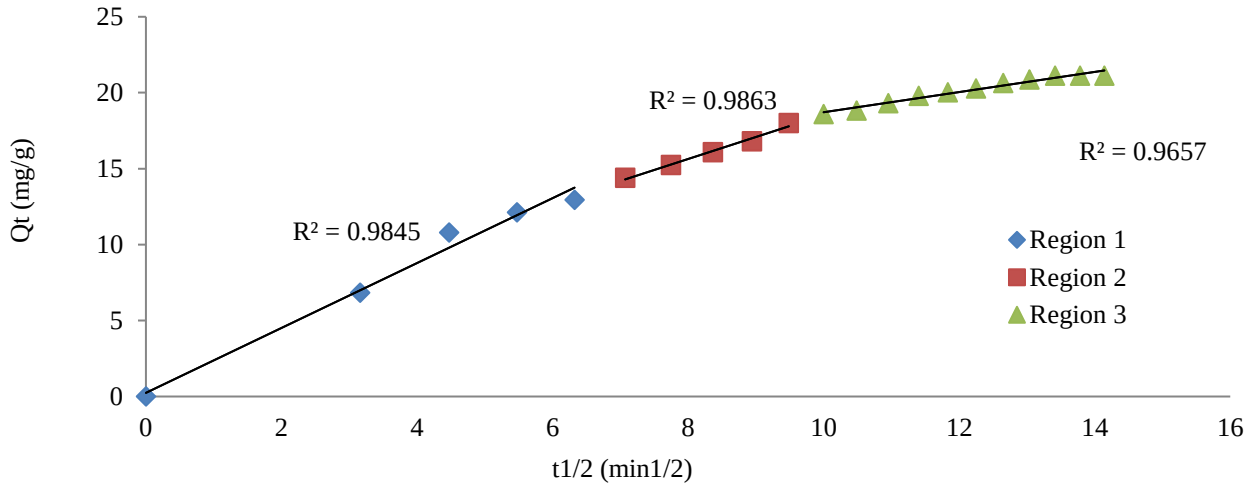

Figure 10. Intraparticle diffusion kinetic model for adsorption of 2,4-DCP onto AC4

As can be seen from Table 6, the value of k_{id} was decreased, whereas value a was increased from region 1 – 3. This showed the domination of the mass transfer process in the initial stage due to the high intraparticle diffusion rate and weak boundary layer effect. Subsequently, at a later stage, the intraparticle diffusion rate became gradually decreased and the boundary layer effect became gradually larger because of the possibility of steric hindrance or pore blockage caused by the adsorbed molecules on surface of AC4. Hence, the adsorption of 2,4-DCP onto AC4 was initially controlled by external mass transfer and then by intraparticle diffusion mass transfer.

Table 6. Kinetic parameters based on the intraparticle diffusion model

Region	k_{id} (mg/g min$^{1/2}$)	a (mg/g)	R^2
1	2.1359	0.2412	0.9845
2	1.4467	4.0633	0.9863
3	0.6636	12.079	0.9657

Adsorption isotherms studies

The data obtained from the initial concentration test was utilised in the adsorption isotherm studies. According to the fitting results shown in Figures 11,12 and 13, the Langmuir isotherm model was more suitable than the Freundlich and Tempkin isotherm models since the correlation coefficient of the Langmuir model (R^2 = 0.8110) was higher than Freundlich (R^2 = 0.7492) and Tempkin (R^2 = 0.5562). This indicated that AC4 had homogenous nature on its surface in which all molecules have equal enthalpies and activation energies during the adsorption process. This result also proved the monolayer adsorption of 2,4-DCP on the surface of AC4. Moreover, chemisorption was further verified through this outcome.

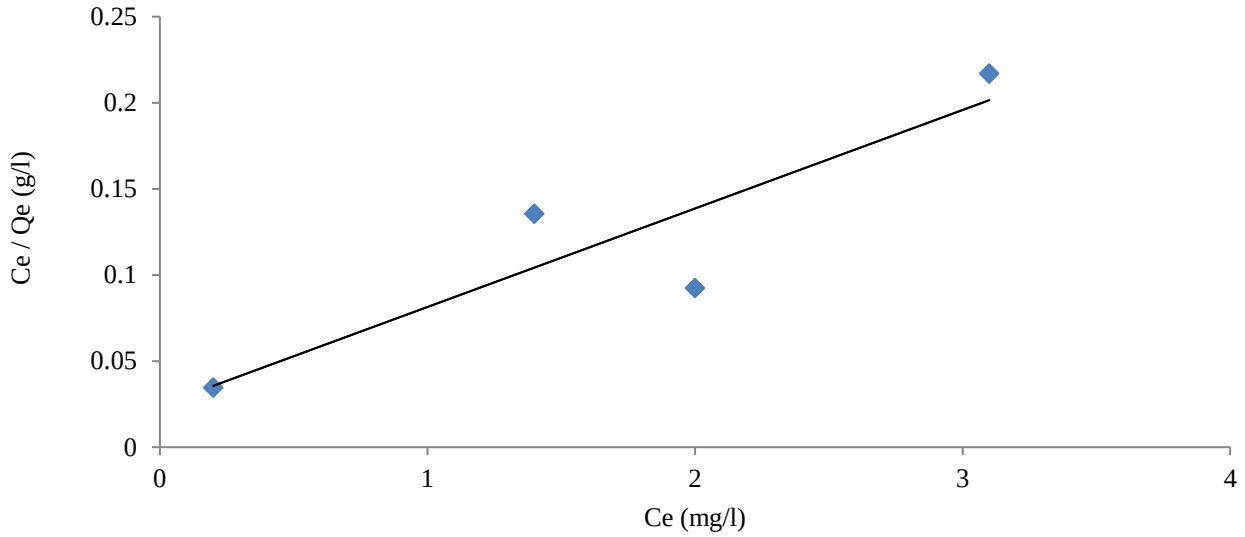

Figure. 11. Langmuir adsorption isotherm for adsorption of 2,4-DCP onto AC4.

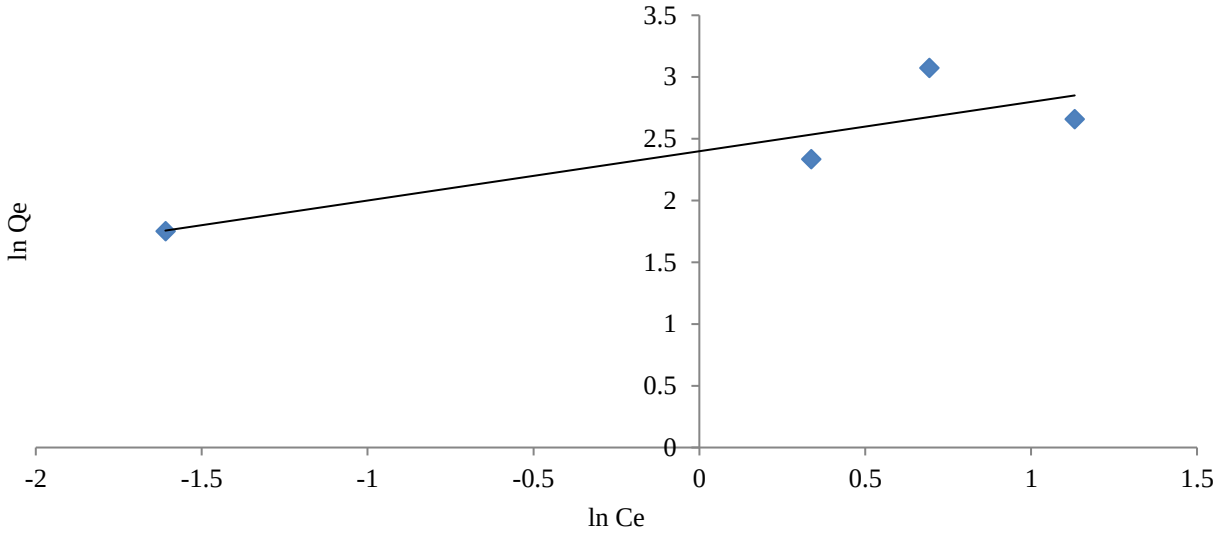

Figure. 12 Freundlich adsorption isotherm of 2,4-DCP onto AC4

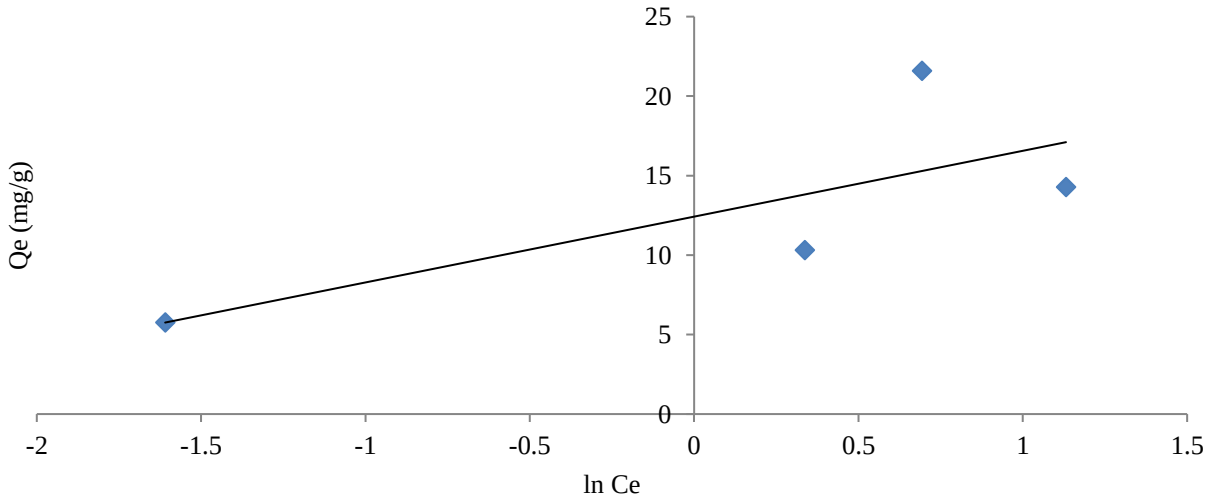

Figure 13. Tempkin adsorption isotherm of 2,4-DCP onto AC4

Comparison of the results from different studies

Table 7 shows the literature values of previous studies of AC using coffee grounds and waste for comparison.

Table 7. Comparison of previous studies of AC using coffee

Precursor	Activation method	Product quality	
Spent coffee grounds	Phosphoric acid activation had been employed as the adsorbent for ethylene and n-butane at room temperature.	BET surface area: 1110 m^2/g, Adsorption isotherms of ethylene and n-butane fitted well with Langmuir equation.	[40]
Coffee extract residue	Prepared ACs using both chemical and physical activation methods (H_3PO_4 at different concentrations: 30, 40 and 50%; heat-treatment temperatures were 500, 600, 700 and 800°C.	Maximum surface area of >640 m^2/g with increased total pore and micropore volumes.	[25]
Coffee husks	Coffee husks were washed with distilled water and dried at 105°C for 5 h in a convection oven. Afterwards they were treated with 2% formaldehyde solution	Biosorption data was best described by Langmuir model and pseudo second-order mechanism was confirmed for the biosorption kinetics. This study was demonstrated that coffee husks are suitable candidates for use as biosorbents in the removal of cationic dyes.	[41]
Coffee ground wastes	Acid black carbons from coffee waste were produced by simple pyrolysis at 673 K and then were sulfonated by sulphuric acid or fuming sulphuric acid.	The "apparent" surface area for all carbons obtained is very small (S_{BET} < 10 m^2/g). However, these acid carbons showed good catalytic activity in glycerol conversion, compared to the commercial resin,	[24]
Coffee residues	Coffee residues were contacted with H_3PO_4 at an impregnation ratio 1:4. This material was dried in air at 100°C for 3 h. The obtained sample was carbonized at 500°C (5 C/min) under N_2 atmosphere (300 cm^3/ min) for 30 min.	BET surface area: 221.55 m^2/g ACs obtained from coffee residues are mesoporous. Their nitroimidazole adsorption capacity per unit of carbon surface area ranges between 0.91 $x10^3$ and 4.02 $x10^3$ $mmol/m^2$ and their sodium diatrizoate adsorption capacity ranges between $0.63x10^3$ and 2.70 $x10^3$ $mmol/m^2$, which are higher capacities than previously reported in the literature.	[23]

Spent Coffee Grounds and Coffee Parchment	AC was prepared from spent coffee grounds and parchment through the co-calcination process and calcium carbonate ($CaCO_3$) was used to optimize the calcinations.	Spent coffee grounds and parchment showed yields after the calcination and washing treatments of around 9.0%. The adsorption of lactic acid was found to be optimal at pH 2. The maximum adsorption capacity of lactic acid was 32.33 and 14.73 mg/g for the parchment and spent coffee grounds ACs, respectively.	[42]
Coffee waste	ACs were prepared from coffee waste via two-stage self-generated atmosphere method after impregnation by $ZnCl_2$.	BET surface area: 951.10 m^2 /g, In this study, the removal of 2,4-DCP in aqueous medium by AC samples was effectively demonstrated and highest adsorption capacity found to be 21.72 mg/g . Kinetics of 2,4-DCP adsorption was best described by pseudo-second order kinetic model.	This study

CONCLUSIONS

Based on the data obtained, it can be concluded that coffee waste can be effectively utilised to prepare AC via $ZnCl_2$ activation in a two-stage self-generated atmosphere method. It was found that the IR of $ZnCl_2$ can affect the characteristics of the AC samples generated. High yield of AC samples was produced using this method in which the yield percentage was decreased from 41.16% to 37.12% for the increasing IR. As for moisture and ash contents, the percentage values were ranged from 4.18% to 6.16% and 9.73% to 10.34% respectively. The ash content increased with the increasing IR. Meanwhile, the AC samples were slightly acidic with pH values varying between 6.06 and 6.56. Besides that, the morphology of AC samples was greatly affected by IR as proved by the SEM micrographs. Various functional groups were present on the surface of AC samples as demonstrated by the FT-IR spectra. However, the surface functional groups of AC samples were generally not influenced by the IR. On the other hand, the removal of 2,4-DCP in an aqueous medium by AC samples was also effectively demonstrated. AC4 yielded the highest 2,4-DCP adsorption capacity which is 21.72 mg/g compared to other samples. Furthermore, the adsorption capacity of AC4 was found to increase with the increased initial concentration of 2,4-DCP and decreasing adsorbent dosage. Nevertheless, an increased in adsorbent dosage resulted in the increment of the percentage of 2,4-DCP removal. The adsorption of 2,4-DCP was found to be more favourable in an acidic solution. The kinetics of 2,4-DCP adsorption by AC4 was best described by the pseudo-second order kinetic model, while the adsorption equilibrium data was well fitted to the Langmuir isotherm model, indicating that chemisorption was a rate limiting step.

ACKNOWLEDGEMENTS

This study was supported by the Research Management Centre of Universiti Malaya in collaboration with the Research Management Centre of Universiti Malaysia Sabah (UMS) (Grant no. GL0111 or UM Project code: CG071-2013). These contributions are gratefully acknowledged. The authors also pay their sincere gratitude to UMS for providing necessary research facilities to accomplish this study.

REFERENCES

Afsharnia, M., Saeidi, M., Zarei, A., Narooie, M. R. and Biglari, H. (2016) Phenol removal from aqueous environment by adsorption onto pomegranate peel carbon, *Electron. Physician*, **8(11),** 3248-3256.

Malakootian, M., Mansoorian, H. J., Alizadeh, M. and Baghbanian, A. (2017) Phenol removal from aqueous solution by adsorption process: Study of the nanoparticles performance prepared from aloe vera and mesquite (Prosopis) leaves, *Sci. Iran.*, **24(6),** 3041-3052.

Palanisamia H, Mohamad R. M. A., Muhammad A. A. Z, Zakariaa Z. A., Alama M. Z. H. Z. and Yunusa M. A. C. (2021) Coffee residue-based activated carbons for phenol removal , *Water Pract. Technol* ., **16(3),** 793-805.

Anku, W. W., Mamo, M. A. and Govender, P. P. (2017) Phenolic compounds in water: sources, reactivity, toxicity and treatment methods. In: Phenolic Compounds – Natural Sources, Importance and Applications (Soto-Hernandez, M., Palma-Tenango, M. & del Rosario Garcia-Mateos, M., eds). IntechOpen, London.

Yousef, R., Qiblawey, H. and El-Naas, M. H. (2020) Adsorption as a process for produced water treatment: a review, *Processes*, **8(1657),** 1-22.

Girish. C. R. and George, G. M. (2017) Phenol removal from wastewater using arecanut husk (areca catechu) as adsorbent, *Int. J. Mech. Eng. Technol*, **8(12),** 1-9.

Tabassi, D., Soumaya, H., Islem, L. and Bechir, H. (2017) Response surface methodology for optimisation of phenol adsorption by activated carbon: Isotherm and kinetic study, *Indian J. Chem. Technol.*, **24(3),** 239-255.

Yan, K. Z., Ahmad-Zaini, M. A., Arsad, A. and Nasri, N. S. (2019) Rubber seed shell based activated carbon by physical activation for phenol removal, *Chem. Eng. Trans.*, **72,** 151–156.

Mohammed, N. A. S., Abu-Zurayk, R. A., Hamadneh, I. and Al-Dujaili, A. H. (2018) Phenol adsorption on biochar prepared from the pine fruit shells: equilibrium, kinetic and thermodynamics studies. J.Environ.Manage., **226,** 377–385.

Tzvetkova, P. G., Nickolov, R. N., Tzvetkova, C. T., Bozhkov, O. D. and Voykova, D. K. (2016) Diatomite/carbon adsorbent for phenol removal, *J. Chem. Technol. Metall,* **51(2),** 202-209.

Huu, S. T., Khu, L. V, Thu, T. L. T. and Thanh, H. H. (2020). Kinetic studies on the adsorption of phenol from aqueous solution by coffee husk activated carbon, *Mediterr. J. Chem.*, **10(7),** 676-686.

Anisuzzaman, S. M., Bono, A., Krishnaiah, D. and Tan, Y. Z. (2016) A study on dynamic simulation of phenol adsorption in activated carbon packed bed column, *J. King Saud Univ. Eng. Sci.*, 28(1), 47-55.

Daffalla, S. B., Mukhtar, H. and Shaharun M. S. (2020) Preparation and characterization of rice husk adsorbents for phenol removal from aqueous systems, *PLoS One,* **15(12):** e0243540.

Crini, G. and Lichtfouse, E. (2018). Advantages and disadvantages of techniques used for wastewater treatment, *Environ. Chem. Lett.*, **17,** 145-155.

Sales, F. R. P., Serra, R. B. G., Figueirêdo, G. J. A. D., Hora, P. H. A. D. and Sousa, A. C. D. (2019) Wastewater treatment using adsorption process in column for agricultural purposes, *Rev. Ambient. Água.*, **14(1),** 1-9.

Agrawal, V. R., Vairagade, V. S. and Kedar, A. P. (2017) Activated carbon as adsorbent in advance treatment of wastewater, *IOSR J. Mech. Civ. Eng.,* **14(4),** 36-40.

Adeleke, O. A., Latiff, A. A. A., Saphira, M. R., Daud, Z., Ismail, N., Ahsan, A., Aziz, N. Adila A., Ndah, M., Kumar, V., Adel Al-Gheethi, Rosli, M. A. and Hijab, M. (2019) Locally derived activated carbon from domestic, agricultural and industrial wastes for the treatment of palm oil mill effluent, *Nanotechnology in Water and Wastewater Treatment,* **2,** 35-62

Gawande, P. R. and Kaware, J. (2017) Characterization and activation of coconut shell activated carbon, *Int. J. Eng. Sci. Invention,* 6(11) 43-49.

Saleem. J., Shahid, U., Hijab, M., Mackey, H. and McKay, G. (2019) Production and applications of activated carbons as adsorbents from olive stones, *Biomass Convers. Biorefin.*, 9, 775-802.

Ukanwa, K. S., Patchigolla, K. Sakrabani, R. and Anthony, E. (2020) Preparation and characterisation of activated carbon from palm mixed waste treated with trona ore, *Molecules.* **25(21): 5028**, 1-18.

Saeed, A. A. H., Harun, N. Y., Sufian, S., Bilad, M. R., Nufida, B. A., Ismail, N. M., Zakaria, Z. Y., Jagaba, A. H., Ghaleb, A. A. S. and Al-Dhawi, B. N. S. (2021) Modeling and optimization of biochar based adsorbent derived from kenaf using response surface methodology on adsorption of Cd2+," *Water,* **13(7),** 1-18.

Ekpete. O. A., Marcus, A. C. and Osi, V. (2017) Preparation and characterization of activated carbon obtained from plantain (*Musa paradisiaca*) fruit stem, *J. Chem.,* **2017 (8635615),** 1-6.

Flores-Cano, J. V., Sanchez-Polo, M., Messoud, J., Velo-Gala, I., Ocampo-Perez, R. and Rivera-Utrilla, J. (2016) Overall adsorption rate of metronidazole, dimetridazole and diatrizoate on activated carbons prepared from coffee residues and almond shells, *J. Environ. Manage.,* **169,** 116-125.

Gonçalves, M., Soler, F. C., Isodaa, N., Carvalhoa, W. A., Mandelli, D. and Sepúlvedac, J. (2016) Glycerol conversion into value-added products in presence of a green recyclable catalyst: Acid black carbon obtained from coffee ground wastes, *J. Taiwan Inst. Chem. Eng.*, **60,** 294-301.

Tehrani, N. F., Aznar, J. S. and Kiros, T. (2015) Coffee extract residue for production of ethanol and activated carbons, *J. Clean. Prod.*, **91,** 64-70.

Ahmad, M. A. and Rahman, N. K. (2011) Equilibrium, kinetics and thermodynamic of Remazol Brilliant Orange 3R dye adsorption on coffee husk-based activated carbon. *Chem. Eng. J.l*, **170(1),** 154-161.

Lamine, S. M., Ridha, C., Mahfoud, H.-M., Chenine, Mouad, Lotfi, B. and Al-Dujaili A. H. (2014) Chemical activation of an activated carbon prepared from coffee residue, *Energy Procedia*, **50**, 393-400.

Boonamnuayvitaya, V., Sae-ung, S. and Tanthapanichakoon, W. (2005) Preparation of activated carbons from coffee residue for the adsorption of formaldehyde, *Sep. Purif. Technol.,* **42(2),** 159-168.

Namanea, A., Mekarzia, A., Benrachedi, K., Belhaneche-Bensemra, N. and Hellal, A. (2005) Determination of the adsorption capacity of activated carbon made from coffee grounds by chemical activation with $ZnCl_2$ and H_3PO_4, *J. Hazard. Mater.,* **119(1-3),** 189-194.

Wang, X., Liang, X., Wang, Y., Wang, X., Liu, M., Yin, D., Xia S., Zhao J. and Zhang Y. 2011. Adsorption of Copper (II) onto activated carbons from sewage sludge by microwave-induced phosphoric acid and zinc chloride activation, *Desalination*, **278**(1-3), 231-237.

Uysal, T., Duman, G., Onal, Y., Yasa, I. and Yanik, J. (2014) Production of activated carbon and fungicidal oil from peach stone by two-stage process, *J. Anal. Appl. Pyrolysis*, **108**, 47-55.

Metin A, Gürses, A. and Karaca, S. 2014. Preparation and characterization of activated carbon from plant wastes with chemical activation, *Microporous Mesoporous Mater.*, **198**, 45-49.

Ozdemir, I., Şahin, M., Orhan, R. and Erdem, M. (2014) Preparation and characterization of activated carbon from grape stalk by zinc chloride activation, *Fuel Process. Technol.,* **125**, 200-206.

Zhong, Z., Yang, Q., Li, X., Luo, K., Liu, Y. and Zeng, G. (2012) Preparation of peanut hull based activated carbon by microwave-induced phosphoric acid activation and its application in Remazol Brilliant Blue R adsorption. *Ind. Crop. Prod.*, **37(1),** 178-185.

Özdemir, M., Bolgaz, T., Saka, C. and Sahin, Ö. (2011) Preparation and characterization of activated carbon from cotton stalks in a two-stage process, *J. Anal. Appl. Pyrolysis*, **92(1),** 171-175.

Anisuzzaman, S. M. Joseph C. G., Krishnaiah D., Bono A., Suali E., Abang S. and Fai L. M. (2016) Removal of chlorinated phenol from aqueous media by guava seed (*Psidium guajava*) tailored activated carbon, *Water Res. Ind.*, **16**, 29-36.

Krishnaiah, D., Joseph, C. G., Anisuzzaman, S. M., Daud, W. M. A. W., Sundang M., and Leow, Y. C. (2017) Removal of chlorinated phenol from aqueous solution utilizing activated carbon derived from papaya (*Carica Papaya*) seeds, *Korean J. Chem. Eng.*, **34(5)**, 1377-1384.

Sathishkumar, M., Binupriya, A. R., Kavitha, D. and Yun, S. E. (2007) Kinetic and isothermal studies on liquid-phase adsorption of 2,4-dichlorophenol by palm pith carbon. *Bioresour. Technol.*, **98(4),** 866-873.

Yakout, S. M. and Elsherif, E. 2010. Batch kinetics, isotherm and thermodynamic studies of adsorption of strontium from aqueous solutions onto low cost rice-straw based carbons. *Carbon - Sci. Tech.*, **1**, 144-153.

Ma, X. and Ouyang, F. (2013) Adsorption properties of biomass-based activated carbon prepared with spent coffee grounds and pomelo skin by phosphoric acid activation, *Appl. Surf. Sci.*, **268,** 566-570.

Oliveira, L. S., Franca, A. S., Alves, T. M. and Rocha, S. D. F. (2008) Evaluation of untreated coffee husks as potential biosorbents for treatment of dye contaminated waters, *J. Hazerd. Mater.*, 155(3), 507-512.

Campos G. A. F., Perez J. P. H., Block I., Sagu S. T., Celis P. S., Taubert A. and Rawel H. M. (2021) Preparation of activated carbons from spent coffee grounds and coffee parchment and assessment of their adsorbent efficiency, *Processes*, 9(1396), 1-18.